Wang, P., Prell, W.L., Blum, P., et al., 2000
Proceedings of the Ocean Drilling Program, Initial Reports Volume 184

7. SITE 1146[1]

Shipboard Scientific Party[2]

BACKGROUND AND OBJECTIVES

The major objectives at Site 1146 (proposed site SCS-4) were to (1) recover a continuous sequence of hemipelagic sediments that would enable reconstruction of East Asian monsoon history from the upper Miocene (~10 Ma) to present; (2) establish the relationship between the orbital-scale variability of East Asian monsoon proxies with orbital forcing, glacial forcing, and internal feedbacks within the climate system; (3) test hypotheses of the relationship between Tibetan Plateau uplift, monsoon evolution, and global cooling by establishing whether monsoonal indices intensify or weaken during the late Miocene and whether the Miocene–Pliocene pattern of accumulation rates is consistent with models of Himalayan-Tibetan Plateau Complex uplift, monsoon intensification, and sea-level changes; and (4) compare the evolution of the East Asian monsoon in the South China Sea (SCS) with that of the Indian monsoon in the Arabian Sea (Ocean Drilling Program [ODP] Leg 117) to identify common causality.

Site 1146 is located at 19°27.40′N, 116°16.37′E, at a water depth of 2091 m (Figs. **F9,** p. 53, in the "Leg 184 Summary" chapter; **F5,** p. 17, in the "Seismic Stratigraphy" chapter). The site was initially located on seismic Line SO95-5 at common depth point 1049 (17:55) in an area of thick sediment fill within a down-dropped block of prerift basement (Fig. **F12,** p. 26, in the "Seismic Stratigraphy" chapter). Based on the *JOIDES Resolution* (JR) seismic survey lines (see **"Site 1146 [SCS-4],"** p. 7, in the "Seismic Stratigraphy" chapter), Site 1146 was moved to shotpoint 3241 on Line JR184-3, ~0.5 nmi east of the originally proposed site (Fig. **F11A,** p. 24, **F11B,** p. 25, in the "Seismic Stratigraphy" chapter). Petroleum wells on the shelf and piston cores on the slope indicated that the sediments at Site 1146 would be hemipelagic muds and silts with moderate carbonate content. The total sediment thickness at the site location is >1.4 seconds below seafloor (sbsf), two-way travel-

[1]Examples of how to reference the whole or part of this volume.
[2]Shipboard Scientific Party addresses.

Ms 184IR-107

time, with a prominent double reflector at ~0.75 sbsf. Two regional reflectors have been identified in this area on the SO95-5 line: T_1, thought to be the Miocene/Pliocene boundary (~5.2 Ma), and T_4, thought to be lower–middle Miocene (15–16 Ma) (H.-K. Wong, pers. comm., 1998). On the JR184-3 line (Fig. **F11,** p. 24, in the "Seismic Stratigraphy" chapter), Reflector T_1 lies at 0.2 sbsf and thus implies a sedimentation rate of ~38 m/m.y. In contrast, the available piston cores near Site 1146 have sedimentation rates of ~200 m/m.y. during the late Quaternary. Reflector T_4 lies at 0.54 sbsf, so that middle to upper Miocene sedimentation rates are estimated at 30 m/m.y. If the interpretation of Reflectors T_1 and T_4 is correct, Site 1146 should recover a middle Miocene to Pliocene sequence that underlies relatively thin Pleistocene deposits. Site 1146 was originally targeted for 520 m penetration; it was deepened to 600 meters below seafloor (mbsf) when the seismic stratigraphy showed that the deeper section at Site 1146 was likely missing at Site 1148 (proposed site SCS-5C). The 600 mbsf penetration at Site 1146 is equivalent to ~0.66 sbsf using the *P*-wave velocity data from physical properties measurements and logging.

Site 1146 lies above the current sill depth of the Bashi Strait (2600 m). Along with Sites 1147 and 1148 (3230 m), it offers both a water-depth transect and a full history of the margin during the Neogene and possibly the Oligocene. The sediments from this site should afford the opportunity to reconstruct a detailed, orbital-scale (Δ = 2 k.y.) record of how East Asian monsoon variability is related to orbital and glacial forcing as well as to internal feedbacks within the climate system. We expect that comparison of the East Asian and Indian monsoons will help to identify common sources of causality and that the long climate record from Site 1146 will enable us to test scenarios for the relationship between the Tibetan Plateau uplift, monsoon evolution, and global cooling. The biostratigraphy and logging data at Site 1146 should help us correlate our findings with the terrestrial record of China and thus make use of the extensive land-based records of climate and monsoon variability. As with its companion site in the southern SCS (Site 1143), the terrigenous accumulation rates at Site 1146 should yield another record of sediment erosion, weathering, and transport related to Himalayan-Tibetan uplift that can be compared with records from the Bengal Fan (ODP Leg 116) and Arabian Sea (Leg 117). The impact of both long-term and short-term sea-level changes will also need to be closely evaluated in interpreting the accumulation rates of these continental margin sediments. In summary, Site 1146 should give a detailed record of Neogene sedimentation and paleoceanographic changes related to the evolution of tectonics as well as global and regional climate.

The drilling program for Site 1146 was to triple core (using the advanced hydraulic piston corer [APC]) to refusal and to use the extended core barrel [XCB] to 520 m (at one or possibly two holes) with a standard logging program (triple combination tool, geological high-resolution magnetic tool [GHMT], and the Formation MicroScanner [FMS]–sonic tool) at one of the deep holes. Permission was received to deepen the hole to 600 m in an effort to recover a section suspected (on the basis of seismic stratigraphy) to be missing at Site 1148.

OPERATIONS

Site 1146 (Proposed Site SCS-4)

The 78-nmi transit to Site 1146 (proposed site SCS-4) was accomplished in 7 hr at an average speed of 11.1 kt. The beacon was dropped on precise Global Positioning System coordinates at 2345 hr on 21 March. The precision depth recorder reading referenced to the dual elevator stool (DES) was 2108.4 m.

Hole 1146A

Hole 1146A was spudded with the APC at 0500 hr on 22 March. The seafloor depth was defined at 2102.6 m from the recovery of the first core. Piston coring advanced with 21 APC cores to 193.9 mbsf. The cores were oriented starting with Core 3H and then continuously from 6H through 21H. During piston coring, downhole temperature measurements were obtained at 32, 61, 99, and 146 mbsf. A temperature gradient of 62°C/km was calculated from the data obtained by the last three measurements (see **"Physical Properties,"** p. 19). The hole was deepened with the XCB to the maximum depth of 607.0 mbsf. The average recovery for this hole was 99.5% (Tables **T1, T2** [both also in **ASCII format**]). Methane concentration increased with depth and peaked at 563 mbsf with 87,000 ppmv, then dropped to 5000 ppmv at the bottom of the hole (see **"Organic Geochemistry,"** p. 14). The maximum ethane concentration of 200 ppmv (and <10 ppmv propane) was found in samples at the bottom of the hole.

T1. Site 1146 coring summary, **p. 72.**

T2. Site 1146 coring summary by section, **p. 75.**

The hole was flushed with 30 bbl of mud and displaced with an additional 190 bbl of sepiolite. No restrictions in hole size were observed by the driller when the pipe was raised to the logging depth of 88 mbsf. Wireline logging began at 1600 hr on 24 March and was completed with three successful runs: triple combo (87–606 mbsf), FMS-sonic (242–606 mbsf), and GHMT (242–606 mbsf) (see **"Wireline Logging,"** p. 22). The drill string was lowered to move the bit from 88 to 239 mbsf after the first run because of numerous washouts and ledges in the upper part of the hole. After logging, the hole was abandoned with 30 bbl of 10.5 lb/gal heavy mud. The drill string was pulled back, and the bit cleared the seafloor at 1330 hr on 25 March.

Floats associated with a long-line fishing array were observed drifting near the ship as Hole 1146A was being displaced with sepiolite mud. As the drill string was pulled up to logging depth, a small amount of monofilament fishing line (30 m) replete with hooks and some live bait was removed from two stands. Two small fishing boats were observed in the area. The drill crew also retrieved two mahi-mahi (3–4 ft long) at the rig floor. The fish had safely passed up through the guide horn and out the DES and ended up in our barbecue grills. A diver inspection of the thrusters and main propeller shafts was planned for the Hong Kong port call.

Hole 1146B

The ship was offset 20 m east of Hole 1146A, and Hole 1146B was spudded with the APC at 1500 hr on 25 March. The seafloor depth inferred from the recovery of the first core was 2103.2 m. Piston coring advanced to 216.3 mbsf, and the cores were oriented starting with Core 3H. The hole was deepened to 245.1 mbsf with three XCB cores. The av-

erage recovery for the hole was 98.7% (Tables T1, T2). The bit was pulled clear of the seafloor at 1415 hr on 26 March.

Hole 1146C

The vessel was offset 10 m east of Hole 1146B. To obtain a stratigraphic overlap with data from the previous holes, the initial APC core of Hole 1146C was shot after placing the bit one meter below the mudline depth of Hole 1146B. Hole 1146C was spudded at 1540 hr on 26 March, and piston coring advanced to 162.5 mbsf. The cores were oriented starting with Core 3H. The hole was deepened to the maximum target depth of 603.5 mbsf with 46 XCB cores. During XCB coring, the interval from 220.1 to 224.1 mbsf was drilled ahead to maintain an overlap with Hole 1146A. The average recovery for the hole was 101.4% (Tables T1, T2).

The total core recovered at this site was 1452.2 m, representing 100.1% of the cored interval of 1450.6 m. The bit cleared the seafloor at 0100 hr on 29 March as the drill string was recovered. Before leaving the site, the components of the bottom-hole assembly were subjected to the routine end-of-leg magnetic particle inspection. At 0615 hr on 29 March, the vessel began the short voyage to Site 1147.

COMPOSITE SECTION

We built a continuous meters composite depth (mcd) scale and a splice (as defined in "Composite Section," p. 3, in the "Explanatory Notes" chapter) that range from the top of Core 184-1146B-1H to the bottom of Section 184-1146C-26X-7. The splice and the mcd extend from 0 to 266.7 mcd. Extension of a continuous splice below this interval was precluded by the alignment of core recovery gaps. However, as described in "Composite Section," p. 3, in the "Explanatory Notes" chapter, we were able to construct a discontinuous ("floating") mcd scale and splice for the interval spanning from 266.7 to 640.9 mcd, which is the bottom of the cored sequence.

The mcd scale and the splice are based on the stratigraphic correlation of whole-core multisensor track (MST) and split-core color spectral reflectance (CSR) data (lightness, L*) collected at 4- to 5-cm intervals (see "Physical Properties," p. 19, for details). From the MST, we used magnetic susceptibility (MS), gamma-ray attenuation (GRA) bulk density, and natural gamma radiation (NGR) data. These data, and the splice constructed from them, are presented on the mcd scale in Figures F1, F2, F3, and F4 (also as Synergy Software KaleidaGraph plots and Microsoft Excel data files [see the "Supplementary Materials" contents list]; the spliced records are also available in ASCII format). The depth offsets that comprise the mcd scale are given in Table T3 (also in ASCII format). The splice tie points (Table T4, also in ASCII format) should be used as a guide for detailed postcruise sampling.

Magnetic susceptibility data were the most useful stratigraphic tool for correlation at this site. The NGR and CSR data were helpful in intervals where structure in the MS profile was ambiguous. As at previous sites on this leg, the GRA data were not particularly useful.

We constructed the mcd scale by assuming that the uppermost sediment (the "mudline") in Core 184-1146B-1H was the sediment/water interface. This core, the "anchor" on the composite depth scale, has the same depth on both the mbsf and mcd scales. We correlated downhole

F1. Smoothed/correlated MS data and splice, p. 27.

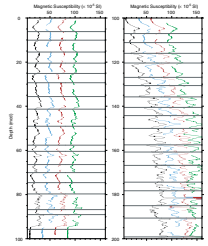

F2. Smoothed/correlated NGR data and splice, p. 31.

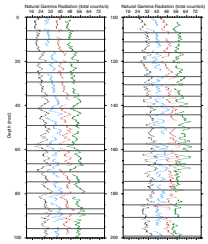

F3. Smoothed/correlated GRA data and splice, p. 35.

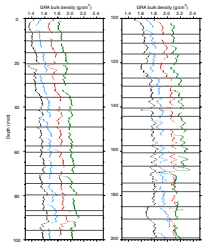

F4. Smoothed/correlated L* values from the CSR data and splice, p. 39.

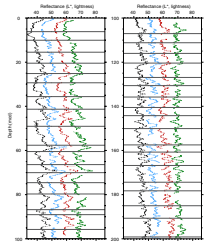

T3. Composite depths, p. 76.

T4. Splice tie points, p. 78.

from this anchor, core by core, until we reached 266.7 mcd. At this point, core gaps prevented further downhole construction of the continuous mcd scale and splice.

Although the cores below 266.7 mcd could not be tied directly to the continuous composite depth scale and thus the splice, they could be correlated with each other. We placed the cores on a discontinuous composite depth scale. This "floating" scale is not tied to the overlying mcd scale (and thus back to the mudline). Instead, the positions of the cores are adjusted such that correlative features match. We chose Core 184-1146C-27X as the top of the floating splice. The depth of this core on the mcd scale is based on the overlying continuous mcd scale. Cores at similar depths from adjacent holes were mapped to Core 184-1146C-27X; correlation then progressed downhole, as in the construction of the continuous mcd.

LITHOSTRATIGRAPHY

Lithologic Units

Three lithologic units were identified at Site 1146 (Fig. F5). Unit I is composed of greenish gray nannofossil clay that extends from 0 to 242.68 mcd. This unit is relatively enriched in quartz, plagioclase, and chlorite and depleted in calcite compared with the lower units. Unit II consists of light brownish gray clayey foraminifer and nannofossil ooze and foraminifer clay nannofossil mixed sediment that continuously grades down into the green nannofossil clay of Unit III at 553.02 mcd. Unit II is divided into two subunits based on shifts in mineralogy determined by X-ray diffraction (XRD) and carbonate coulometry of sediments from Hole 1146A (Fig. F6). The XRD analyses indicate an increase in illite, kaolinite, and quartz concentrations across the Subunit IIA/IIB boundary. A decrease in the calcite concentration and the disappearance of dolomite also occur across this boundary. Subunit IIA includes sediments from 242.68 mcd through 434.22 mcd and contains slightly more carbonate-rich sediment than Subunit IIB, which continues down to 553.02 mcd. The green nannofossil clay of Unit III dominates below this level to the bottom of Holes 1146A and 1146C (642.31 mcd). This unit is defined by changes in color and "iron sulfide" concentration; there is little mineral change across the Unit II/III boundary.

F5. Recovered section summary, p. 43.

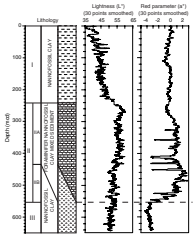

F6. Hole 1146A bulk mineralogy, p. 44.

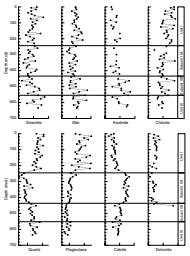

Unit I (0.0–242.68 mcd)

Interval: Cores 184-1146A-1H through 24X; Cores 184-1146B-1H through 23H; Core 184-1146C-1H through Section 24X-3, 13 cm
Depth: 0–222.40 mbsf (Hole 1146A); 0.–216.31 mbsf (Hole 1146B); 0–227.23 mbsf (Hole 1146C)
Age: late Pliocene–Pleistocene

Unit I mainly consists of clay, nannofossil clay, and clayey nannofossil ooze. The greenish gray nannofossil clay contains abundant foraminifers. Pteropods, including individuals >1 cm across (e.g., Section 184-1146A-2H-2, 102 cm; 7.37 mcd), are common in the upper part of Unit I. Nannofossils are common throughout the unit. Sedimentary structures are rarely noted in the core since the clay is completely homogenized by bioturbation. However, shifts in color toward lighter tones correspond to higher nannofossil content (clayey nannofossil ooze), for ex-

ample, at interval 184-1146A-7H-4, 0–70 cm (58.4–59.1 mcd), and at interval 184-1146A-9H-5, 10 cm, to 9H-6, 100 cm (80.1–82.5 mcd) (Table T5). Foraminifer turbidites are absent in Unit I but are observed in Units II and III. An ~10-cm-thick red-brown oxidized sediment layer is observed at the top of Cores 184-1146A-1H and 184-1146B-1H and is presumed to be the modern seafloor. This layer was not recovered in Hole 1146C.

The bulk mineralogy as determined by X-ray diffraction (Fig. F6) indicates that the sediments in Unit I are relatively enriched in quartz, plagioclase, and chlorite relative to Units II and III, and dolomite is usually a trace component of the mineral assemblage.

T5. Light-colored, carbonate-rich layers, p. 80.

Carbonate-Rich Intervals

Slightly lighter intervals, with higher carbonate content, are observed throughout Unit I in all three holes (Table T5; Fig. F5). Internal sedimentary features of the light layers include abundant visible foraminifers, common green clay layers (typically 1–3 cm thick), well-defined bioturbation, and slightly yellowish gray patches or mottles, which probably represent traces of bioturbation. Smear-slide estimates indicate calcareous nannoplankton contents of >30%, compared to ~10% in the background clay. The light layers are characterized by a stiff clay, which often shows a rough surface caused by the cutting wire.

Green Layers and Mottles

Green layers and less distinct green mottles, which resemble the green clay layers observed at Sites 1143, 1144, and 1145 (see "Lithostratigraphy," p. 8, in the "Site 1143" chapter; "Lithostratigraphy," p. 6, in the "Site 1144" chapter; and "Lithostratigraphy," p. 4, in the "Site 1145" chapter), occur frequently in the upper part of Unit I, principally above ~185 mcd (Fig. F7). They are characterized by a stiffer clay than the dominant clay lithology of the section and have a lower water content and higher *P*-wave velocity.

F7. Occurrence of "iron sulfides," pyrite, and green layers, p. 45.

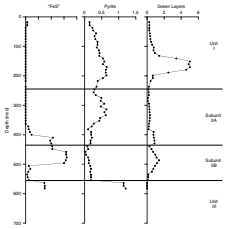

Bioturbation

Bioturbation is intense throughout Unit I. The sediment is generally completely homogenized, and individual burrows are rarely observed. Pyrite-filled burrows are the exception to this pattern. They occur at a frequency of about one to two burrows per section throughout the lower part of the unit. Large pyrite-filled burrows reach several centimeters in length and up to 2 cm in diameter. Pyrite-filled burrows first appear at ~39 mcd, although small, disseminated pyrite crystals are present at shallower depths (Fig. F7). They probably form by the diagenetic replacement of organic matter–rich sediment fills.

Fossils

Macrofossils are a volumetrically small but regular component of the sediments at Site 1146. Large (>1 cm in length) pteropods of the genus *Cavolinia* are observed in Cores 184-1146A-2H and 3H (4.85 mcd and 25.5 mcd). Additionally, large benthic and planktonic foraminifers were observed. Diatoms, silicoflagellates, radiolarians, and sponge spicules are commonly observed in smear slides. Several large pyrite nodules preserve organic structures that may be interpreted as xenophyophorians (large agglutinating multicellular organisms, which show some similarities to agglutinated foraminifers). Xenophyophorians are often observed on the sediment surface in the deeper parts of the South China Sea (Hess, 1998).

Volcaniclastic Layers

The stratigraphic distribution of ash layers in the upper part of Unit I exhibits a pattern similar to previous Leg 184 sites: thin, light gray ash layers, often dispersed by bioturbation, as well as isolated pumice clasts (Cores 184-1146A-1H through 8H). In contrast, the lower part of Unit I is characterized by a small number of dark gray or black ash layers with larger pumice clasts (Table T6). Finely dispersed volcanic glass is observed in smear slides from Section 184-1146B-2H-2, 27 cm (10.32 mcd), and this level coincides with a significant peak in magnetic susceptibility (see "Physical Properties," p. 19).

T6. Volcanic ash layers, p. 81.

Black ashes are present in the lower part of Unit I and include thin (<1–2 cm) layers at intervals 184-1146A-9H-7, 28–29 cm (83.28–83.29 mcd), and 184-1146B-12H-5, 57–60 cm (115.87–115.90 mcd). The latter contains large volcanic glass shards as long as 1 cm. A prominent 4-cm-thick black ash interval with a sharp base and with pumice debris in the lower part of the layer is observed at intervals 184-1146A-19H-5, 10–14 cm (181.65–181.69 mcd), 184-1146B-19H-2, 58–62 cm (181.63–181.67 mcd), and 184-1146C-19X-1, 0–4 cm (182.40–182.44 mcd). This ash is easily correlated between the three holes at this site.

Unit II (242.68–553.02 mcd)

Interval: Core 184-1146A-25X through Section 55X-CC, 22 cm; Core 184-1146B-24X through Section 26X-CC, 27 cm; Sections 184-1146C-24X-3, 13 cm, through 54X-6, 87 cm
Depth: 222.40–512.97 mbsf (Hole 1146A); 216.30–245.10 mbsf (Hole 1146B); 227.23–515.51 mbsf (Hole 1146C)
Age: middle Miocene–late Pliocene

Lithologic Unit II differs from Unit I mainly in its significantly higher carbonate content (50–60 wt% instead of 10–30 wt%) and the resulting lighter colors. In addition, the mineralogy shifts from a plagioclase and quartz-rich assemblage to a finer grained and biogenic calcite-rich assemblage (inferred from smear slides). Dolomite occurs in Subunit IIA but not in Subunit IIB. The unit consists mainly of homogeneous to rarely mottled, light brownish gray foraminifer and nannofossil clay mixed sediment. A few intercalations of light bluish green nannofossil clay occur in the lower part of the unit. This unit is subdivided into two subunits based on the mineralogy (Fig. F6).

Subunit IIA (242.68 –434.22 mcd)

Interval: Core 184-1146A-25X through Section 44X-4, 10 cm; Core 184-1146B-24X through Section 26X-CC, 27 cm; Sections 184-1146C-24X-3, 13 cm, through 43X-6, 125 cm
Depth: 222.40–409.9 mbsf (Hole 1146A); 216.30–245.10 mbsf (Hole 1146B); 227.23–410.75 mbsf (Hole 1146C)
Age: late Miocene–late Pliocene

Subunit IIB (434.22–553.02 mcd)

Interval: Sections 184-1146A-44X-4, 10 cm, through 55X-2, 67 cm; Sections 184-1146C-43X-6, 125 cm, through 54X-6, 89 cm
Depth: 409.9–512.97 mbsf (Hole 1146A); 410.75–515.51 mbsf (Hole 1146C)
Age: middle–late Miocene

Subunit IIA is dominated by biogenic calcite, which increases sharply across the Unit I/Unit II boundary and represents an increase in the flux and/or preservation of nannofossil ooze. Calcite remains relatively high until the Subunit IIB boundary at 434.22 mcd, where it decreases; dolomite is not detected below this level. Kaolinite becomes a significant contributor to the mineral composition within Subunit IIB, and quartz also increases at the Subunit IIA/Subunit IIB boundary. These mineralogy changes mark the onset of the gradational change in the lithology from a carbonate-rich Unit II to the green clays of Unit III; they represent either a change in source region or a change in weathering regime at the source area.

Bluish Green Pyrite-Rich Nannofossil Ooze Intervals

The most noteworthy features within lithologic Unit II are several intervals of characteristically bluish green nannofossil clay, which contain large amounts of pyrite as nodular irregular layers or as finely disseminated specular particles within the sediment. Contacts with the overlying and underlying gray or light brownish gray background sediment are generally gradational. In some cases (e.g., interval 1146A-42X-3, 80 cm, through 42X-4, 20 cm; 414.06–414.96 mcd) a broad transition zone is observed, characterized by intense visible bioturbation. Two bluish green intervals contain foraminifer turbidites within the middle of the layer (Fig. F8). One of these turbidites (324.6–324.8 mcd) is directly overlain by a fine-grained green ash layer. A typical pyrite layer with calcite is observed in interval 184-1146A-44X-2, 27–36 cm (431.38–431.47 mcd) (Fig. F9). These units are evident in the reflectance red parameter (a*) as a drastic decrease to more green values (Fig. F5).

F8. Foraminifer turbidite covered by a volcanic ash layer, p. 46.

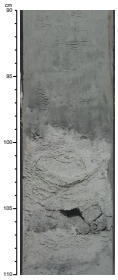

F9. Pyrite layer in green calcareous sediment, p. 47.

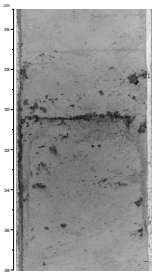

Bioturbation

Bioturbation is common to abundant throughout the cored interval of Unit II, although individual burrows are difficult to identify because of the homogeneous sediment color. In most cases, faint black "iron sulfide" staining and some mottled intervals are the only visible traces of burrowing. In the lower part of Subunit IIB, a large number of individual *Zoophycos* burrows are observed.

Volcanic Ash Layers

Volcanic ash is a volumetrically small and rare component of the sediments in Subunit IIB. A stiff, dark gray, altered volcanic ash, with a sharp base and normal grading, is observed at interval 184-1146A-26X-CC, 30–33 cm (258.78–258.81 mcd). This layer is composed of quartz, feldspar, and volcanic glass altered to clay and zeolites, as shown by smear-slide analysis.

Unit III (553.02–642.31 mcd)

Interval: Section 184-1146A-55X-2, 67 cm, through Core 64X; Section 184-1146C-54X-6, 89 cm, through Core 63X
Depth: 512.97–607.12 mbsf (Hole 1146A); 515.51–603.77 mbsf (Hole 1146C)
Age: early–middle Miocene

The transition between Unit II and Unit III corresponds to an important progressive change in the sediment color. The sediment at the base of Unit II is brownish gray but shows an increasing number of green intervals downsection, becoming a distinct greenish gray below Section 184-1146A-55X-CC, 22 cm (553.02 mcd). We define this color change as

the boundary between Unit II and Unit III (Fig. F5, a* values curve). The sediment is clearly poorer in foraminifers in the upper part of the unit compared to Unit II, whereas the proportion of nannofossils seems to increase slightly. The abundance of foraminifers increases again toward the bottom of Unit III. The carbonate content of Unit III is in the range of 30–50 wt% and is clearly lower than in Unit II (50–60 wt%). Unit III is characterized by relatively high concentrations of smectite and illite (Fig. F6).

Bioturbation

Bioturbation is intense and most of the sediment is homogenized, although a number of well-defined traces can still be detected. Only a few burrows are replaced by pyrite. The most common trace fossils are *Zoophycos* and composite burrows with *Chondrites,* a classic bathyal assemblage. The density of *Zoophycos* burrows increases toward the bottom of the hole. They are generally filled with brownish sediment and clearly visible (Fig. F10). A well-preserved escape trace is observed in interval 184-1146A-64X-4, 144–150 cm (638.45–638.51 mcd).

F10. *Zoophycos*-rich interval, p. 48.

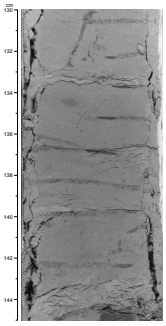

Discussion

Three main lithologic units have been recognized at Site 1146. This division is also shown in the mineralogy and color data. Unit I is characterized by an alternation of darker and lighter intervals, usually with gradational boundaries. According to smear-slide observation and carbonate analysis, the lighter intervals correspond to significant increases in the carbonate content. The uppermost light intervals are clearly correlative between the three holes. Their formation may be caused by changes in marine productivity, the relative amount of terrigenous deposition to the site, or differential dissolution caused by changing bottom-water chemistry and/or glacial–interglacial variation. We propose an interpretation in which the light intervals correspond to the interglacial isotopic stages (Table T5) (e.g., Shackleton and Opdyke, 1976), based on the similarity of the L* value curve and the deep-sea oxygen isotope curve. Smear-slide analyses indicate no noticeable change in the character of the terrigenous material between dark and light layers. In the lower part of Unit I, the correlation of the L* value curve with global isotopic stages becomes more difficult. This could be because of the overall increase of carbonate that results in a lower contrast between light and dark intervals. Unit II is characterized by high intensity in lightness (reflectance L* parameter) as a result of its high carbonate content. Only a few darker intervals (e.g., interval 184-1146C-30X-3, 10–40 cm [299.25–299.55 mcd]) indicate an increase of clay content because of lower primary productivity, higher continental detrital sediment supply, or decreased preservation of carbonate. Unit III does not show a change in lightness, but there is a color shift toward green values at the Unit II/III boundary (Fig. F5).

Despite the variation in carbonate content, no evidence suggests a significant change in the water depth at Site 1146 during the sedimentation of the recovered section. The sediment character is one typical of deposition at bathyal depths on a continental slope, with oxygenated bottom water implying water depths exceeding the oxygen minimum zone (~600 m). However, the bulk mineralogy suggests that either a change in the source of the terrigenous material or a change in the weathering regime of the source region took place over time. The relatively high concentration of quartz and plagioclase, and to a lesser ex-

tent chlorite, in Unit I suggests that the terrigenous component in this unit is coarser grained and characteristic of source-area environments where physical weathering was more important than chemical weathering compared with the older sediments.

The relative increase in kaolinite in at the Subunit IIA/IIB boundary suggests a change to a more chemical weathering–dominated source-area environment during the middle to late Miocene. The complete lack of dolomite below the Subunit IIA/IIB boundary suggests either a change in terrigenous source area, or a change in the diagenetic regime in the sediment column.

Overall, the terrigenous component of the sediment suggests aridification of the source regions from the late Miocene through the Pleistocene.

BIOSTRATIGRAPHY

Calcareous Nannofossils

Calcareous nannofossil biostratigraphy for Site 1146 used core-catcher samples of Hole 1146A, selected samples within the cores of Hole 1146A, and core-catcher samples from Hole 1146B (Tables **T7, T8;** Fig. **F11**). Sediments recovered at Site 1146 yield abundant nannofossils that are generally well preserved above 531.2 mcd but are moderately overgrown below that level. Many samples exhibited some degree of reworking; however, this was more pronounced in the interval between 419.9 and 460.4 mcd.

Thirty-two nannofossil biostratigraphic datums were recognized in the lower Miocene to Pleistocene sediment sequence at Site 1146 (Table **T7**). The last occurrence (LO) of *Sphenolithus* spp. (*Sphenolithus abies* and *Sphenolithus neoabies*) was noted in Sample 184-1146B-25X-CC (250.6 mcd); no sediments were recovered from Core 184-1146A-25X.

The Pliocene/Miocene boundary is constrained by the LO of *Triquetrorhabdulus rugosus* and the LO of *Discoaster quinqueramus* between 308.4 mcd and 317.9 mcd, respectively. *Discoaster loeblichii* and *Discoaster neorectus* are marker species used by Okada and Bukry (1980) to subdivide late Miocene Zone CN8. At Site 1146, specimens that resemble these two species were found to occur down to 438.7 mcd (Zone CN7) and 460.4 mcd (Zone CN6) in Hole 1146A. Thus, these two species are not useful markers for the South China Sea. *Sphenolithus belemnos* was observed between 635.3 and 643.1 mcd, which places the bottom of Hole 1146A in Zone NN3 (18.3 to 19.2 Ma).

Planktonic Foraminifers

Planktonic foraminifers were examined in all core-catcher samples from Hole 1146A and selected core-catcher samples from Hole 1146C. Site 1146 yields abundant, well-preserved planktonic foraminifers as documented by infrequent test breakage (fragmentation <10%), little to no evidence of dissolution or diagenetic alteration, and the observation of numerous clear tests. In addition, the soft clay in the samples was easily removed by soaking in a warm Calgon and hydrogen peroxide solution and washing through a 150-µm sieve.

A complete planktonic foraminiferal biostratigraphy for Site 1146 is based on all core-catcher samples from Hole 1146A and three core-catcher samples from Hole 1146C (see Tables **T7, T9** for details). The

T7. Summary of biohorizons, **p. 82.**

T8. Calcareous nannofossil checklist, **p. 84.**

F11. Age-depth plot, **p. 49.**

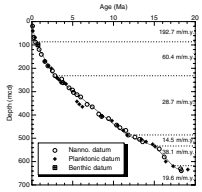

T9. Planktonic foraminifer checklist, **p. 86.**

biostratigraphy of Site 1146 had several notable conventions and exceptions.

Within Zone N22, we used the LO (0.12 Ma; Thompson et al., 1979) and first occurrence (FO) (0.40 Ma; Li, 1997) of pink *Globigerinoides ruber* as two biostratigraphic control points. The FO of *Globorotalia truncatulinoides* was used to mark the bottom of Zone N22 (185.4) (Blow, 1969).

For Zone N21, the LO of *Globorotalia multicamerata* was found to occur at 206.1 mcd, which corresponds to an age of 2.4 instead of 3.09 Ma (see Table **T3,** p. 43, in the "Explanatory Notes" chapter). This observation is supported by studies of the South China Sea northern shelf (Wang et al., 1991). Because there was no recovery for Core 184-1146A-25X, we used three core-catcher samples from Hole 1146C to constrain the LOs of *Globoquadrina altispira* and *Sphaeroidinellopsis seminulina* and the FO of *Globorotalia tosaensis* (Table **T7**). The coiling change of *Pulleniatina* from sinistral to dextral was quite distinct and served as a marker for the bottom of Zone N20 (256.5 mcd). At Site 1146, we observed that the FO of *Sphaeroidinella dehiscens* appeared at 337.7 mcd and used it as a marker for the bottom of Zone N19.

Although *Pulleniatina primalis* is observed higher in the section, we did not find its FO to be a useful marker of the bottom of Subzone N17b. Instead, we relied on the FO of *Globigerinoides conglobatus* as an indicator of N17b (360.3 mcd). Because we observed both dextral and sinistral forms of *Neogloboquadrina acostaensis* throughout Subzone N17a, its coiling change was not used as a datum to mark 6.6 Ma. At this site, we used the FO of *N. acostaensis* and the LO of *Globorotalia mayeri* to define the top (419.8) and bottom (449.1 mcd), respectively, of biozone N15. No transitional specimens of these two species were found within this biozone. The FO of *Globigerina nepenthes* was quite distinct and clearly marked the bottom of Zone N14 (460.4 mcd).

The FOs of *Orbulina* spp. and *Praeorbulina sicana* were used to mark the lower boundary of Zones N9 (531.2 mcd) and N8 (594.7 mcd), respectively. In the last core-catcher sample, we observed *Globoquadrina binaiensis* but not *Paragloborotalia kugleri*. This confines the bottom of Hole 1146A (643.1 mcd) to within Zone N5, with an age between 19.1 and 21.5 Ma.

Benthic Foraminifers

Site 1146 yields rare to common deep-sea benthic foraminifers, but the ratio of benthic to planktonic foraminifers increased greatly in the lower part of Hole 1146A, indicating a shallower water depth for sediments below ~560 mcd (*Heterolepa, Gavelinopsis, Uvigerina,* and *Globocassidulina* were observed). However, we found no clear evidence for reworked benthic foraminifers from the shelf and upper slope. The LO of *Stilostomella* was observed at a depth of 104.8 mcd, which is assigned an age of 0.75 Ma for the latitude of this site (Schönfeld, 1996).

Summary

At Site 1146 calcareous nannofossils are abundant and well preserved, although preservation deteriorates below ~530 mcd. Planktonic foraminifers are abundant and have good preservation for the site's entire interval. Benthic foraminifers are generally few but become more abundant in the lower part.

An age-depth plot shows that the biohorizons from the three fossil groups generally agree with each other (Fig. F11). The Pleistocene/Pliocene boundary is constrained by the FO of medium-sized *Gephyrocapsa* spp. and the LOs of *Globigerinoides fistulosus* and *Discoaster brouweri* and is located between 185.4 and 195.1 mcd. The Pliocene/Miocene boundary is constrained by the LO of *T. rugosus* and the LO of *D. quinqueramus,* between 308.4 and 317.9 mcd, respectively. The sedimentation rate at Site 1146 has been calculated based on biostratigraphic data (Table T7) and is depicted in Figure F11.

PALEOMAGNETISM

Shipboard paleomagnetic measurements for Holes 1146A, 1146B, and 1146C consisted of long-core measurements of the natural remanent magnetization (NRM) at 8-cm intervals before and after alternating field (AF) demagnetization (usually up to 20 mT) carried out on the archive halves of all APC cores. Measurements of XCB cores were pursued until the overprint was so severe that no information could be retrieved after demagnetization at 30 mT. In addition, 380 discrete samples were collected from the working halves of Hole 1146A (APC and XCB cores), at an average spacing of two samples per section (1.5 m). Half of these samples were subjected to progressive AF demagnetization with 10 steps up to 50 mT; further analysis will be carried out postcruise. For Hole 1146B, the nonmagnetic cutting shoe was used with a standard core barrel on every second core. Cores 184-1146A-6H through 21H, 184-1146B-3H through 21H, and 184-1146C-3H through 17H were oriented using the Tensor tool.

Hole 1146A

Long-core measurements of NRM and subsequent demagnetization steps were carried out at 8-cm intervals. Cores 184-1146A-1H through 4H and 13H were measured with two demagnetization steps at 10 and 20 mT; the remaining cores were measured with only one AF demagnetization step at 20 mT.

The direction of the NRM (after demagnetization at 20 mT and correction using the Tensor tool data where available) is shown in Figure F12. Above 115 mcd, declination and inclination generally oscillate around values expected for a geocentered dipole field at this latitude (0° and 38°, respectively), with an amplitude consistent with the secular variation of the geomagnetic field. At 116.7 mcd, the Brunhes/Matuyama boundary is identified by a sudden swing of the declination to 180°.

Farther downcore, the data are highly scattered, possibly as a result of incomplete removal of the overprint resulting from the coring process. As noted at previous sites, this increasing contribution of the overprint to the magnetization is revealed by positive inclinations: although some core intervals are undoubtedly reversed according to the declination, inclinations remain positive, showing that the overprint along the z-axis has not been entirely removed. Because of this, the occurrence of the Jaramillo and Olduvai Subchrons was largely obscured and could not be precisely located.

Every second discrete sample was AF demagnetized with 10 steps of demagnetization up to 50 mT. This treatment proved to be very efficient in removing the overprint in discrete samples from APC cores. An

F12. Declination and inclination for Hole 1146A, 0–300 mcd, p. 50.

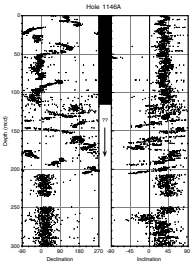

initial look at the data suggests it is consistent with the long-core measurements; further postcruise analysis should resolve some of the problems below the Brunhes/Matuyama boundary.

Hole 1146B

Only long-core measurements were made at Hole 1146B at 8-cm intervals and two demagnetization steps at 10 and 20 mT. Hole 1146B yielded better results, with the Jaramillo and possibly the Olduvai Subchrons evident (Fig. F13).

Between 99.7 and 101.3 mcd, a swing in declination with very low correlative inclinations could document a geomagnetic event. From its estimated age, we suggest that this could be a record of the Big Lost geomagnetic Event (dated at 510 to 650 ka). The Brunhes/Matuyama boundary was found just below at a depth of 114.9 mcd. Farther downcore, the upper Jaramillo transition is situated at a depth of 132.5 mcd; the lower Jaramillo, at 137.7 mcd. Additional declination swings are present farther downcore. Their identification with a known polarity chron, however, is made difficult by the large overprint present on inclination data, even after demagnetization at 20 mT. A transition from reverse declinations to normal occurs between 160.5 and 165.8 mcd, possibly marking the Olduvai Subchron. Comparison with the magnetic polarity time scale and with subsequent biostratigraphic results (see "Biostratigraphy," p. 10) yields the age-depth relation shown in Table T10.

F13. Declination and inclination for Hole 1146B (APC cores), p. 51.

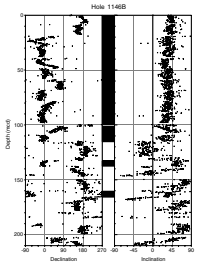

T10. Age-depth relationship from the magnetic polarity time scale, p. 88.

Hole 1146C

Long-core measurements in Hole 1146C were conducted with only one step of demagnetization at 15 mT down to Core 184-1146C-10H. Based on the results of Hole 1146B, Cores 184-1146C-11H through 17H were then demagnetized with two steps at 10 and 15 mT. The one-step procedure was then resumed for the XCB cores from Cores 184-1146C-18X through 28X. For this last core, both the archive and working halves of Section 184-1146C-28X-4 were measured after demagnetization. Although the AF treatment removed >90% of the magnetization, the archive and the working halves still have the same declination, indicating that the radial overprint is still dominating. Therefore, measurements were stopped at this level.

The Brunhes/Matuyama boundary was found at a water depth of 114.8 mcd. The upper Jaramillo transition is located at a depth of 132.5 mcd; the lower Jaramillo, at 138.1 mcd. At 162.3 mcd, a change from reverse to normal declination and inclination could mark the start of the upper Olduvai Subchron (Fig. F14). Unfortunately, Core 184-1146C-17H suffered a horrible fate, and the last three sections had to be extruded from the core barrel. Therefore, interpretations from this core are tentative at best.

The switch to XCB for Core 184-1146C-18X and below along with the increasing strength of the overprint made identification of other geomagnetic chrons below this level impossible.

F14. Declination and inclination for Hole 1146C (APC cores), p. 52.

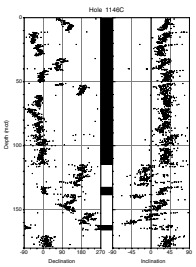

SEDIMENTATION AND ACCUMULATION RATES

The chronostratigraphy of Site 1146 is derived from a combination of calcareous nannofossil and planktonic foraminiferal events and paleo-

magnetic polarity stratigraphy. The Neogene section at Site 1146 yielded 32 calcareous nannofossil events, 27 planktonic and one benthic foraminiferal events, and three paleomagnetic datums (see "Biostratigraphy," p. 10, and "Paleomagnetism," p. 12).

Figure F15 (also given as Synergy Software KaleidaGraph plots and Microsoft Excel data files [see the "Supplementary Materials" contents list]) shows the linear sedimentation rate and mass accumulation rate curves based on calculations described in "Sedimentation and Accumulation Rates," p. 13, in the "Explanatory Notes" chapter. The sedimentation rates generally decrease downhole from a maximum of 350 m/m.y. over the uppermost 20 mcd to a minimum of ~30 m/m.y. in the lower Miocene (587–643 mcd) (Fig. F15; Table T11). Sedimentation rates in the Pleistocene average ~110 m/m.y.; in the Pliocene, ~38 m/m.y.; and in the Miocene, ~27 m/m.y. When converted to mass accumulation rates and partitioned into carbonate and noncarbonate components, extremely high total accumulation rates (>19 g/cm²/k.y.) are observed over the past 0.26 Ma (Fig. F15). Accumulation rates over the entire Pleistocene average 9.5 g/cm²/k.y., with noncarbonate components dominant. Pliocene and Miocene total accumulation rates are relatively constant and average 7 and 4 g/cm²/k.y., respectively; carbonate accounts for about half of the accumulation. An increase in rates occurs near the early/middle Miocene boundary at ~17 Ma. The carbonate accumulation rates at Site 1146 are high for a midslope basin, which should accumulate mostly terrigenous sediments. The reasonably high sedimentation and carbonate accumulation make Site 1146 an excellent record for the identification of orbital-scale variability well into the Miocene.

F15. Age-depth model, LSR, and MAR, p. 53.

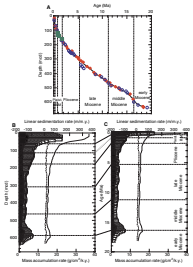

T11. Sedimentation and accumulation rates for selected intervals, p. 89.

ORGANIC GEOCHEMISTRY

Overview

The concentration of methane (headspace analysis) in sediments from Hole 1146A increased downhole from <10 ppmv at the top to a maximum of 85,000 ppmv at 599 mcd. Ethane (C_2H_6) and propane (C_3H_8) initially appeared at 536 mcd and peaked at 608 mcd with concentrations of 155 and 7 ppmv, respectively. The C_1/C_2 ratio reached a minimum of 345 at the bottom of the hole. A similar distribution was detected in the lower 100 m of Hole 1146C. Carbonate concentrations varied from <10 to >60 wt%, with the highest values in a distinct lithologic unit below 225 mcd. Total organic carbon (TOC) obtained by difference (total carbon [TC] – inorganic carbon [IC]) decreases systematically from 1 wt% at the top of Hole 1146A to trace abundance (<0.2 wt%) below 225 mcd, with occasional exceptions coincident with low carbonate. All sediments exhibit low C/N values, suggesting a marine organic source. However, organic C and total N are very low, and the C/N ratio is only reliable for a limited number of samples that yield higher C concentrations in the top 100 m of the hole.

Hydrocarbon (HC) Gases

Headspace gas analysis was performed on every core taken from Hole 1146A and on the bottom 100 m of Hole 1146C. Sampling and analysis were conducted as described in "Organic Geochemistry," p. 14, in the "Explanatory Notes" chapter. Methane concentrations are low (<10

ppmv) above 110 mcd and relatively constant (<30 ppmv) between 110 and 231 mcd in Hole 1146A. Below this depth, concentrations rise sharply, reaching 1000 ppmv by 303 mcd, 10,000 ppmv by 415 mcd, and a maximum of 85,000 ppmv at 599 mcd (Table **T12;** Fig. **F16A**). Ethane (C_2H_6) was first detected at 536 mcd and peaked (155 ppmv) at 608 mcd. Propane (C_3H_8) was first detected at 568 mcd and peaked (7 ppmv) between 608 and 619 mcd. The C_1/C_2 ratio rapidly decreased from 2460 at 536 mcd to 345 at the bottom of the hole (Fig. **F16B**). No alkenes or higher (than C_3) hydrocarbons were detected. A very similar pattern was observed in Hole 1146C.

Dissolved sulfate in interstitial waters was essentially zero (<0.5 mM) by 65 mcd (see **"Inorganic Geochemistry,"** p. 17). A constant but low level of methane (10–30 ppmv) along with relatively low TOC (0.2–1.0 wt%) (Fig. **F17B**) was detected between this depth and the lithologic change at 225 mcd. This suggests predominantly microbial generation of methane in this upper unit. Dissolved NH_4^+, a product of both sulfate reduction and methanogenesis, is present below the zone of sulfate reduction (0–68 mcd) to ~225 mcd (see **"Inorganic Geochemistry,"** p. 17).

Sediment methane concentrations begin to increase substantially below 231 mcd. Because TOC decreases downhole and is <0.2 wt% (with a few exceptions) below ~210 mcd, this methane cannot be produced from an increased amount of organic matter (OM) for methanogens (see **"Organic Matter Characterization,"** p. 16). Further, the presence of ethane (below 500 mcd) and propane (568 mcd), as well as the decreasing C_1/C_2 ratio, suggest the presence of thermogenic hydrocarbons. These increased HC concentrations also coincide with a significant decrease in chloride ions in interstitial water at 568 mcd (see **"Inorganic Geochemistry,"** p. 17). However, from the lack of evidence of thermal maturity from thermal gradient measurements and Rock-Eval pyrolysis (see **"Organic Matter Characterization,"** p. 16), it appears that these HC gases are migrated from either a deeper or a lateral source. Seismic survey profiles indicate a possible basement high ~2 km north-northwest and two prominent faults at a similar distance. A marked seismic reflector, T_4 (see **"Background and Objectives,"** p. 1), exists near the depth of maximum HC abundance. Physical properties measurements (see **"Physical Properties,"** p. 19) also indicate a lithologic change, which may be associated with a conduit for HC migration. If lateral instead of vertical migration is most significant, then the nearby fault scarp is a good source candidate. However, methane concentrations are persistently >25,000 ppmv to the bottom of Holes 1146A and 1146C, and the C_1/C_2 ratios appear to decrease with depth (Fig. **F16;** Table **T12**), indicating possible vertical HC migration.

T12. Methane, ethane, and propane concentrations, Holes 1146A and 1146C, **p. 90.**

F16. Methane, ethane, and propane concentrations and C_1/C_2 ratio vs. depth, Holes 1146A and 1146C, **p. 54.**

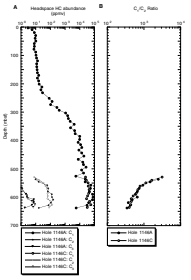

F17. Carbonate, TOC, and organic C/N ratio vs. depth, **p. 55.**

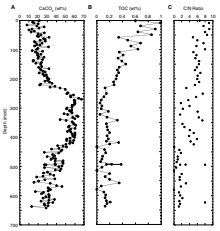

Inorganic Carbon

Sampling for carbonate analysis was conducted in three sections per core from Hole 1146A (Table **T13**). Carbonate varies from 7.9 to 68.1 wt%, with low but gradually increasing concentrations from 0 to 225 mcd (average [AV] = 22.2 wt%; standard deviation [SD] = 5.9). Carbonate undergoes a marked increase from 225 to 425 mcd from ~20 to generally >50 wt% (AV = 55.4 wt%; SD = 6.0). Carbonate abundance again decreases to ~20–40 wt% (AV = 34.4 wt%; SD = 9.1) below 425 mcd to the bottom (641 mcd [Fig. **F17A**]). The upper two zones of significantly

T13. IC, $CaCO_3$, TC, TOC, TN, and TS contents, **p. 92.**

different carbonate abundance approximate lithologic Units I and II (see "Lithostratigraphy," p. 5).

Organic Carbon

Total organic carbon concentration by difference (TC – IC) was determined for one sample per core (Table T13). The TOC decreases systematically from ~1.0 wt% at the top of Hole 1146A to 0.2 wt% at 220 mcd and remains below 0.2 wt% to the bottom of the hole, with a few notable exceptions (Fig. F17B). Samples 184-1146A-35X-3, 107–108 cm; 50X-3, 107–108 cm, and 56X-3, 107–108 cm, all correspond to intervals of higher TOC levels and may represent localized OM enrichment. Likely explanations include bioturbation, burrows, and the numerous dark bands observed in the lower cores from Hole 1146A (see "Lithostratigraphy," p. 5). On close inspection, the presence of green layers does not correlate with the high or anomalous TOC values. Rock-Eval measurement of eight samples from below 280 mcd that gave TOC (by difference) results >0.3 wt% produced no values above 0.1 wt% TOC (Table T14). This is consistent with lower values obtained by Rock-Eval analysis at previous sites.

T14. Rock-Eval pyrolysis results, p. 95.

Organic Matter Characterization

Our analytical methods only allow organic matter to be characterized where TOC exceeds 0.5 wt%. Most of the TOC values (by difference) for Hole 1146A are therefore too low to characterize sediments precisely. Ratios of TOC (by difference) to total nitrogen (C/N) (Table T13; Fig. F17C) range from ~5 to 9 in the upper 225 m of the hole, suggesting a dominance of marine organic material in these immature sediments. The C/N values below 225 mcd are not necessarily diagnostic of marine OM because the TOC concentration is low, and the N is probably associated with clay as NH_4^+ (see "Organic Geochemistry," p. 11, in the "Site 1145" chapter).

Rock-Eval results (Table T14) for samples from the upper 300 m of Hole 1146A show low T_{max} indicating immature OM, but a poorly defined S_2 peak may render this unreliable. Samples from the zone of high methane and higher HC give similarly low T_{max} values, suggesting thermally immature sediments. This supports the earlier conclusion that the abundant HCs are migrated. Known gas and oil reservoirs are hosted in lower Miocene formations of the nearby continental shelf in a stratigraphic unit that may exist only a few hundred meters below the bottom of Hole 1146A (Wang and Wong, 1998). Drilling at Site 1148 through the Miocene (see "Organic Geochemistry," p. 16, in the "Site 1148" chapter), however, has not revealed a substantial reservoir or source rocks. The source of the high values for methane and accompanying ethane and propane, therefore, awaits explanation from shore-based laboratory analysis.

Sulfur

Total sulfur was measured with the carbon-nitrogen-sulfur analyzer (see "Organic Geochemistry," p. 14, in the "Explanatory Notes" chapter). Sulfur is higher in the top 170 mcd of the core, varying between 0.1 and 0.5 wt% (except for three lower values [Table T13]). These are also the sediments with the highest TOC values, and this occurrence of

higher S and TOC together is expected (Berner, 1984). Because of the depositional environment and the presence of pyrite in the sediments (see "Lithostratigraphy," p. 5), we assume that the sulfur measured is pyrite. Below 170 mcd, sulfur is <0.1%.

Examination of the S data (Table T13) reveals discrepancies with the abundance of observed sulfides (see "Lithostratigraphy," p. 5). Observed "iron sulfide" that is disseminated in millimeter- to centimeter-sized areas (but is amorphous or microcrystalline) is greatest from 110 to 210 mcd, from 275 to 360 mcd, and in the lowermost 30 m. Pyrite as centimeter-sized crystal masses filling burrows is reported mainly between 425 and 530 mcd and also in the bottom 30 m. Although not quantitative, these lithology descriptions seem at odds with the measured S contents. This can be explained by two factors. First, pyrite concretions are rare and almost never found in the discrete 2-cm carbonate (CARB) sample that is taken for S analysis. Second, the finely disseminated S is too small to be recognized by the unaided eye or hand lens in the dark brown-gray matrix encountered in the top 170 mcd of the core, where our measured S abundance is greatest.

INORGANIC GEOCHEMISTRY

Inorganic chemical analyses were conducted on 27 interstitial water samples from Hole 1146A squeezed from whole-round samples at a frequency of one per core in the first nine cores and one every third core thereafter. Analytical methods are detailed in "Inorganic Geochemistry," p. 17, in the "Explanatory Notes" chapter. The concentrations of dissolved interstitial constituents are presented in Table T15, and the profiles with depth are shown in Figure F18. Interstitial water profiles at Site 1146 are characteristic of sediments in which sulfate reduction, alteration of volcanic material, and dissolution-recrystallization of biogenic minerals are the primary reactions controlling the concentrations of dissolved constituents.

T15. Interstitial water composition, p. 96.

F18. Interstitial water measurements, p. 56.

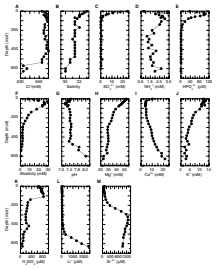

Chloride and Salinity

Chloride (Cl^-) concentrations in interstitial waters at Site 1146 are relatively constant above 550 mcd, ranging from 555 to 560 mM (Fig. F18A; Table T15). Below 550 mcd, Cl^- begins to decrease to values <540 mM by 569 mcd. Interstitial water salinities decrease from 34.5 to 32 between 3 and 109 mcd, are relatively constant (~32) between 109 and 476 mcd, and then decrease from 32 to 30 between 476 mcd and the base of the hole (Fig. F18B; Table T15). The decrease in salinity from the top of the core down to 109 mcd is most likely related to the removal of dissolved sulfate from interstitial waters during sulfate reduction. The decreases in Cl^- and salinity below ~476 mcd correspond to a large increase in methane concentration, the appearance of ethane and propane in headspace gas samples (see "Organic Geochemistry," p. 14, and "Background and Objectives," p. 1), a change in sediment color (see "Lithostratigraphy," p. 5), and a major decrease in magnetic susceptibility (see "Physical Properties," p. 19). A series of seismic reflectors at a depth of ~530 mcd (see discussion, "Site 1146 [SCS-4]," p. 7, in the "Seismic Stratigraphy" chapter; "Organic Geochemistry," p. 14), may correspond to the changes in lithology observed at this depth. One possible explanation for these changes is dissociating gas hydrates, which would dilute pore waters and elevate methane levels. At present,

little direct evidence exists for gas hydrates at this site beyond the low chlorinity/salinity and the hydrocarbons, no gas hydrates were observed upon core recovery, no disturbance was observed in the split core (see "Lithostratigraphy," p. 5), and other interstitial water signals are not diluted (Fig. F18; Table T15), although this last change would be small (~4% dilution). A second possibility is that major changes in clay mineralogy occur at this depth, leading to the release of water and changes in some other dissolved constituents (see pH and lithium below). However, no major changes in clay mineralogy were observed at these depths in the shipboard X-ray diffraction data. Clay mineralogy also would not explain the changes in the hydrocarbons, unless the two were linked through some parameter such as temperature. A third possibility is the migration of low-chlorinity water and hydrocarbons, either laterally or from depth. At present this seems the most viable theory. The depth of the events in the chlorinity and hydrocarbons correlates with seismic Reflector T_2 (see "Site 1146 [SCS-4]," p. 7, in the "Seismic Stratigraphy" chapter), which could be linked to a fault that can be seen extending to basement within 1 nmi of this site. Fluid and hydrocarbons could migrate laterally along this surface, and the changes in lithology could be diagenesis caused by conditions imposed by these fluids.

Sulfate, Ammonium, Phosphate, Alkalinity, and pH

Sulfate decreases from 24.1 mM near the surface to 0 mM by 68 mcd (Fig. F18C; Table T15) indicating that sulfate reduction is completed by this depth. Below the zone of sulfate reduction, methane levels begin to increase, indicating that methanogenesis takes over at this depth (see "Organic Geochemistry," p. 14). Ammonium (NH_4^+) increases to a maximum of 3.34 mM in the interval of sulfate reduction, decreases to a minimum of 1.14 mM at 262 mcd, and finally increases gradually downhole (Fig. F18D; Table T15). Dissolved phosphate (HPO_4^{2-}) concentrations increase to a maximum of 103.9 mM in the zone of sulfate reduction and then begin to decrease rapidly to reach near-zero values by 201 mcd (Fig. F18E; Table T15). Alkalinity increases to a maximum of 28.82 mM in the zone of sulfate reduction then decreases downhole to a minimum of 0.51 mM near the base (Fig. F18F; Table T15). The depletion of NH_4^+, HPO_4^2, and alkalinity—all products of methanogenesis—with depth supports the idea that methanogenesis is active only in the uppermost sediments and that increases in methane at depth are related to the migration of thermogenic hydrocarbons into the sediments. A pH minimum is centered at the depth of the maximum in NH_4^+, HPO_4^2, and alkalinity (Fig. F18G; Table T15). Below this level, pH is relatively constant down to 444 mcd, then increases to a maximum of 8.2 near the base of the hole.

Potassium, Magnesium, and Calcium

Magnesium (Mg^{2+}) concentrations decrease with depth from 51.7 mM at the top to a minimum of ~23.6 mM at the bottom of the hole (Fig. F18H; Table T15). Dissolved calcium concentrations (Ca^{2+}) decrease slightly in Cores 184-1146-1H through 4H in response to sulfate reduction (Fig. F18I; Table T15). Then Ca^{2+} increases slowly downhole to a maximum of 21.30 mM at 628 mcd. Dissolved potassium (K^+) concentrations decrease downhole from ~11.8 mM near the surface to 4.1

mM at 628 mcd (Fig. F18J; Table T15). The most likely cause of changes in the profiles of these three elements is uptake of Mg^{2+} and K^{+} and release of Ca^{2+} during the alteration of clay minerals and, to a secondary extent, alteration of basaltic volcanic ash, which is present in smaller quantities at this site than at other sites during this leg (see "Lithostratigraphy," p. 5).

Silica, Lithium, and Strontium

Dissolved silica (H_4SiO_4) concentrations are high, 744 ± 60 mM, in the upper part of the hole and then decrease sharply to <300 mM at 170 mcd (Fig. F18K; Table T15). This decrease corresponds to a major decrease in siliceous microfossils in the sediments (see "Sedimentation and Accumulation Rates," p. 13). Below this depth, H_4SiO_4 values decrease gradually downhole to a minimum of 71 mM at the base (Fig. F18K; Table T15). Lithium (Li^{+}) is very low, <60 mM down to 323 mcd, and then increases sharply, reaching a maximum of 2390 mM at the base of the hole (Fig. F18L; Table T15). This increase correlates with the increase in pH (Fig. F18G; Table T15). Given the correspondence of increasing Li^{+} with lowered Cl^{-} and increased hydrocarbons, the release of Li^{+} may be occurring because of alteration of clay minerals in response to changing environmental conditions in the sediments. This conclusion, however, is highly tentative and awaits shore-based investigation. Dissolved strontium concentrations (Sr^{2+}) are <150 mM above 109 mcd, then increase to a maximum of 1268 mM at 356 mcd and remain high to the base of the hole (Fig. F18M; Table T15). This increase in Sr^{2+} occurs in conjunction with an increase in the percent carbonate from 20 to 60 wt% in Hole 1146A (see "Organic Geochemistry," p. 14). Although Sr^{2+} concentrations increase downhole in carbonate sediments in response to calcite recrystallization (Baker, 1986), the simultaneous increase of Sr^{2+} and carbonate percentage at depth at Site 1146 suggests that large changes in carbonate content can also affect the extent of recrystallization.

PHYSICAL PROPERTIES

Sampling

At Site 1146, physical properties were measured on whole-round sections, split-core sections, and discrete samples from the latter. Whole-core logging with the MST included GRA bulk density, MS, NGR, and *P*-wave velocity logging on all cores. Sampling intervals were 5 cm for all cores in the three holes. The *P*-wave logger (PWL) data were bad because of instrument problems and/or cracks or voids in the sediment cores. The PWL data are not shown in this report but are available from the ODP JANUS database (see the "Related Leg Data" contents list). One thermal conductivity measurement per core was also performed on whole-round sections from Holes 1146A and 1146B as long as sediment conditions allowed. Color reflectance was measured on the archive halves of all split cores at 4-cm intervals. Moisture, density, and *P*-wave velocity were measured on discrete samples from split-core sections at intervals of one measurement per section (1.5 m) (see "Physical Properties," p. 18, in the "Explanatory Notes" chapter).

Results

Similar to the previous sites, one major feature affecting the core physical properties measurements is related to the change from APC to XCB coring (207.2 mcd in Hole 1146A, 216.30 mcd in Hole 1146B, and 170.5 mcd in Hole 1146C). The XCB cores are moderately disturbed by partial remolding and incorporation of drilling slurry, and the reduced diameter of these cores is probably the main component of the pronounced offset of GRA and somewhat slighter offset in MS and NGR values at those depths (Figs. F19, F20, F21). This effect is not compensated for because there was no time to perform a careful correction on board ship.

The other primary features in the physical properties data can be ascribed to changes in sediment composition. We can distinguish five major intervals, which are represented by clear changes in the physical properties of the sediment.

Interval 1, 0–110 mcd

The first interval shows constant or slightly increasing values in MS and NGR (Figs. F19, F20). The GRA, bulk density (Fig. F21), and *P*-wave values (Fig. F22) increase normally with depth, having a steeper slope in the top 25 mcd and a distinct depression between 25 and 35 mcd. The porosity reveals an inverse pattern in this interval, and grain density displays a large scatter (2.62–2.75 g/cm^3) (Fig. F23). This short feature in the first interval appears to be related to changes in the carbonate content (see "Organic Geochemistry," p. 14) and may result from glacial–interglacial cycles. The L* reflectance record (Fig. F24) and NGR (Fig. F20) also denote the slightly increasing trend, with superimposed high-amplitude variations showing patterns very similar to stable oxygen isotope records. Much lower amplitude variations, which appear to correlate with glacial–interglacial cycles, are also displayed by MS, which does not exhibit a general downhole trend. The chromaticity ratio a*/b* reflects neither the cycles nor a general trend (Fig. F24).

Interval 2, 110–235 mcd

The second interval is characterized by lower porosity and an increase in bulk density, MS, and NGR (Figs. F19, F20, F21, F23), indicating a major change in lithology and/or sedimentation rate. The most drastic increase is observed in the MS record, where values rise from ~20 (10^{-5} SI) above 110 mcd to >80 (10^{-5} SI) between 140 and 210 mcd. Several ash layers within this interval give high MS signals and can be found in all three holes. Both the carbonate content (see "Organic Geochemistry," p. 14) and the L* value (Fig. F24) stay almost constant until 235 m.

Interval 3, 235–420 mcd

The third interval is characterized by a dramatic increase in carbonate (see "Organic Geochemistry," p. 14) together with a strong decrease in NGR (Fig. F20) and a slighter decrease in MS signals (Fig. F19) (probably a carbonate dilution effect). Bulk density starts to increase slowly from a low around 230 mcd, with little variation in the discrete moisture and density (MAD) values. The GRA bulk density values are slightly lower on average and display a very prominent sawtooth pat-

F19. Magnetic susceptibility measurements, p. 57.

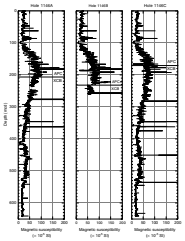

F20. Natural gamma radiation measurements, p. 58.

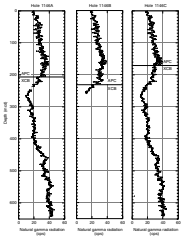

F21. Bulk density measurements from GRA and MAD methods, p. 59.

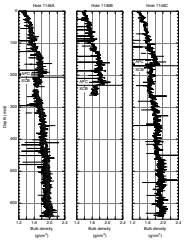

F22. *P*-wave velocity measurements for Hole 1146A, p. 60.

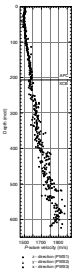

tern (Fig. F21). This is likely to be an artifact induced by stretching and compression during coring and recovery. The lower GRA values result from reduced core diameter through the XCB coring; no correction has yet been applied. At ~410 mcd in Hole 1146A and 435 mcd in Hole 1146C, the sawtooth pattern becomes less obvious, indicating that the sediment is less sensitive to the coring influences. Porosity is characterized by long-period (tens of meters) fluctuations superimposed on a generally decreasing downhole trend, as is typical for the entire drilled interval. Grain density in this third interval varies around 2.72 g/cm³, with some low values and stronger scattering in the lower part until ~400 mcd (Fig. F23). The values of *P*-wave velocity in this third interval increase steadily with some scattering because of the core conditions (Fig. F22). Negative excursions in the chromaticity ratio at 325, 355, and 418 mcd present in Holes 1146A and 1146C indicate compositional changes in the sediment that are not always visible as color changes (Fig. F24). The relatively high L* values still reflect a high carbonate content. The strong negative chromaticity excursion observed in Hole 1146A at 408–416 mcd is not found in Hole 1146C. These negative chromaticity excursions are accompanied by drastic drops in MS at the same depths, indicating short but major changes in lithology/chemistry in these intervals.

Interval 4, 420–550 mcd

The fourth interval is marked at 420 mcd with a pronounced downhole increase in NGR and MS (Figs. F19, F20), most likely the result of the lower carbonate content below that depth. The NGR values increase more or less steadily down to 550 mcd, with a small peak at ~460 mcd. As in the interval above, the MS record again drops to near zero in some short intervals that are accompanied by negative excursions in the chromaticity ratio. The L* reflectance record (Fig. F24) decreases very similarly to the carbonate content (see "Organic Geochemistry," p. 14; Fig. F17). The GRA and discrete bulk density increase without major excursions (Fig. F21); the GRA values still exhibit a sawtooth pattern but to a far lesser extent than in the third interval. *P*-wave values vary between 1700 and 1800 m/s with a very small downhole increase to 515 mcd, where a sharp increase in value up to 1920 m/s is observed (Fig. F22). Below 515 mcd down to 532 mcd, no *P*-wave velocities could be measured because the response signal was too low. From 532 to 550 mcd the velocity values were again received, but they dropped to a lower level around 1800 m/s. Porosity decreases normally; grain density stays constant within a narrow bandwidth at ~2.74 g/cm³ down to 505 mcd. Below this depth the grain density values are significantly more scattered, and overall values decrease to a low of 2.68 g/cm³ at 550 mcd (Fig. F23).

Interval 5, 550–642 mcd

The fifth interval is best documented in the chromaticity ratio a*/b*, which drops sharply between 540 and 550 mcd (Fig. F24). The change in sediment color is also observed visually (see "Lithostratigraphy," p. 5). The MS values also drop at this depth (Fig. F20), indicating that the drop in chromaticity may be accompanied by a change in mineralogy. Grain density increases from a low at 550 mcd to values around 2.74 g/cm³ and then stays fairly constant. *P*-wave velocities first increase to a high of ~580 mcd with values up to 1960 m/s, then decline.

F23. Porosity, grain density, and dry density, p. 61.

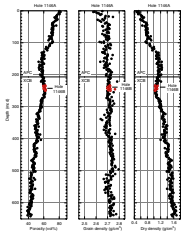

F24. Color reflectance measurements, p. 62.

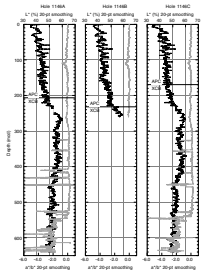

At 620 mcd, no measurements were possible because no signal could be received. We ascribe this to the high gas content prevalent in the lower part of the hole (see "Organic Geochemistry," p. 14). A similar archlike feature in the *P*-wave velocity record (Fig. F22) of the lowermost part of the hole was noted in the downhole logging data (see "Wireline Logging," p. 22).

Thermal Conductivity

Thermal conductivity data from the APC and XCB cores range from 0.85 to 1.30 W/(m·K) (Table T16, also in ASCII format; Fig. F25). The values from XCB cores are compromised by poor core quality, particularly in the upper XCB interval. The values from APC cores show a gradual downhole increasing trend. A slight increase at ~80 mcd is observed, which corresponds to a downhole rise in bulk density at that depth.

Downhole Temperature Gradient

Four downhole temperature measurements with the APC temperature tool were taken in Hole 1146A at depths of 32.4, 60.9, 98.9, and 150.0 mbsf, respectively. In addition, a bottom-water temperature measurement was taken before coring in Hole 1146B (Fig. F26). The objective was to establish the local heat flow. Original temperature records were analyzed using "Tfit" software to establish the equilibrium temperature at depth. Measurements at 32.4 mbsf seem problematic. The estimated errors in equilibrium temperature vary from 0.3° to 0.5°C, reflecting the amount of frictional heat introduced near the sensor by the ship's heave during the 10-min measurement. Depth errors are on the order of ±0.5 m. The measurements between 0 and 150 mbsf yielded a thermal gradient of 59°C/km (Fig. F27).

WIRELINE LOGGING

Logging Operations

After reaching the coring depth of 607 mbsf, Hole 1146A was filled with viscous mud, reamed, and flushed of debris. We first ran one full pass and a shorter repeat pass with the triple combo tool string, including the hostile environment natural gamma-ray sonde (HNGS), accelerator porosity sonde, hostile environment lithodensity sonde (HLDS), and dual-induction tool (DIT; resistivity) (Fig. F28). (See the "Related Leg Data" contents list.) The Lamont-Doherty temperature/acceleration/pressure tool was not run because it failed during Hole 1143A operation, and attempts to fix it were unsuccessful.

Next, we ran two full passes with the FMS, long-spaced sonic (LSS), and natural gamma-ray spectrometry tool (NGT) string (Fig. F28). Before this descent, the pipe was lowered to 242 mbsf, below an interval of swollen clays where the triple combo tool string had slight difficulty passing through. Finally, we ran three full passes with the GHMT string including the nuclear magnetic remanence sonde, susceptibility measurement sonde, and NGT (Fig. F28). The magnetic intensity recording failed in a prior run but was fixed before the two successful passes. The wireline heave compensator (WHC) performed well. Sea heave was between 0.5 and 1.5 m for the duration of the logging. Logging operations

T16. Thermal conductivity measurements, p. 97.

F25. Thermal conductivity measurements for Holes 1146A and 1146B, p. 63.

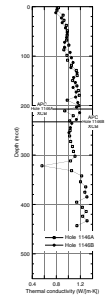

F26. Downhole temperature measurements, p. 64.

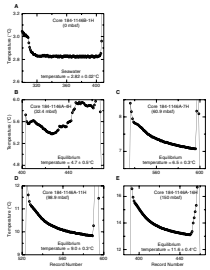

F27. Downhole temperature gradient, p. 65.

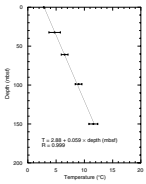

F28. Graphic summary of downhole logging operations for Hole 1146A, p. 66.

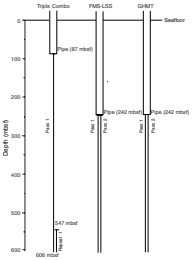

started at 1600 hr on 24 March and finished at 1235 hr on 25 March (Table T17).

T17. Summary of logging operations, p. 101.

Log Quality

All three tool strings reached within several meters of the bottom, indicating that little debris fell from the borehole wall. The two passes for the three tool string runs showed generally excellent repeatability for all the log parameters. The interval from 124 to 188 mbsf featured alternating large washouts and swollen clays. Above this depth and all the way up to 87 mbsf, the caliper saturated or nearly saturated. Below 250 mbsf, the hole was in good condition other than some fine rugosity (Fig. F29).

F29. Downhole logs of hole diameter from Hole 1146A, p. 67.

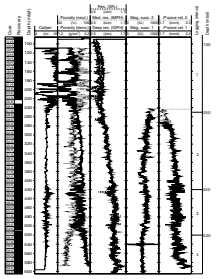

The HNGS data were poor in the upper interval, where caliper saturation resulted in a poor hole-size correction. The values of standard (total) gamma ray (HSGR) were consequently too low; elsewhere, the data were of good quality. The DIT was effective in the lower interval. However, in the poor-contact section of the hole, both the spherically focused log (SFL) and the medium induction phasor-processed resistivity (IMPH) read somewhat lower than the values from deep induction phasor-processed resistivity (IDPH), reflecting borehole influences (Fig. F29).

The FMS tool performed well. The first pass showed regular 0.25-m tool heave, as usual. Apparently the WHC did a better job compensating for sea heave during the second pass. The observed stick-slip of the tool string was on the order of 0.25 m. This effect on the data was corrected during the processing of the FMS images with the Geoframe software. The LSS log is of good quality for the entire hole. The two *P*-wave velocity measurements are almost completely superimposed (Fig. F29).

The magnetic intensity data recorded during the GHMT runs displayed the typical random spikes that were expected from this tool. Most of these spikes were on the order of 20 nT, but a few were hundreds of nT. In general, the spikes do not repeat between the two passes, so a good splice should be possible. These spikes were edited out in the data presented in this report.

In general, HSGR and computed gamma ray (HCGR) from the HNGS tool in the triple combo run read 10% to 25% higher than spectroscopy gamma ray or computed gamma ray from the NGT in the FMS-LSS run, a difference easily accounted for by eccentricity and hole-size correction. Contrary to the NGT, the HNGS corrects for borehole diameter and potassium in the borehole fluid, although the corrections near individual large washouts were apparently inadequate. The HNGS is more sensitive than the NGT; hence, its results are presented in Fig. F30 (column 1).

F30. Downhole logs of HSGR, HCGR, potassium, thorium, and uranium, p. 68.

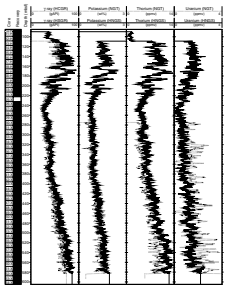

Results

The downhole logging and core-sample data together suggest that below the logging depth of 87 mbsf, Hole 1146A could be divided into four main intervals of distinct physical properties. The general dividing lines seem to be at ~250, ~420, and ~520 mbsf (Fig. F29).

Interval 1 (above 250 mbsf)

Above 250 mbsf the caliper frequently saturated, indicating severe hole washouts. Correspondingly, neutron porosity and bulk density

values from downhole logging are spiky, and the shallow resistivity (SFL) is less than the medium (IMPH) and deep (IDPH) resistivity (Fig. F29). Gamma ray (reflecting the combined effects of potassium, thorium, and uranium) and density values from both downhole and core logging all increase from 100 to 170 mbsf and then decrease from 170 to 250 mbsf (Figs. F30, F31). The porosity profiles either remain constant or increase slightly with depth from 170 to 240 mbsf, in contrast to the typical, compaction-related decrease with depth found in sections both above and below this interval (Fig. F32).

Interval 2 (250–420 mbsf)

Caliper measurements show that the hole condition in interval 2 is not only significantly better than that of interval 1 above but is also better than that of interval 3 below (Fig. F29). In this interval, several physical properties indicators increase with depth, including bulk density, electric resistivity, *P*-wave velocity, and gamma ray (Figs. F29, F30, F31, F32). Neutron porosity and magnetic susceptibility decrease with depth in this interval, although a change in the trend of magnetic susceptibility was observed at 385 mbsf (Fig. F29). The decrease in magnetic field with depth in this interval is likely to be caused by the influence of the drill pipe on the upper ~80 m of the log (Fig. F32).

Interval 3 (420–520 mbsf)

Caliper data show slight rugosity in interval 3 (Fig. F29). Apparently the rugosity was sufficient to cause moderate spikes in bulk density, *P*-wave velocity, and photoelectric effect (PEF) data from downhole logging (Figs. F29, F31, F32). Relatively low values of these parameters, as well as of magnetic susceptibility, were observed at 407, 426, and 499 mbsf, where the caliper reached local maxima. Within interval 4, bulk density, resistivity, *P*-wave velocity, and gamma ray all increase with depth, whereas porosity decreases slightly with depth (Figs. F29, F30, F31, F32). Magnetic susceptibility remains constant for most of interval 3 but decreases from 510 to 520 mbsf.

Interval 4 (520–606 mbsf)

This interval has an excellent hole condition as revealed by a smooth caliper curve (Fig. F29). Within this interval, several parameters increase with depth, including bulk density, *P*-wave velocity, and gamma ray (Figs. F29, F30, F31, F32). Magnetic susceptibility, PEF, and magnetic field remain nearly constant for the interval, whereas porosity decreases slightly with depth.

The trends in gamma ray from the NGT and HNGS tool strings agree well despite some constant offsets (Fig. F30). The trend in magnetic susceptibility from downhole logging is also in good agreement with that from MST measurements (Fig. F31). The trends of thorium and PEF agree above 200 and below 50 mbsf but are opposite between 200 and 520 mbsf (Fig. F31). $CaCO_3$ measurements of core samples and PEF from downhole logging show similar trends, especially above 200 mbsf and between 280 and 460 mbsf (Fig. F31). Natural gamma rays from downhole logging and MST measurements agree in their general trends as well (Fig. F32).

Bulk density from downhole logging agrees with that from both MAD measurements of core samples and core logging, although the

F31. MS from MST measurements of core logs vs. downhole measurements of thorium, p. 69.

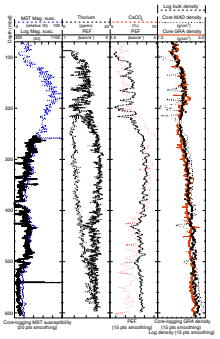

F32. Comparison of core MAD porosity, downhole log bulk density porosity, and NGR, p. 70.

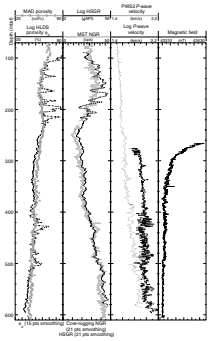

downhole logging data show considerably greater spikes above 220 mbsf and between 440 and 500 mbsf (most likely because of poor hole contact where washouts are severe [Fig. **F31**]). Porosity calculated from downhole bulk density is ~10%–15% less than that calculated from the moisture content of core samples in intervals 2 and 4. The logging porosity is very spiky in intervals 1 and 3, presumably also a result of poor hole condition (Fig. **F32**). Finally, *P*-wave velocity from core-sample measurements is ~0.3 km/s smaller than that from downhole logging at 280–420 mbsf. The discrepancy between these two types of measurement decreases gradually to 0.1 km/s at 580 mbsf (Fig. **F32**). The FMS data showed alternating layers of relatively high and low conductive layers (Fig. **F33**).

F33. FMS image from downhole logging data, **p. 71.**

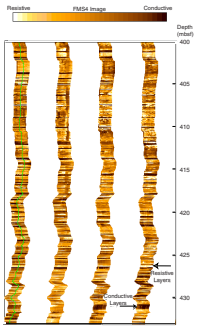

REFERENCES

Baker, P.A., 1986. Pore-water chemistry of carbonate-rich sediments, Lord Howe Rise, Southwest Pacific Ocean. *In* Kennett, J.P., von der Borch, C.C., et al., *Init. Repts. DSDP,* 90: Washington (U.S. Govt. Printing Office), 1249–1256.

Berner, R.A., 1984. Sedimentary pyrite formation: an update. *Geochim. Cosmochim. Acta,* 48:605–615.

Blow, W.H., 1969. Late middle Eocene to Recent planktonic foraminiferal biostratigraphy. *In* Brönnimann, P., and Renz, H.H. (Eds.), *Proc. First Int. Conf. Planktonic Microfossils, Geneva, 1967:* Leiden (E.J. Brill), 1:199–422.

Hess, S., 1998. Vereilungsmuster rezenter benthischer Foraminiferen im Südchinesischen Meer. *Ber. Rep., Geol. Palaeontol. Inst. Univ. Kiel,* 93.

Li, B., 1997. Paleoceanography of the Nansha Area, southern South China Sea since the last 700,000 years [Ph.D. dissert.]. Nanjing Inst. Geol. Paleontol., Academica Sinica, Nanjing, China. (in Chinese, with English abstract)

Okada, H., and Bukry, D., 1980. Supplementary modification and introduction of code numbers to the low-latitude coccolith biostratigraphic zonation (Bukry, 1973; 1975). *Mar. Micropaleontol.,* 5:321–325.

Schönfeld, J., 1996. The "*Stilostomella* Extinction": structure and dynamics of the last turnover in deep-sea benthic foraminiferal assemblages. *In* Mogurlevsky, A., and Whatly, R. (Eds.), *Microfossils and Oceanic Environments:* Aberystwyth (Univ. Wales, Aberystwyth Press), 27–37.

Shackleton, N.J., and Opdyke, N.D., 1976. Oxygen isotope and palaeomagnetic evidence for early Northern Hemisphere glaciation. *Nature,* 270:216–219.

Thompson, P.R., Bé, A.W.H., Duplessy, J.-C., and Shackleton, N.J., 1979. Disappearance of pink-pigmented *Globigerinoides ruber* at 120,000 yr BP in the Indian and Pacific oceans. *Nature,* 280:554–558.

Wang, P., Xia, L., Wang, L., and Cheng, X., 1991. Lower boundary of the marine Pleistocene in northern shelf of the South China Sea. *Acta Geol. Sinica,* 2:176–187.

Wang, P., and Wong, H.K., 1998. *ODP Leg 184 Safety Report:* Shanghai (Tongji Univ.).

Figure F1. Smoothed (11-point running average)/correlated MS data and the splice for the three holes at Site 1146 (spliced MS data for this figure are also available in **ASCII format**). The order of the four arrays (the splice and Holes 1146A through 1146C) increases outward from the origin. The hole arrays are offset from each other—and from the splice—by a constant (25.0×10^{-5} SI units) so that only the splice is plotted relative to the absolute MS value. Lines identify the splice tie points; those below 266 mcd are connecting "floating" tie points. (Continued on next three pages.)

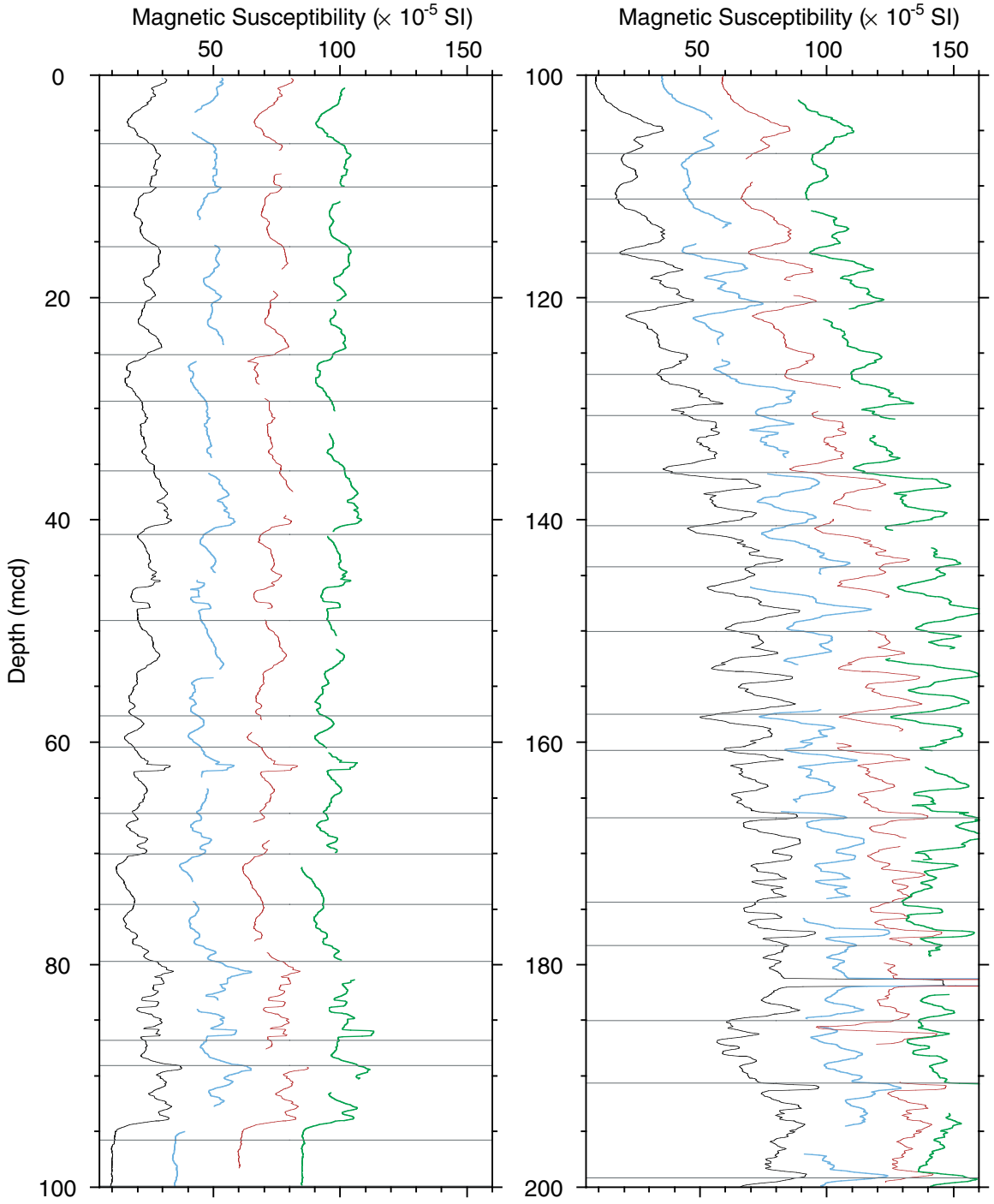

Figure F1 (continued).

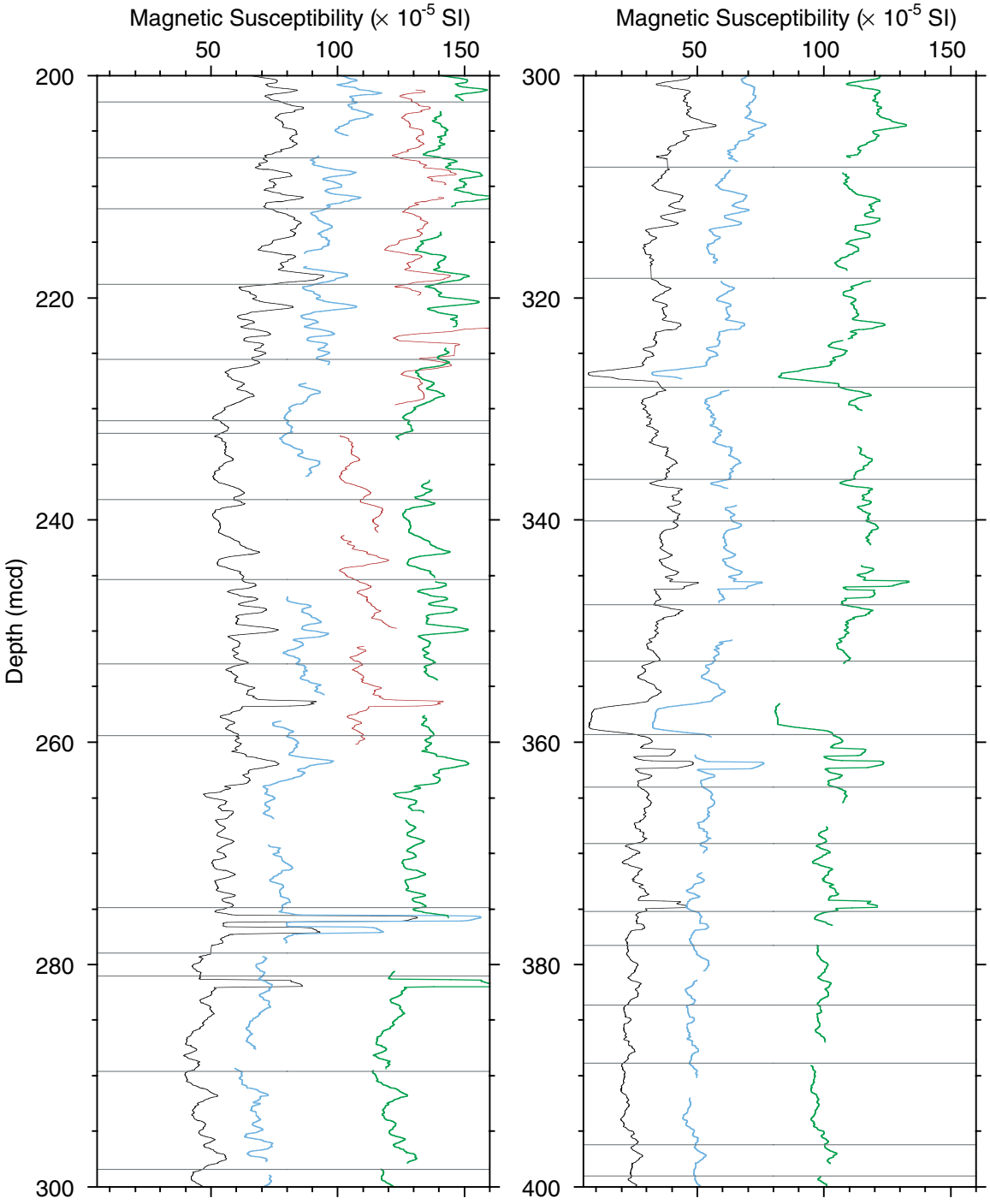

Figure F1 (continued).

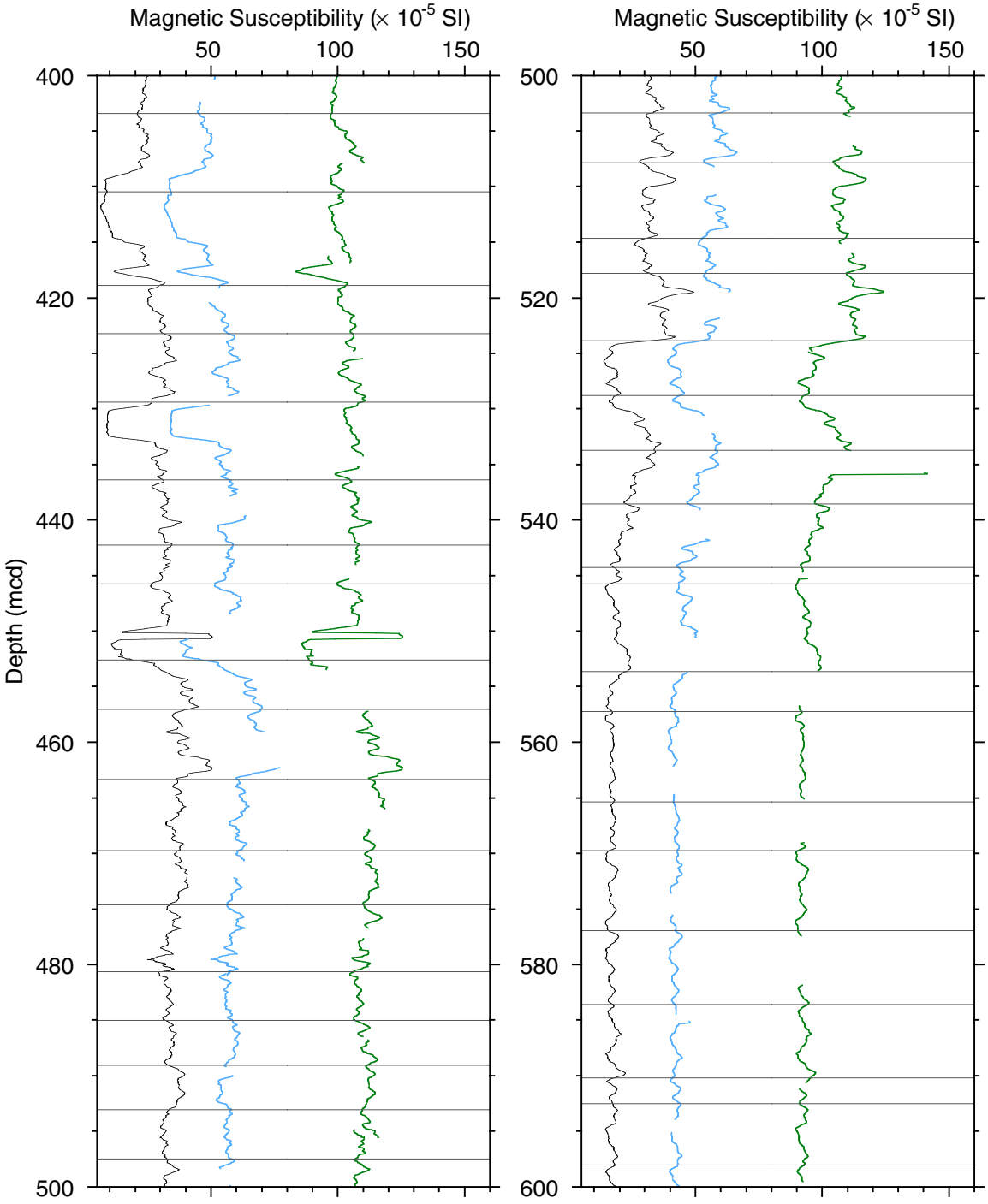

Figure F1 (continued).

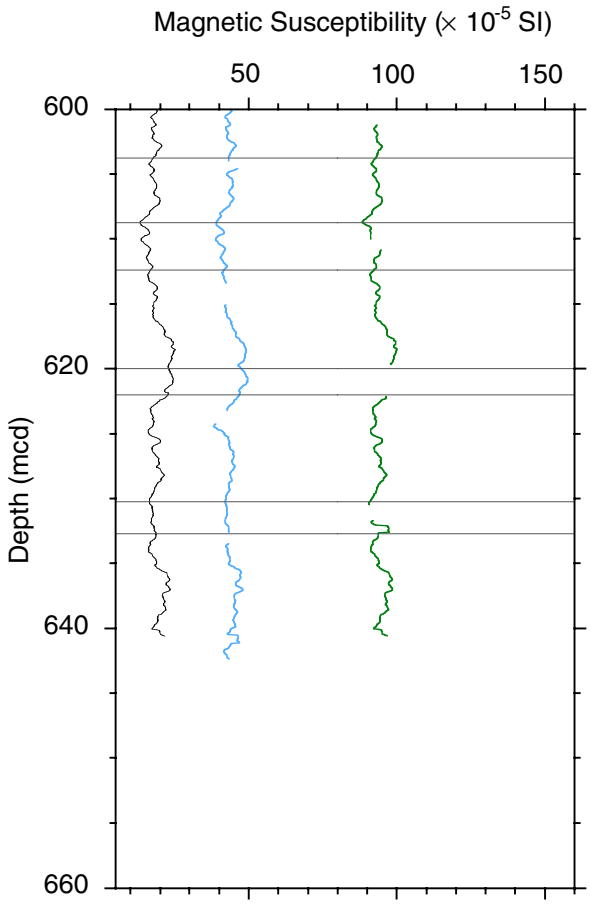

Figure F2. Smoothed (11-point running average)/correlated NGR data and the splice for the three holes at Site 1146 (spliced NGR data for this figure are also available in **ASCII format**). The order of the four arrays (the splice and Holes 1146A through 1146C) increases outward from the origin. The hole arrays are offset from each other—and from the splice—by a constant (9 cps) so that only the splice is plotted relative to the absolute NGR value. Data from the top and bottom 7 cm of the first and last section of each core have been culled. Lines identify the splice tie points; those below 266 mcd are connecting "floating" tie points. (Continued on next three pages.)

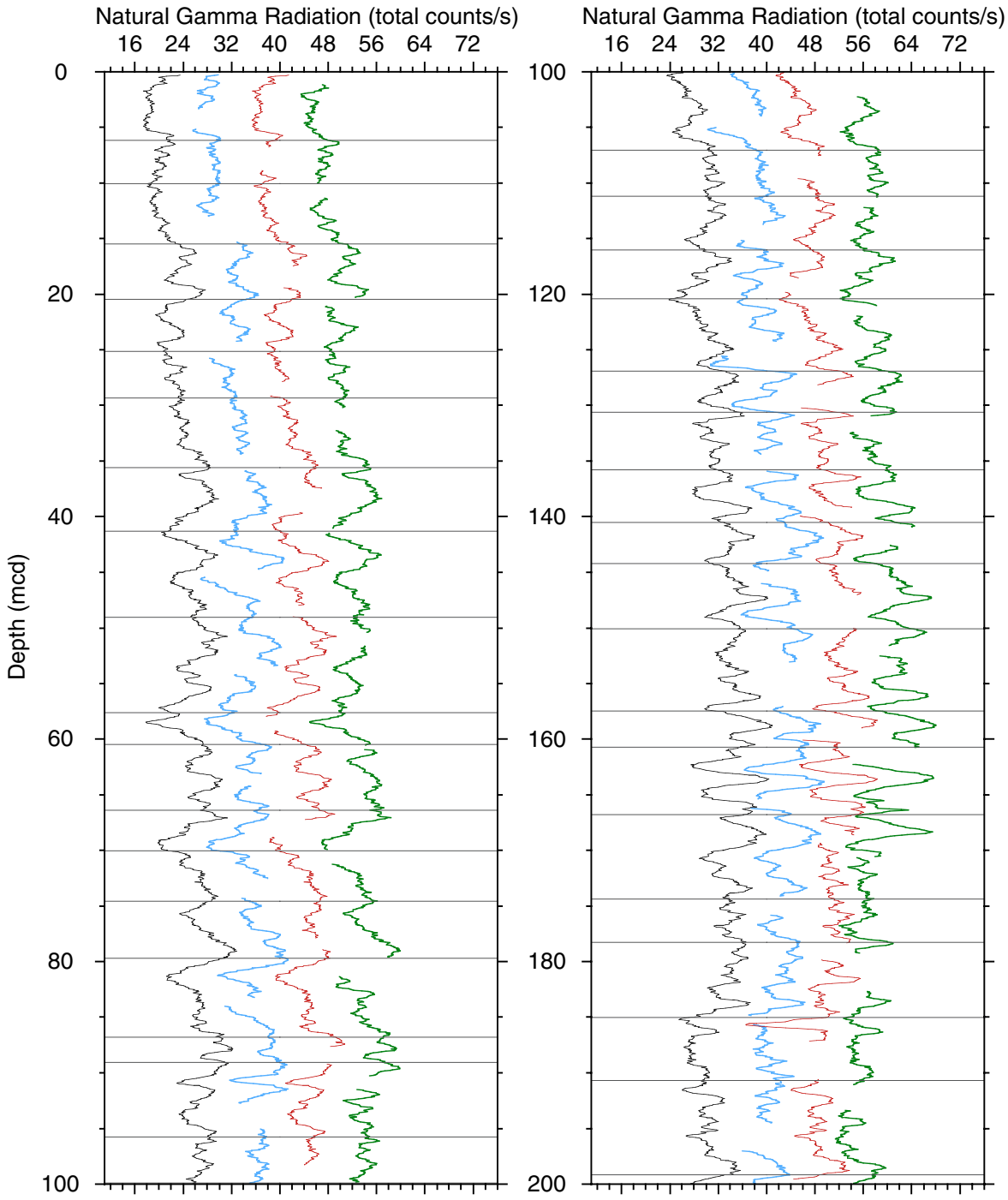

Figure F2 (continued).

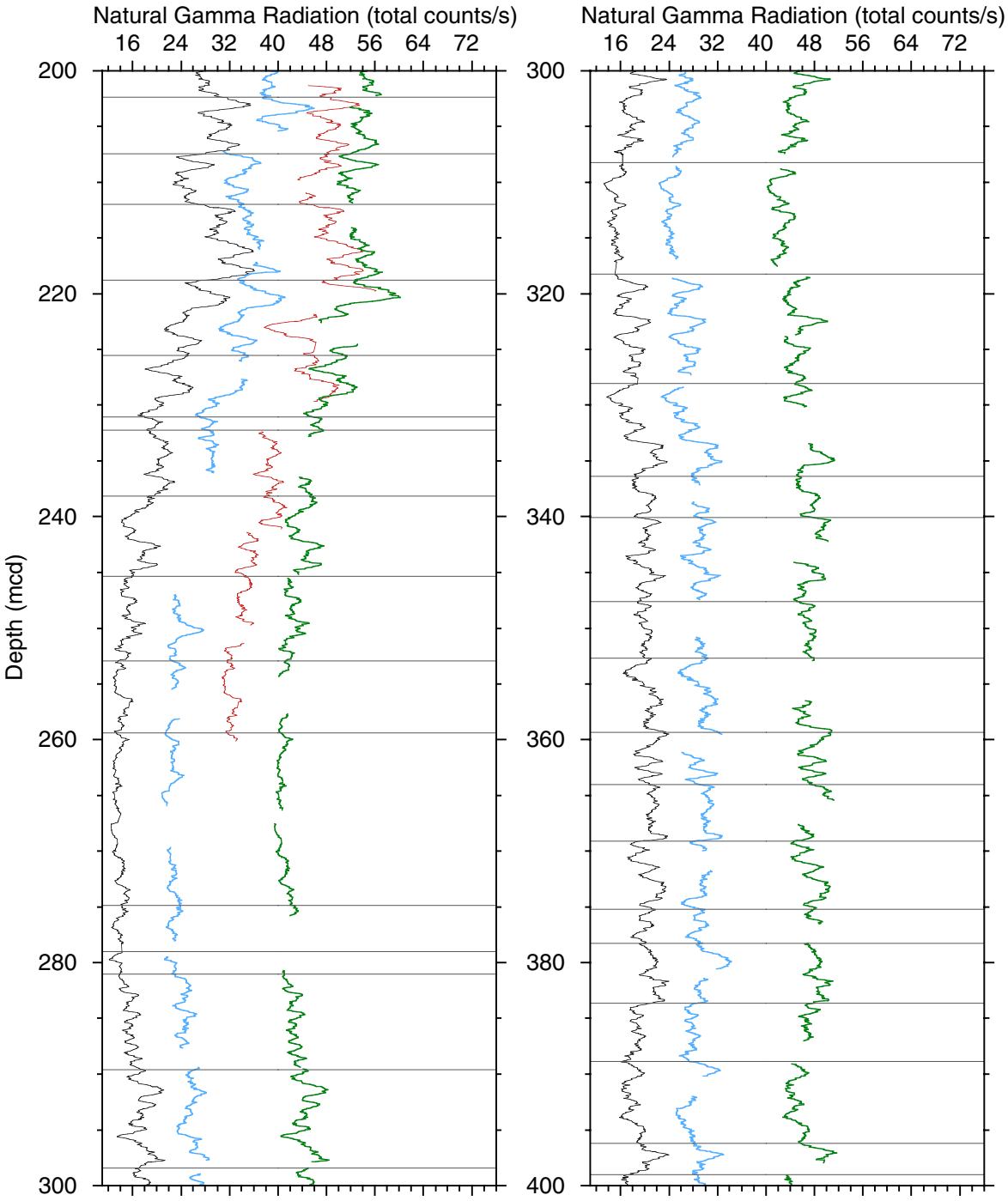

Figure F2 (continued).

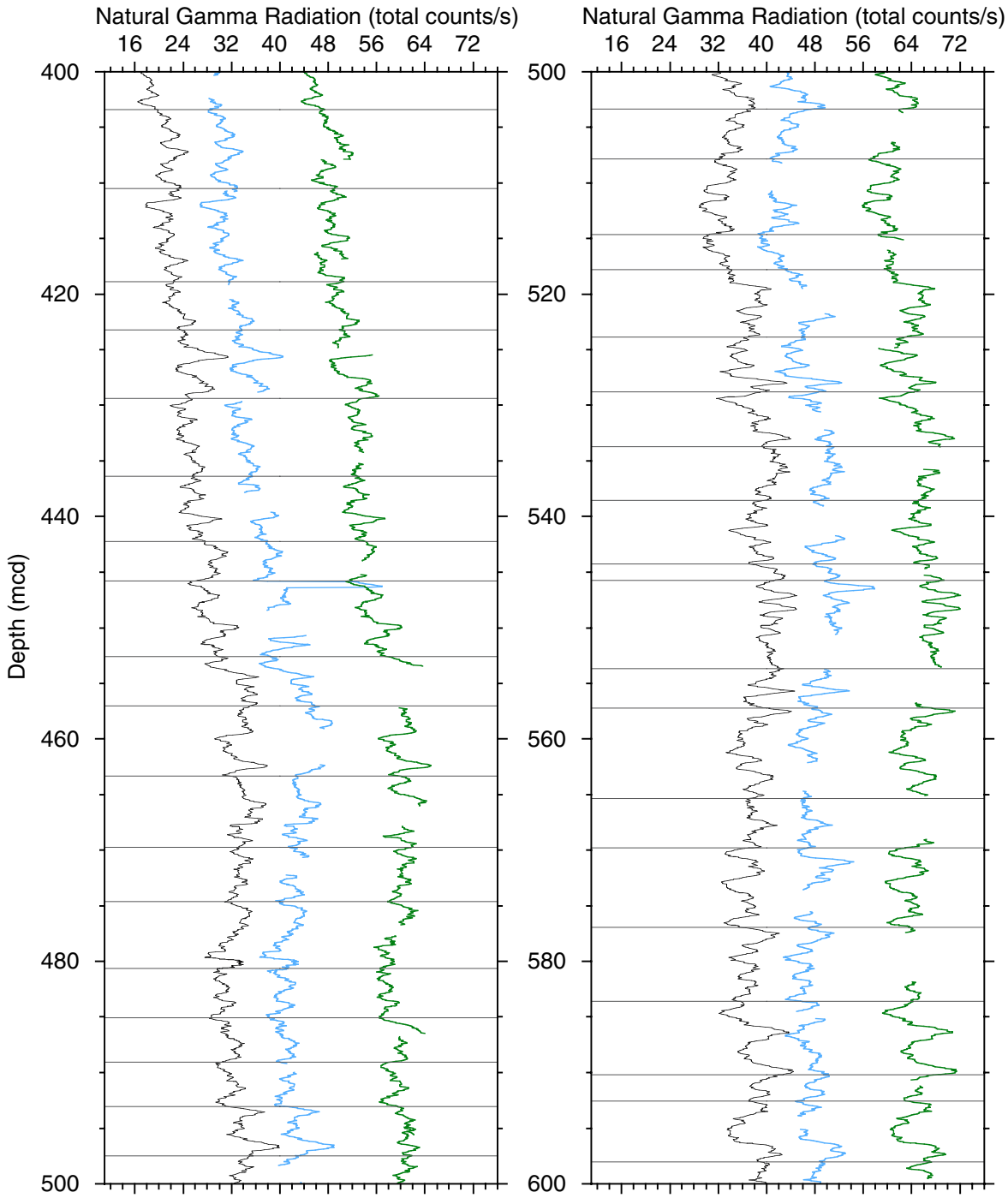

Figure F2 (continued).

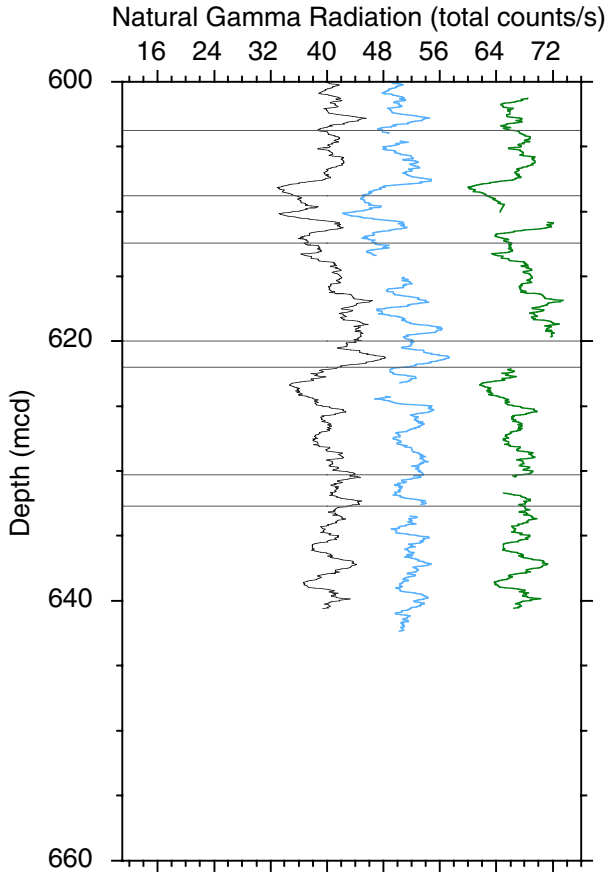

Figure F3. Smoothed (11-point running average)/correlated gamma-ray attenuation (GRA) data and the splice for the three holes at Site 1146 (spliced GRA data for this figure are also available in **ASCII format**). The order of the four arrays (the splice and Holes 1146A through 1146C) increases outward from the origin. The hole arrays are offset from each other—and from the splice—by a constant (0.15 g/cm³) so that only the splice is plotted relative to the absolute GRA value. Values ≤1.03 and ≥2.4 (g/cm³) have been culled. Lines identify the splice tie points; those below 266 mcd are connecting "floating" tie points. (Continued on next three pages.)

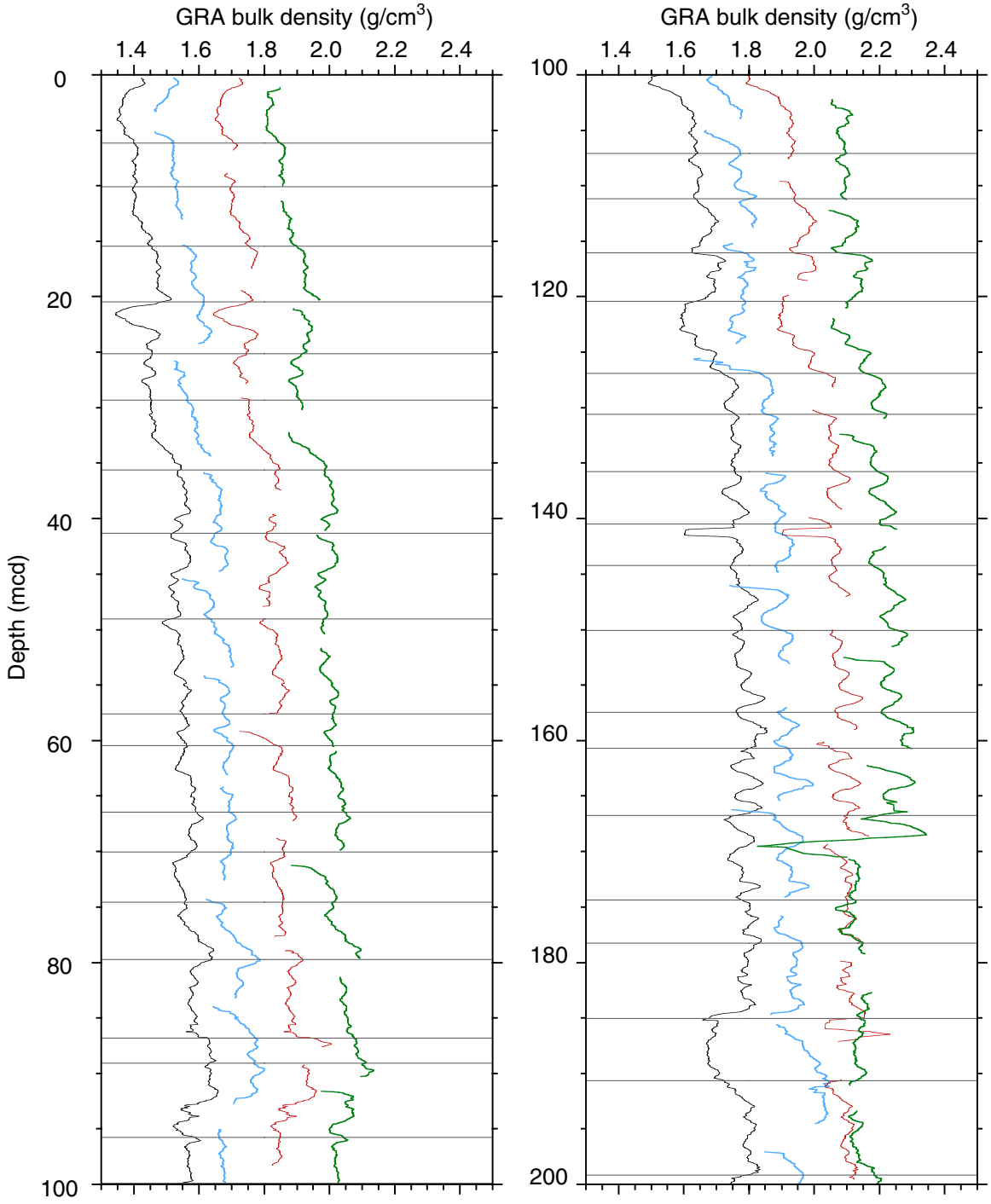

Figure F3 (continued).

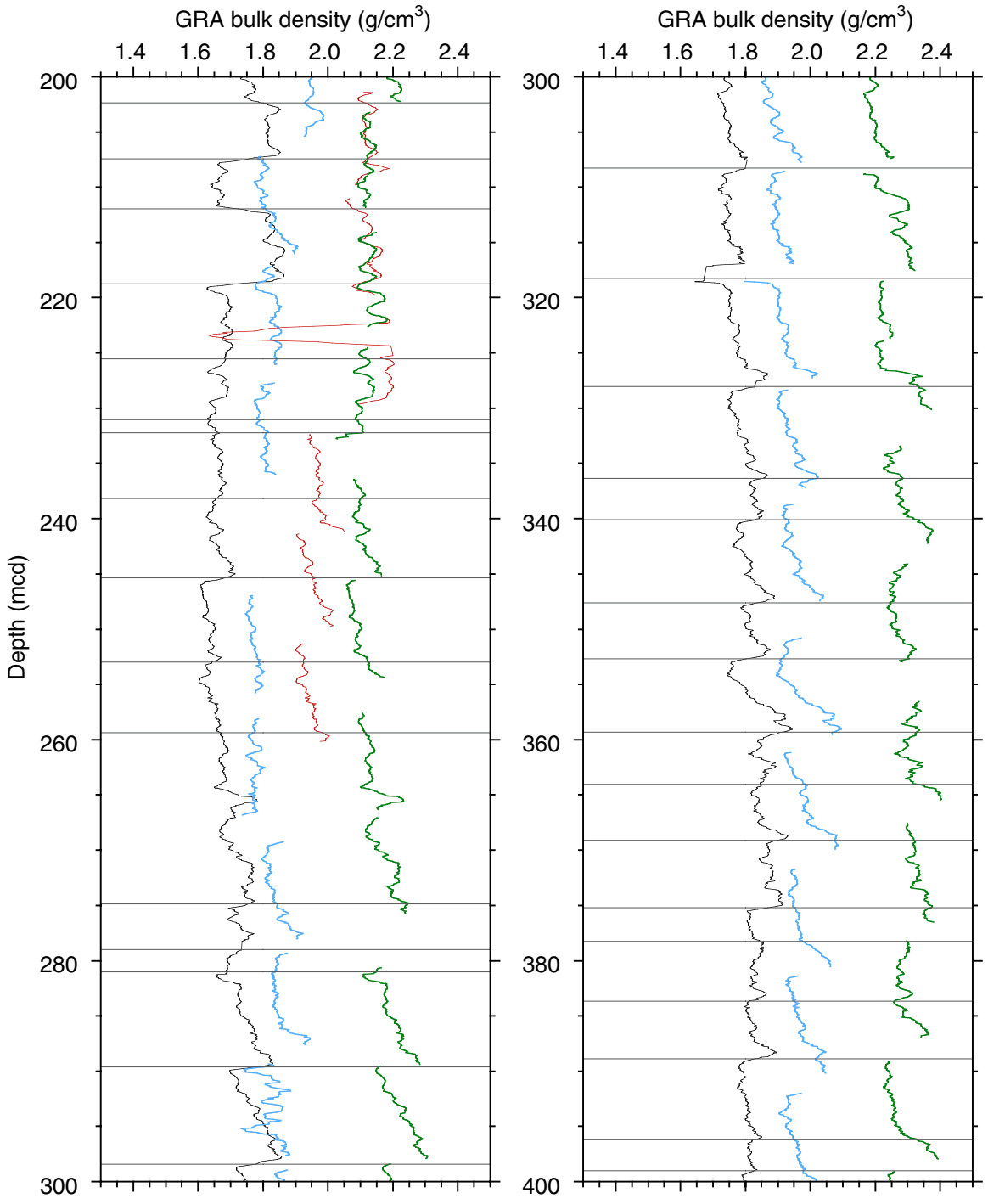

Figure F3 (continued).

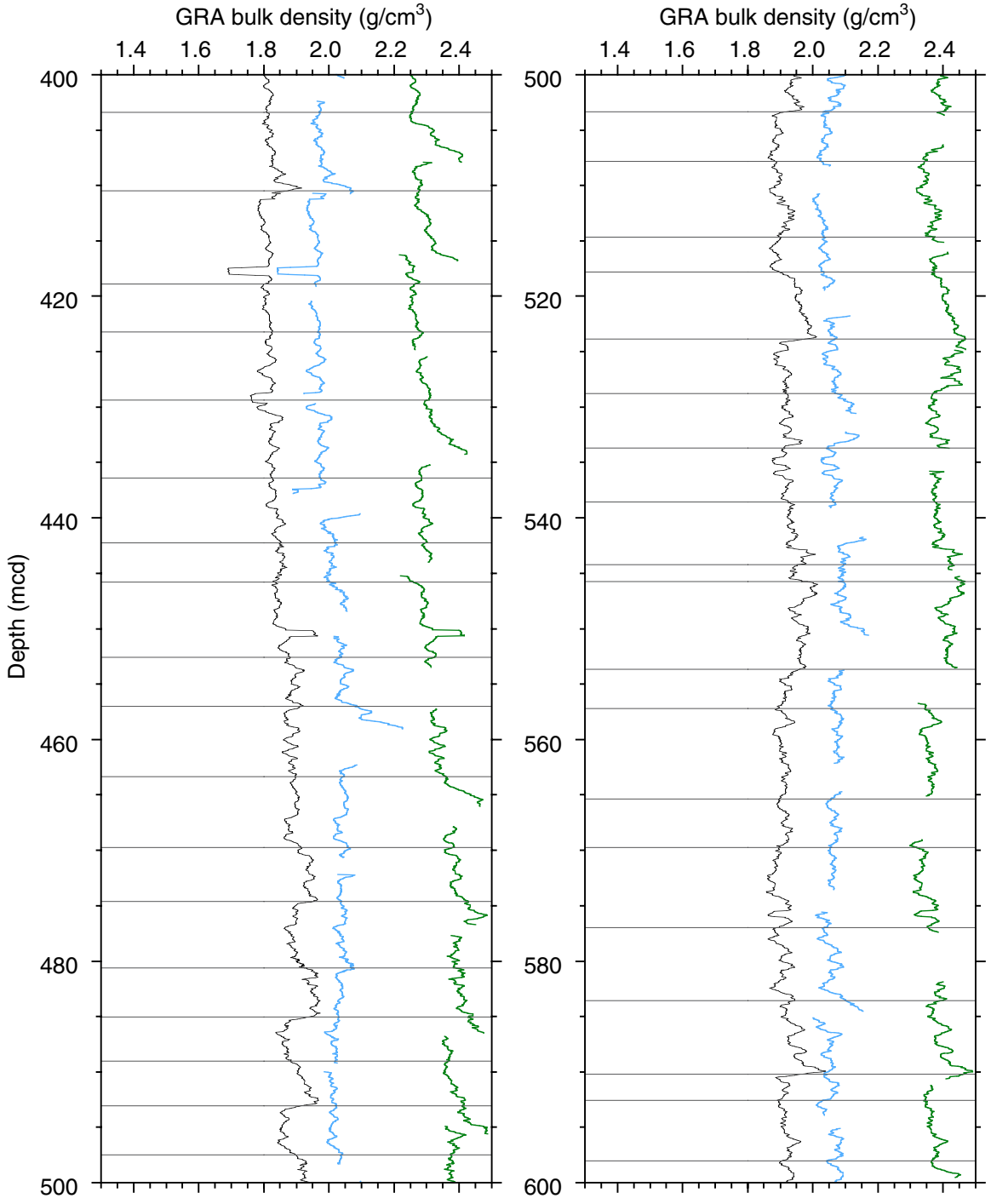

Figure F3 (continued).

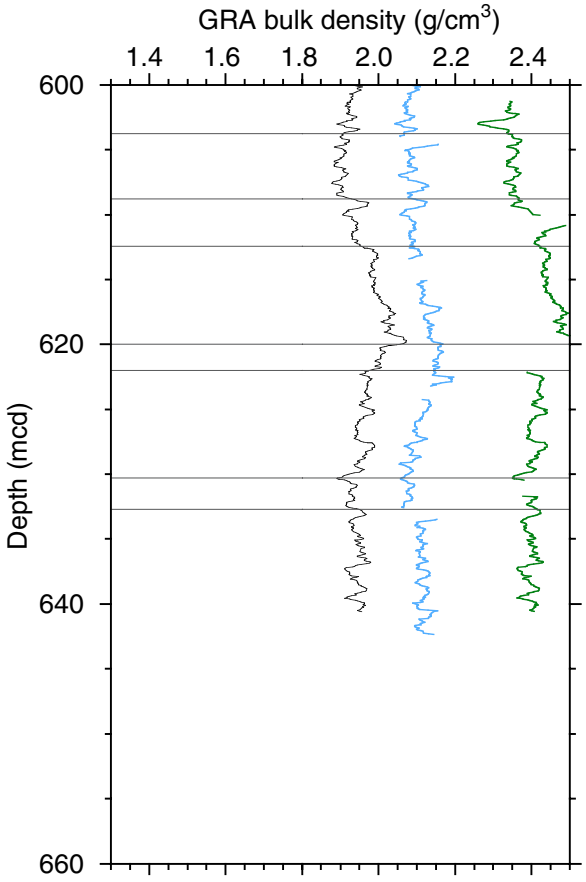

Figure F4. Smoothed (11-point running average)/correlated L* ("lightness") values from the CSR data and the splice for the three holes at Site 1146 (spliced CSR data for this figure are also available in **ASCII format**). The order of the four arrays (the splice and Holes 1146A through 1146C) increases outward from the origin. The hole arrays are offset from each other—and from the splice—by a constant (8%) so that only the splice is plotted relative to the absolute L* value. Values ≤1% have been culled. Lines identify the splice tie points; those below 266 mcd are connecting "floating" tie points. (Continued on next three pages.)

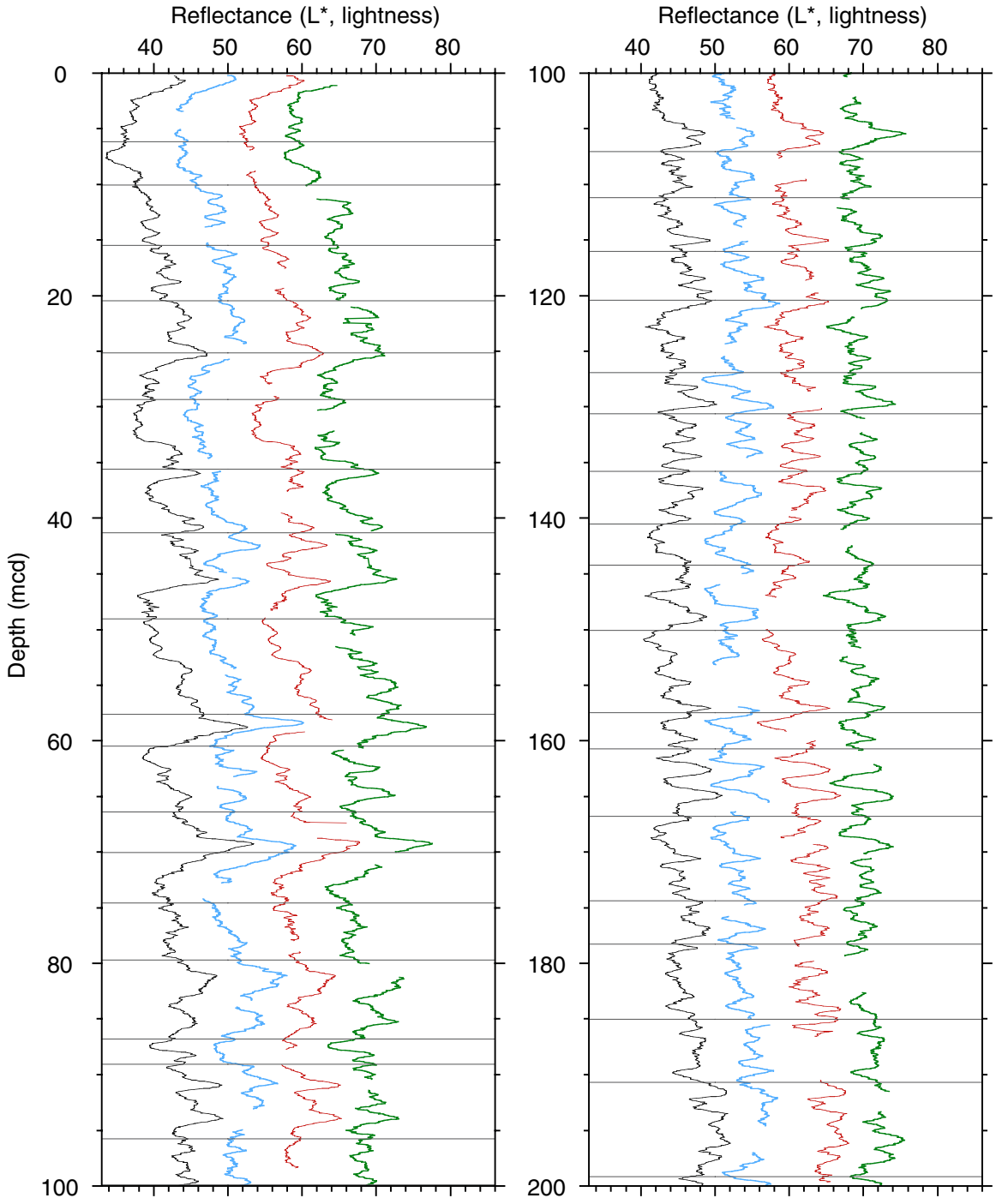

Figure F4 (continued).

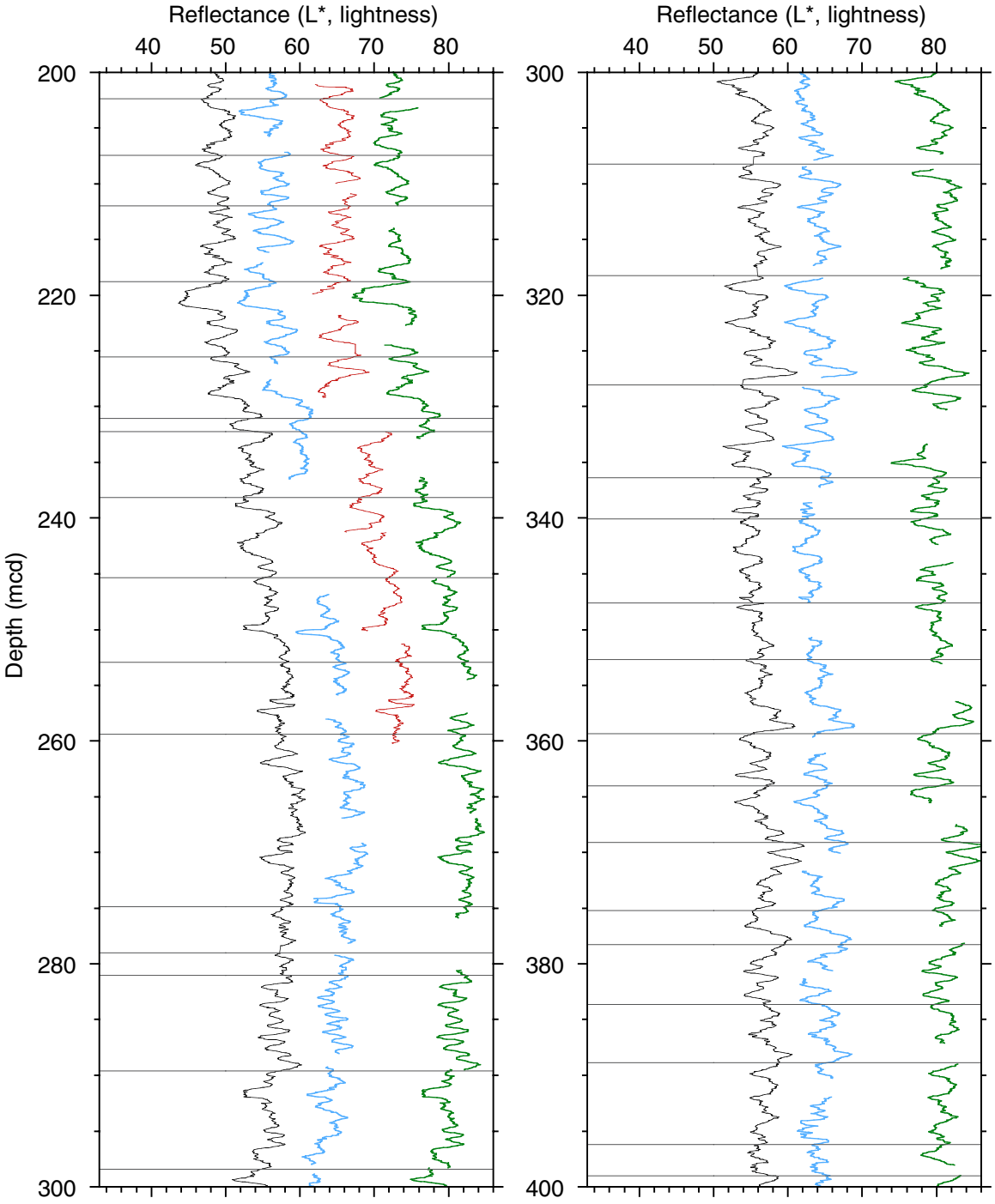

Figure F4 (continued).

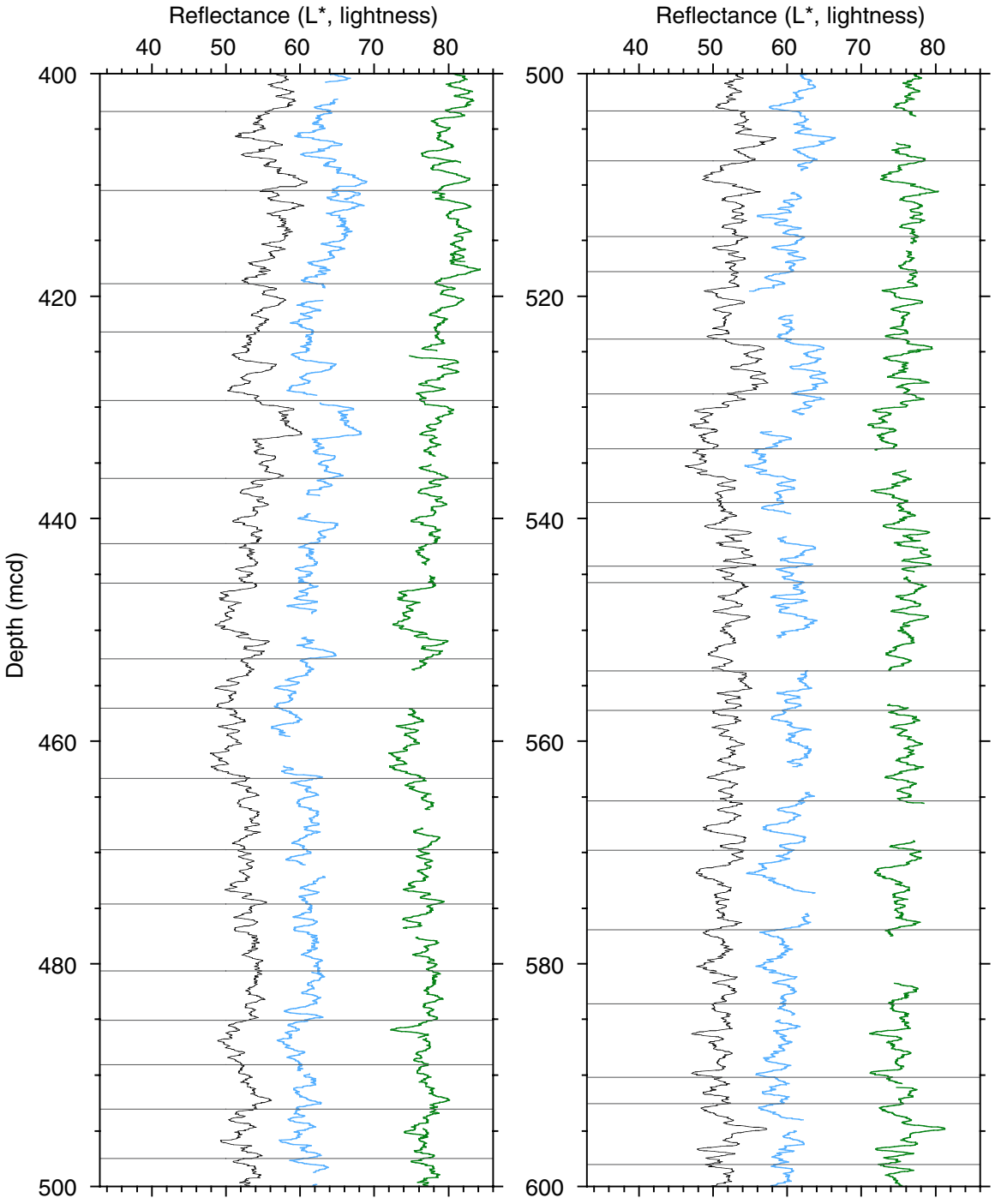

Figure F4 (continued).

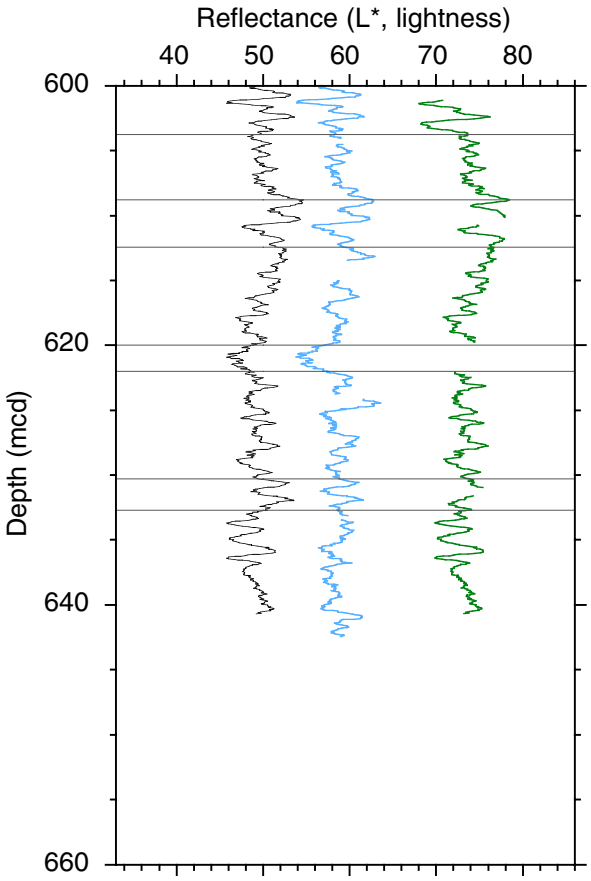

Figure F5. Summary of the recovered section at Site 1146, showing lithologic units, sediment types, lightness intensity (L* parameter), and the a* parameter. High positive values of a* correspond to high red intensity, whereas high negative values correspond to high green intensity.

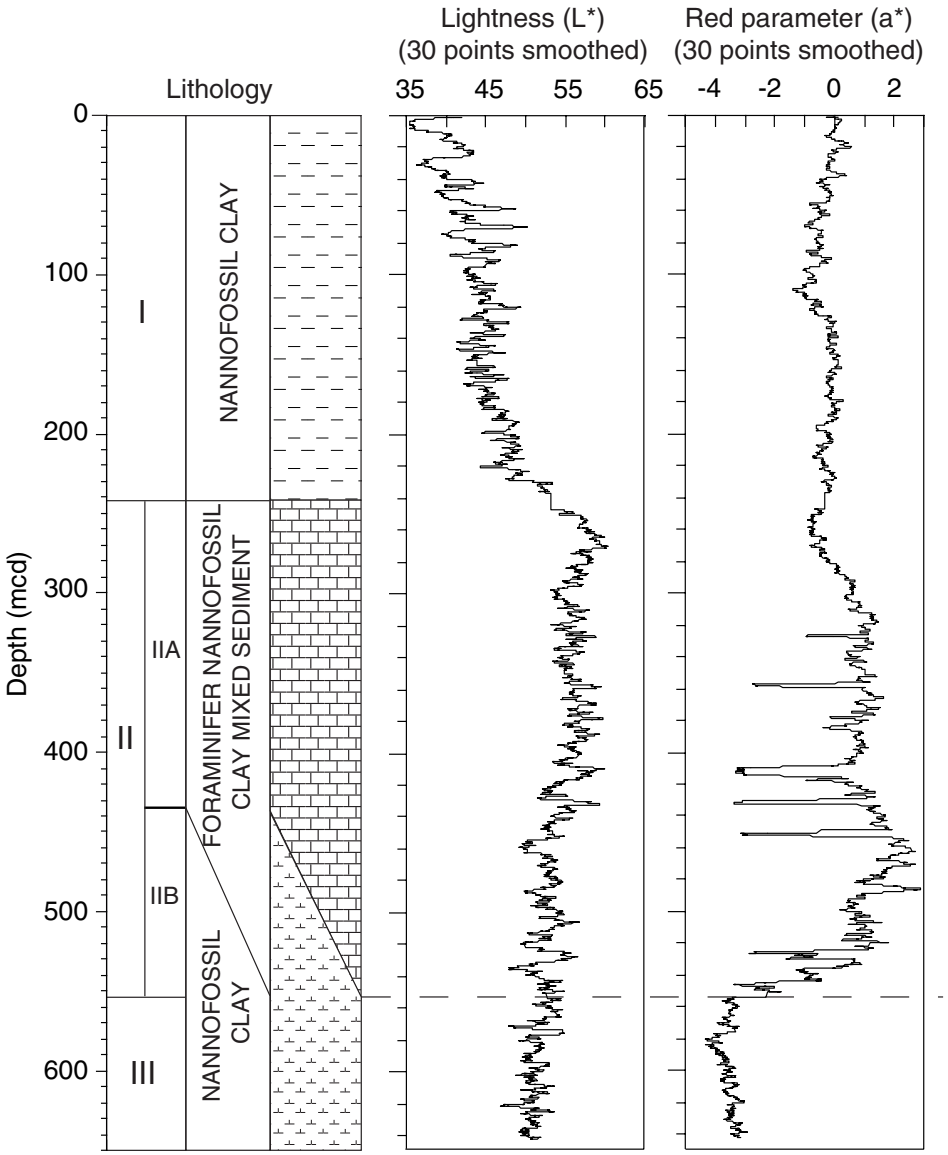

Figure F6. Bulk mineralogy as determined by X-ray diffraction of samples from Hole 1146A.

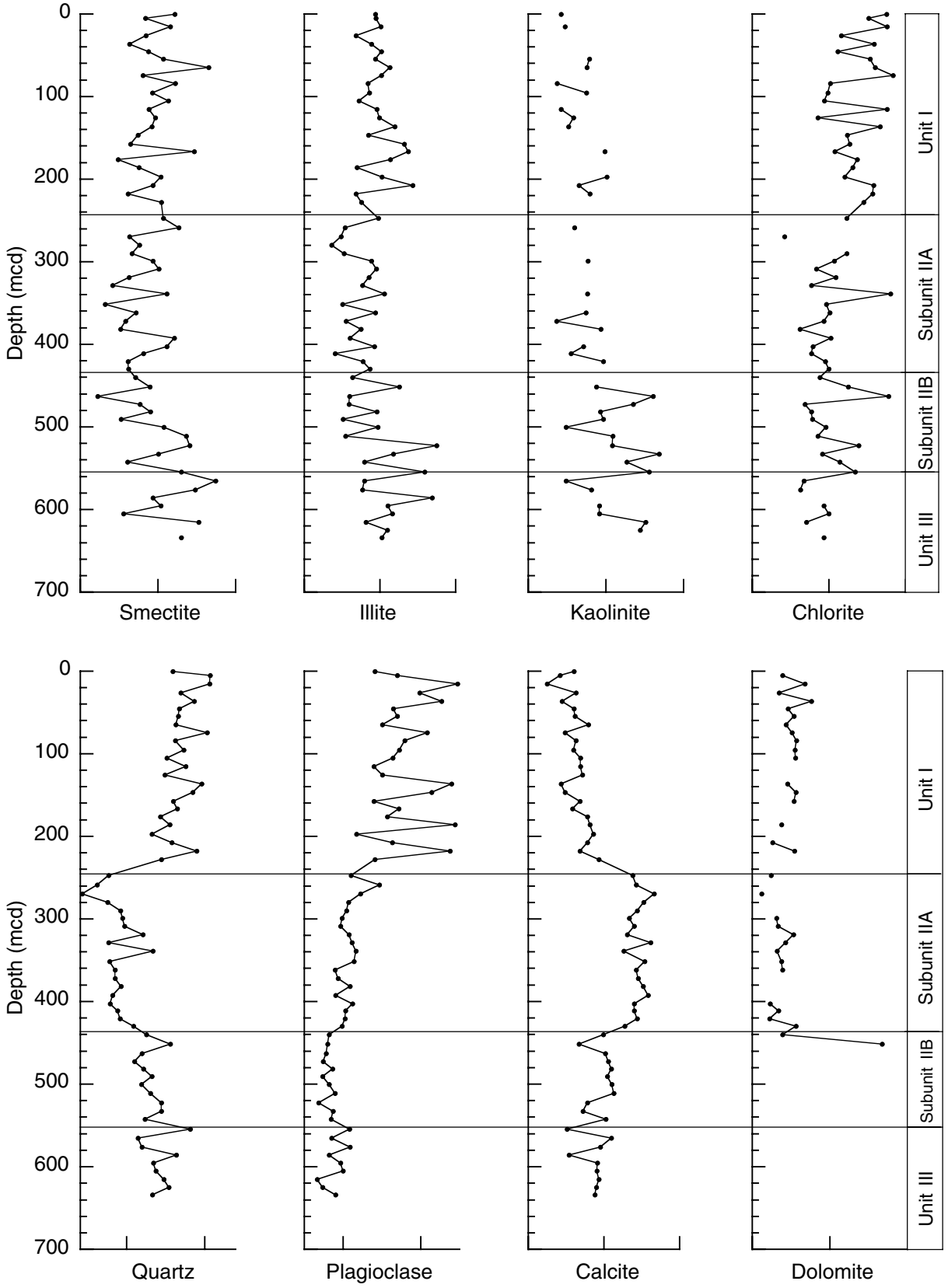

Figure F7. Occurrence of "iron sulfides," pyrite, and green layers in Hole 1146A. Units are occurrences per section.

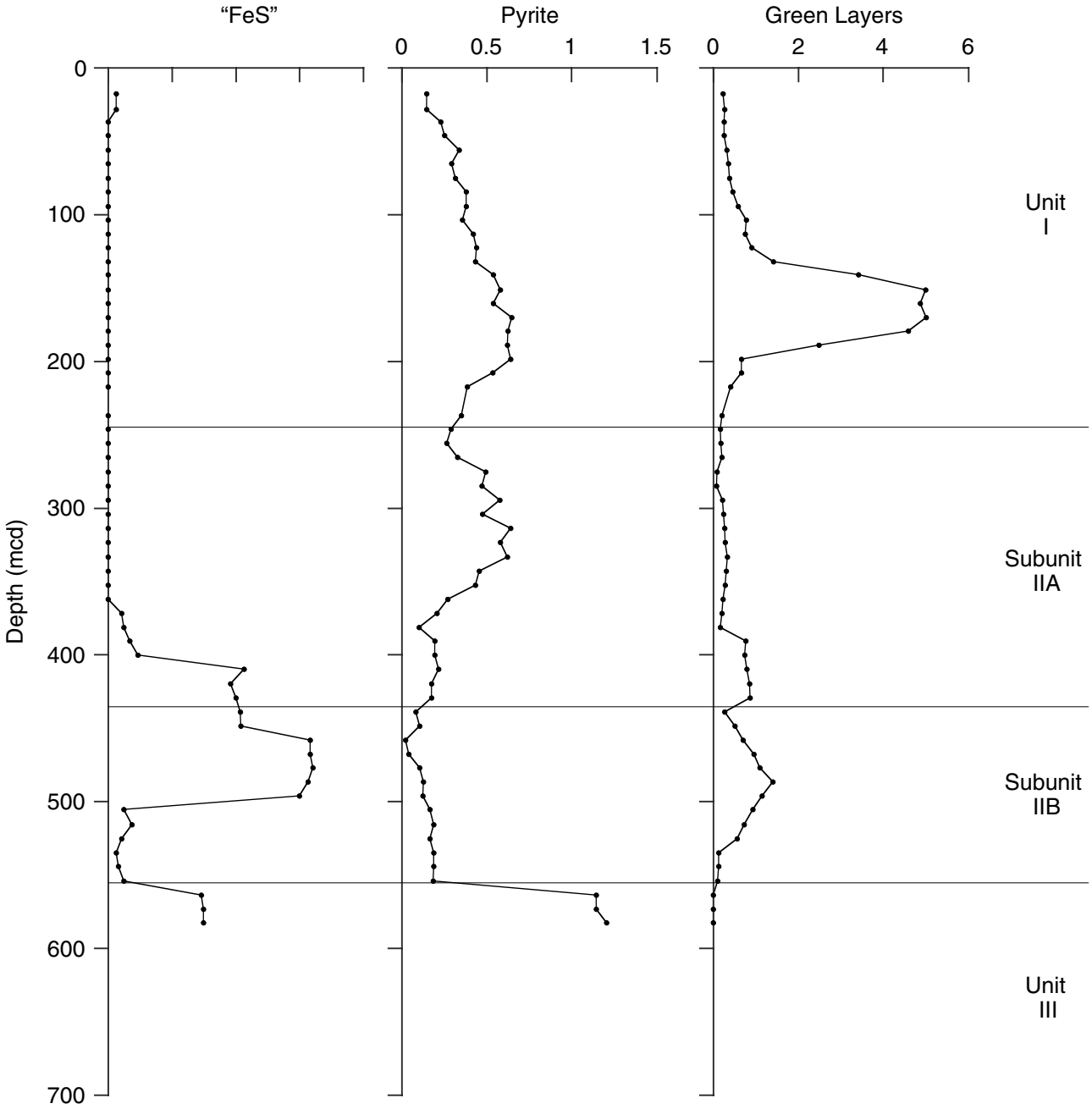

Figure F8. Close-up view of a foraminifer turbidite (107–99 cm) covered by a volcanic ash layer (99–97 cm): interval 184-1146A-33X-6, 90–110 cm.

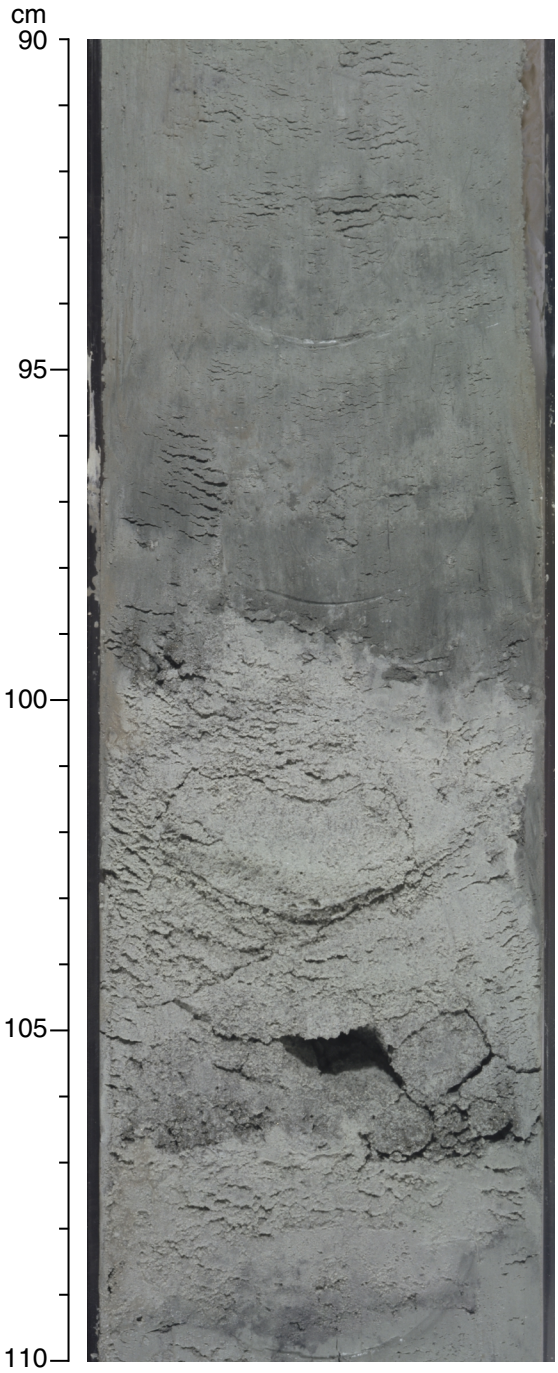

Figure F9. Close-up of pyrite layer in green calcareous sediment (interval 184-1146A-44X-2, 25–38 cm).

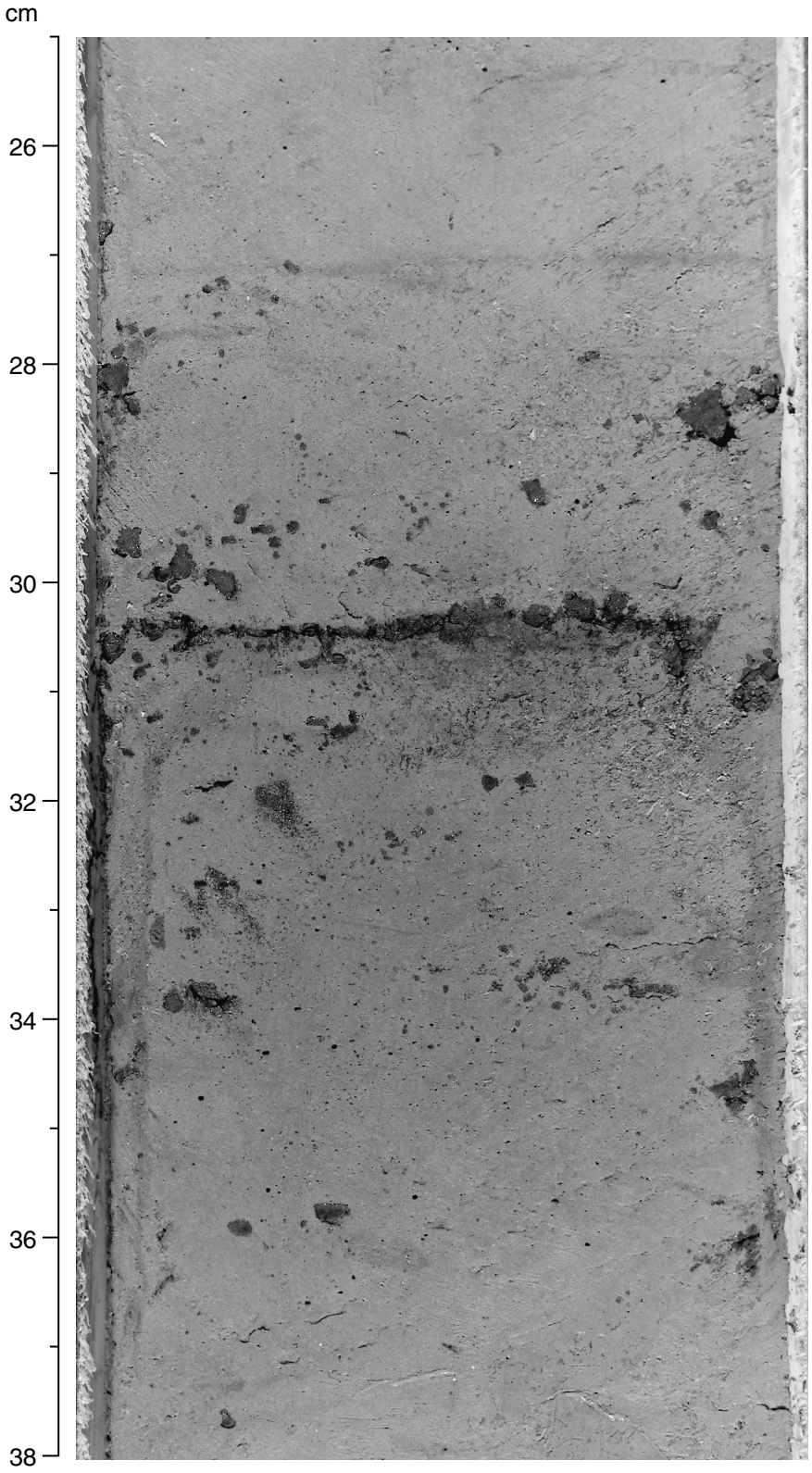

Figure F10. Close-up view of a *Zoophycos*-rich interval (interval 184-1146A-63X-6, 130–145 cm).

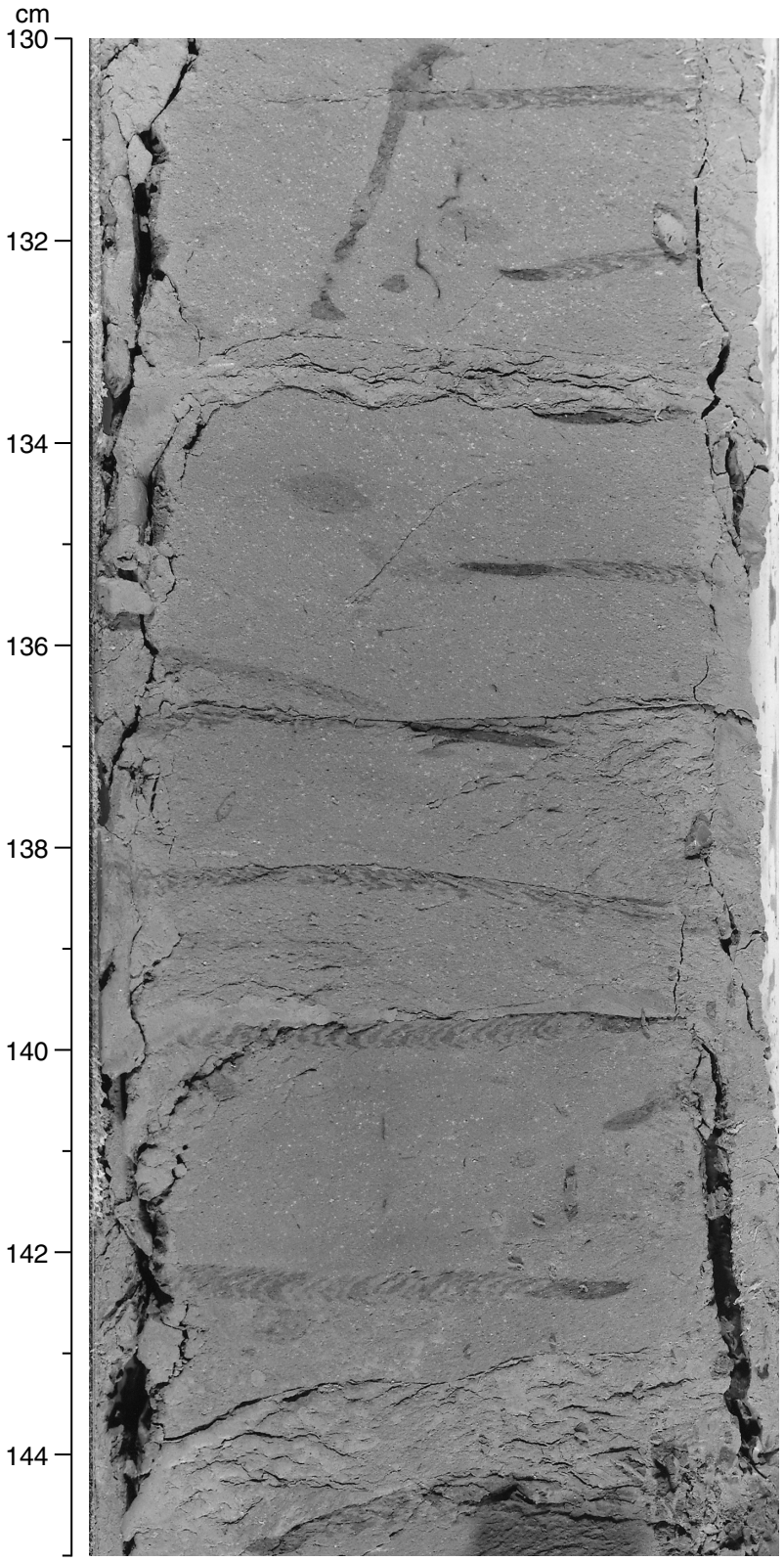

Figure F11. Age-depth plot for Site 1146. All biostratigraphic events are listed in Table T7, p. 82. The average sedimentation rate is calculated based on six control points (marked by * in Table T7, p. 82).

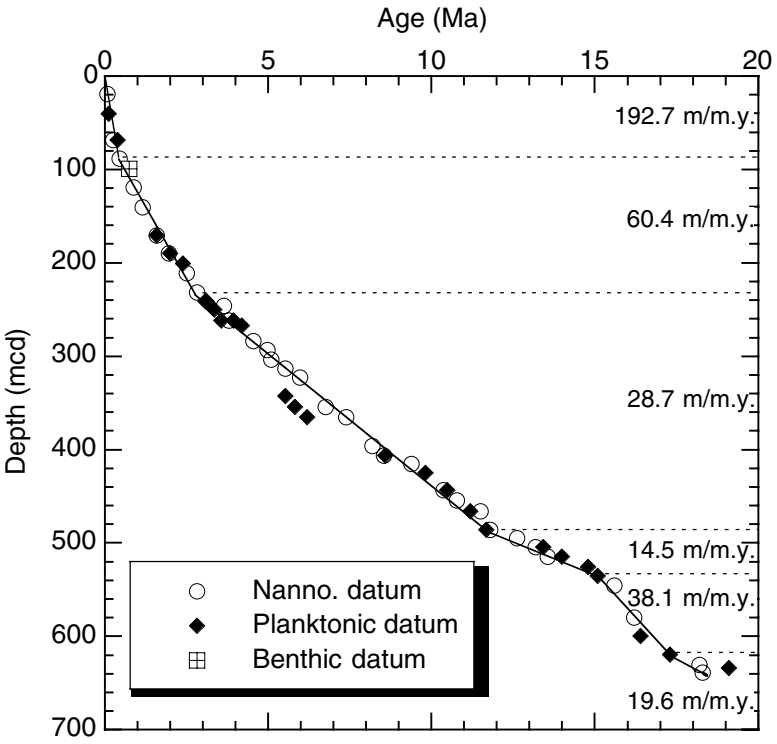

Figure F12. Declination and inclination for Hole 1146A, 0–300 mcd, obtained from long-core measurements (Cores 184-1146A-1H and 2H are not oriented). Below 210 mcd declinations cluster around 0°, and inclinations are very scattered as a result of XCB cores.

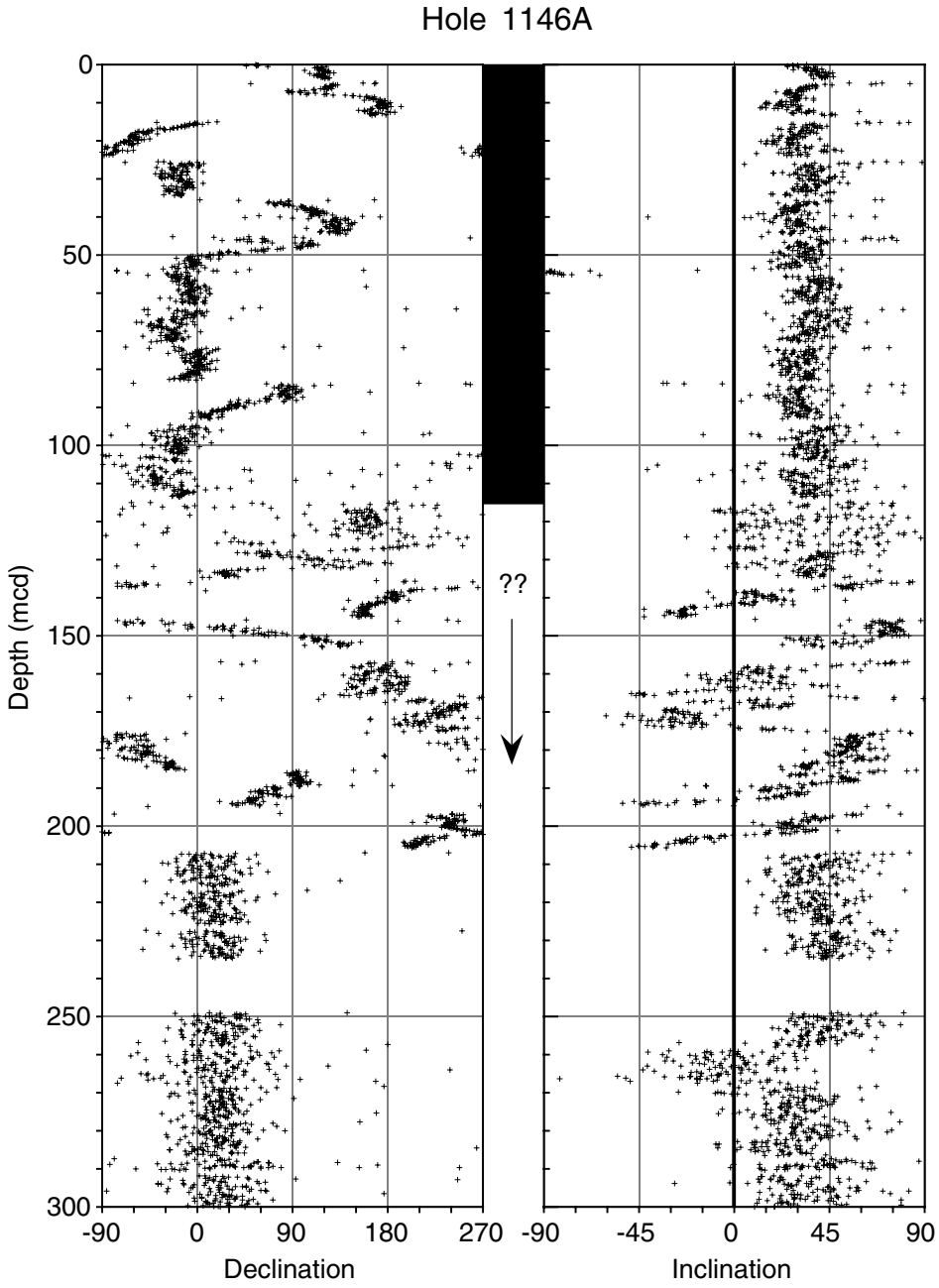

Figure F13. Declination and inclination for Hole 1146B (APC cores).

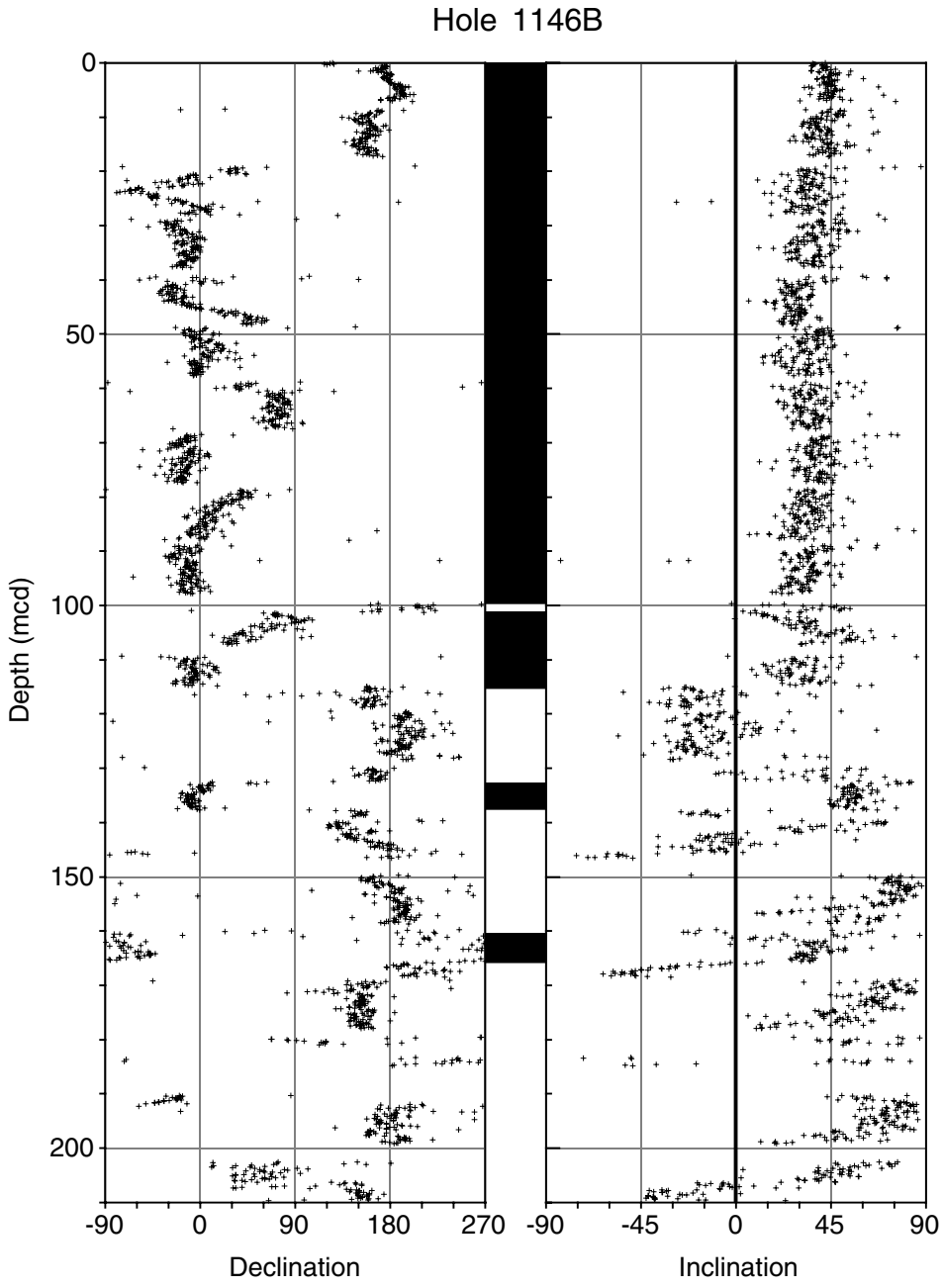

Figure F14. Declination and inclination for Hole 1146C (APC cores).

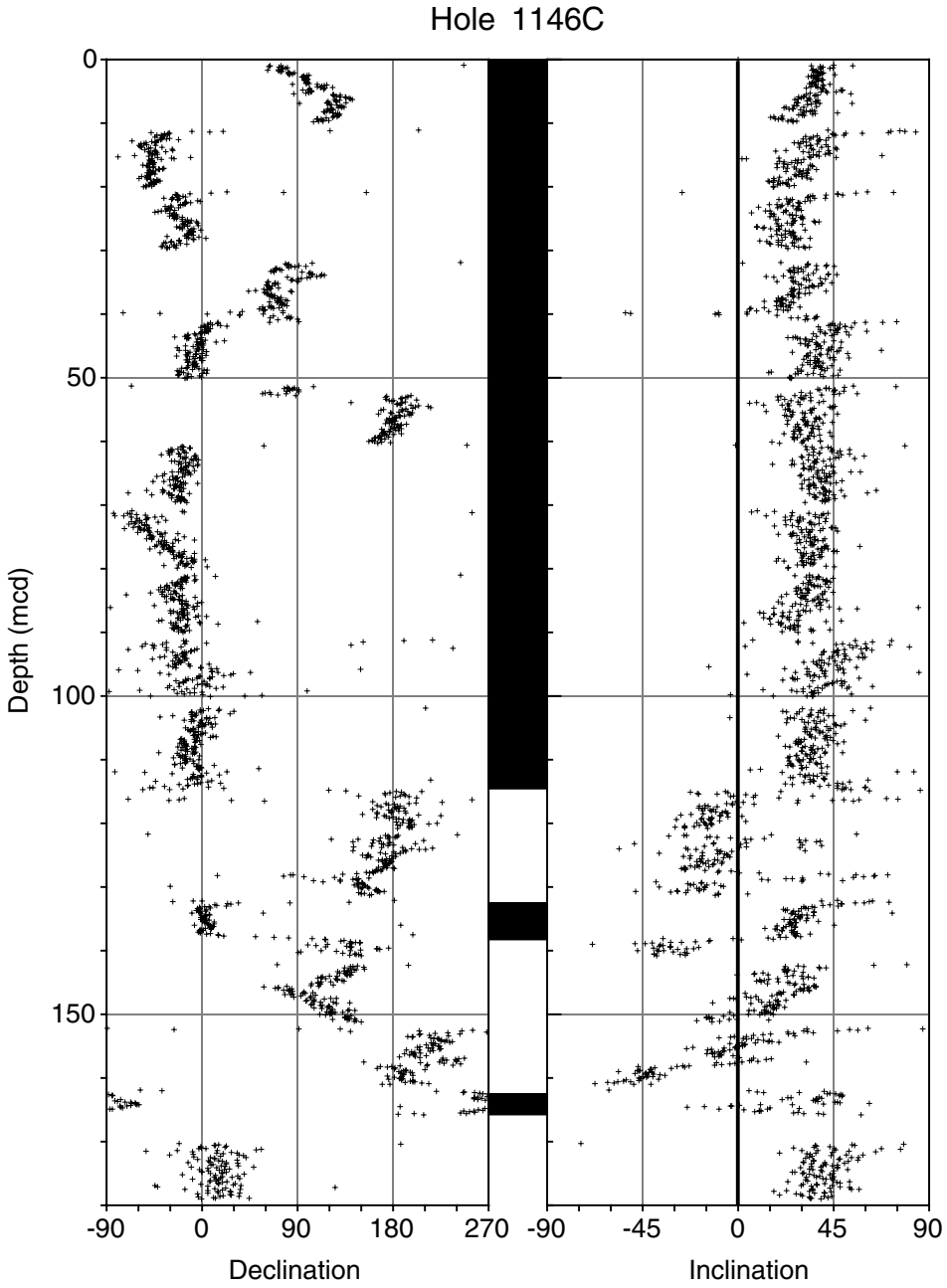

Figure F15. (**A**) Age-depth model, (**B**) linear sedimentation rates (LSR) and mass accumulation rates (MAR) vs. depth, and (**C**) LSR and MAR vs. age for Site 1146. Construction of model rates, LSR, and MAR is explained in "Sedimentation and Accumulation Rates," p. 13, in the "Explanatory Notes" chapter. In (A), diamonds = calcareous nannofossils, circles = foraminifers, squares = paleomagnetic reversals; in (B) and (C), solid lines = total sediment LSR, dashed lines = carbonate LSR, stippled columns = total sediment MAR, solid columns = carbonate MAR. B/M = Brunhes/Matuyama.

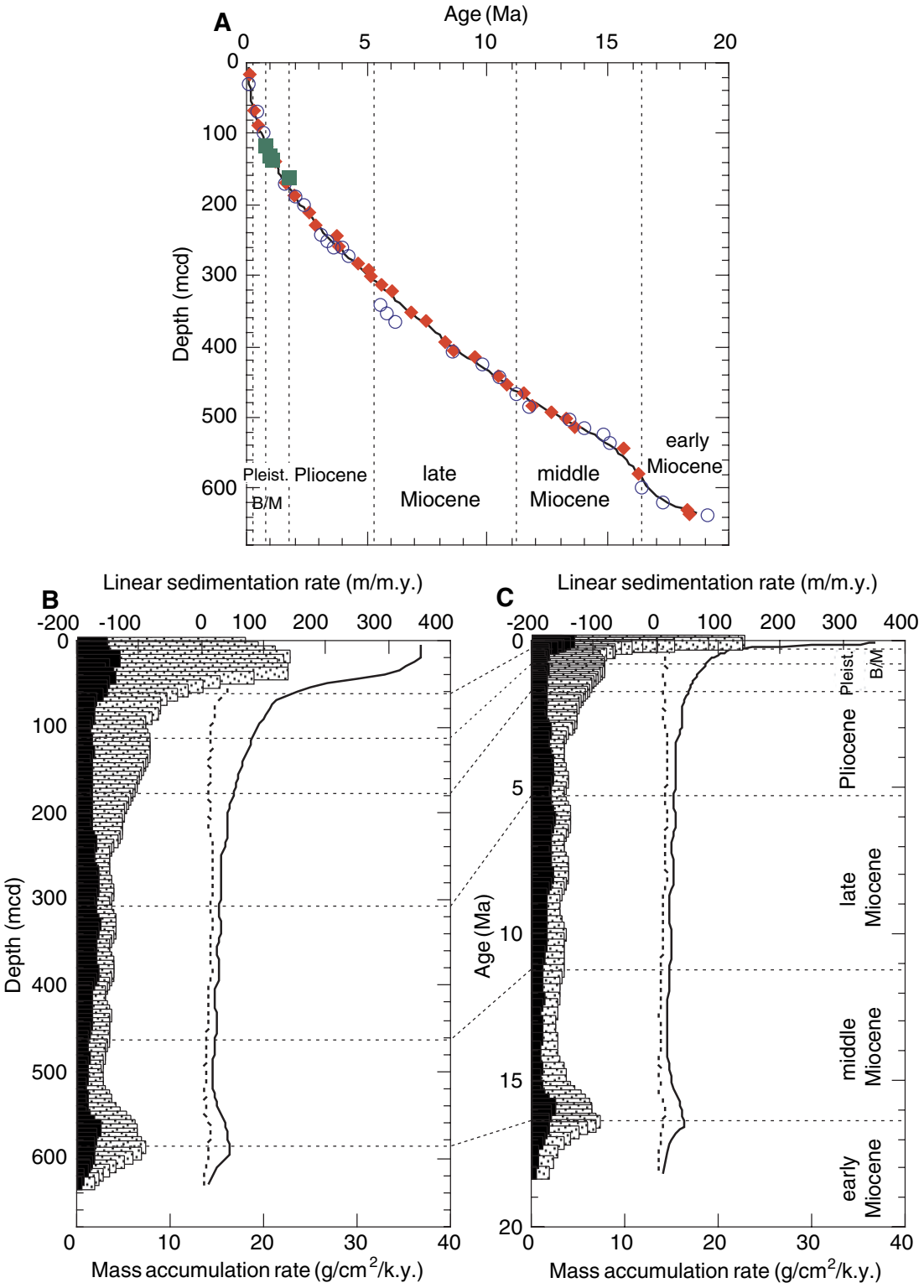

Figure F16. (**A**) Methane (C_1), ethane (C_2), and propane (C_3) concentrations (ppmv) and (**B**) C_1/C_2 ratio vs. depth, as obtained by the headspace technique for Holes 1146A and 1146C (530–635 mcd).

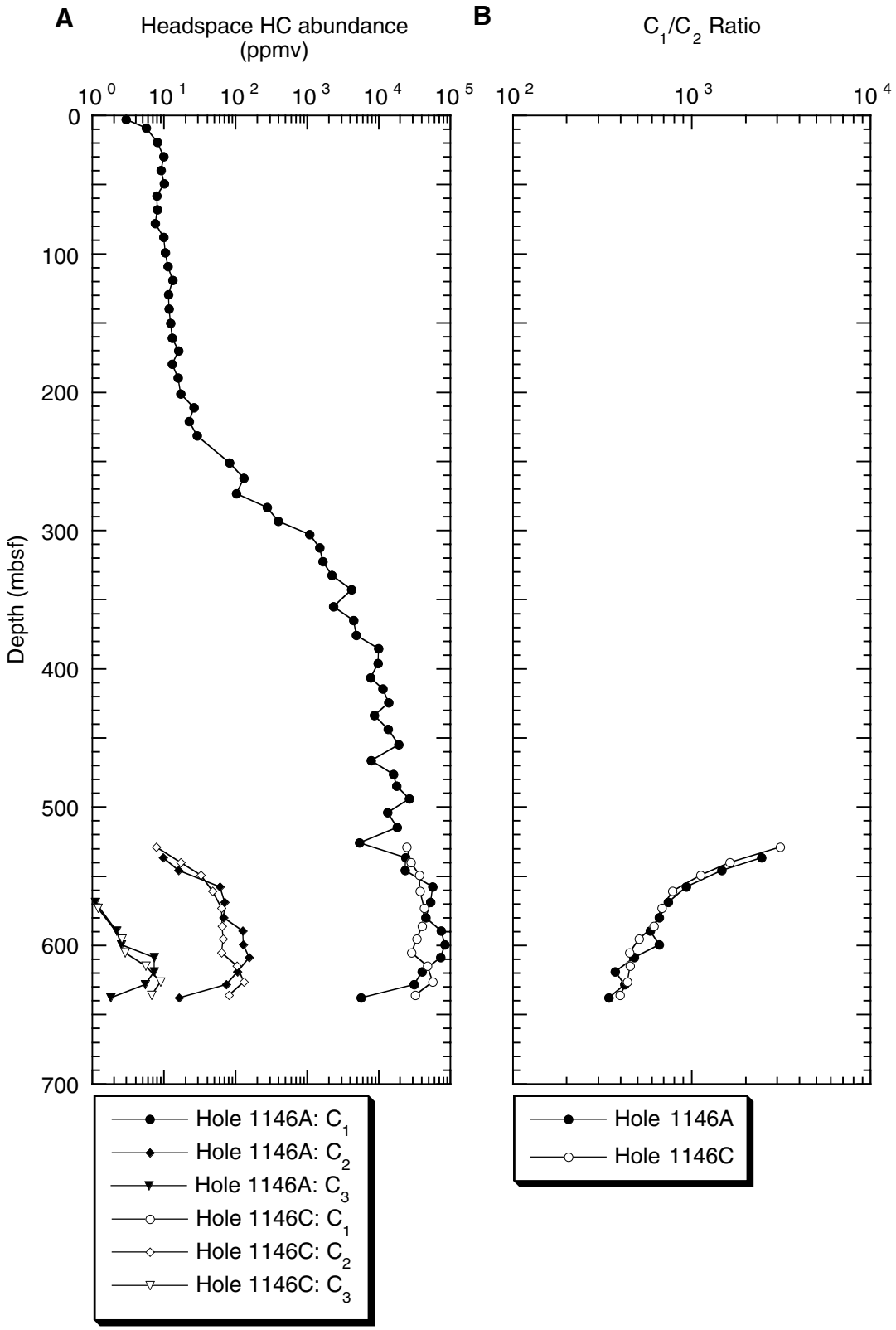

Figure F17. (**A**) Carbonate, (**B**) total organic carbon, and (**C**) organic C/N ratio at Site 1146 vs. depth (Hole 1146A).

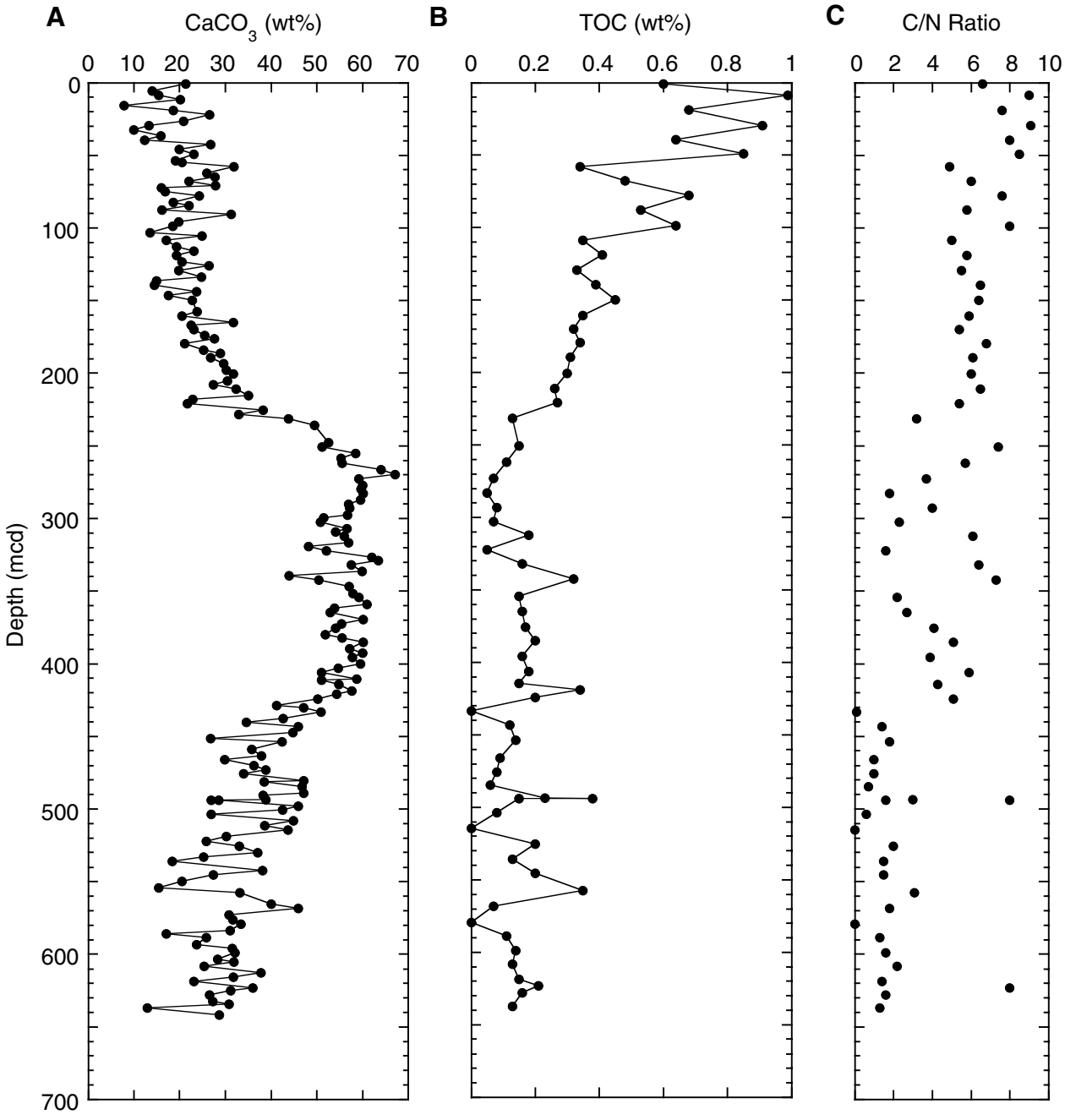

Figure F18. Vertical profiles of interstitial water measurements at Site 1146 (concentrations). **A.** Chloride. **B.** Salinity. **C.** Sulfate. **D.** Ammonium. **E.** Phosphate. **F.** Alkalinity. **G.** pH. **H.** Magnesium. **I.** Calcium. **J.** Potassium. **K.** Silica. **L.** Lithium. **M.** Strontium.

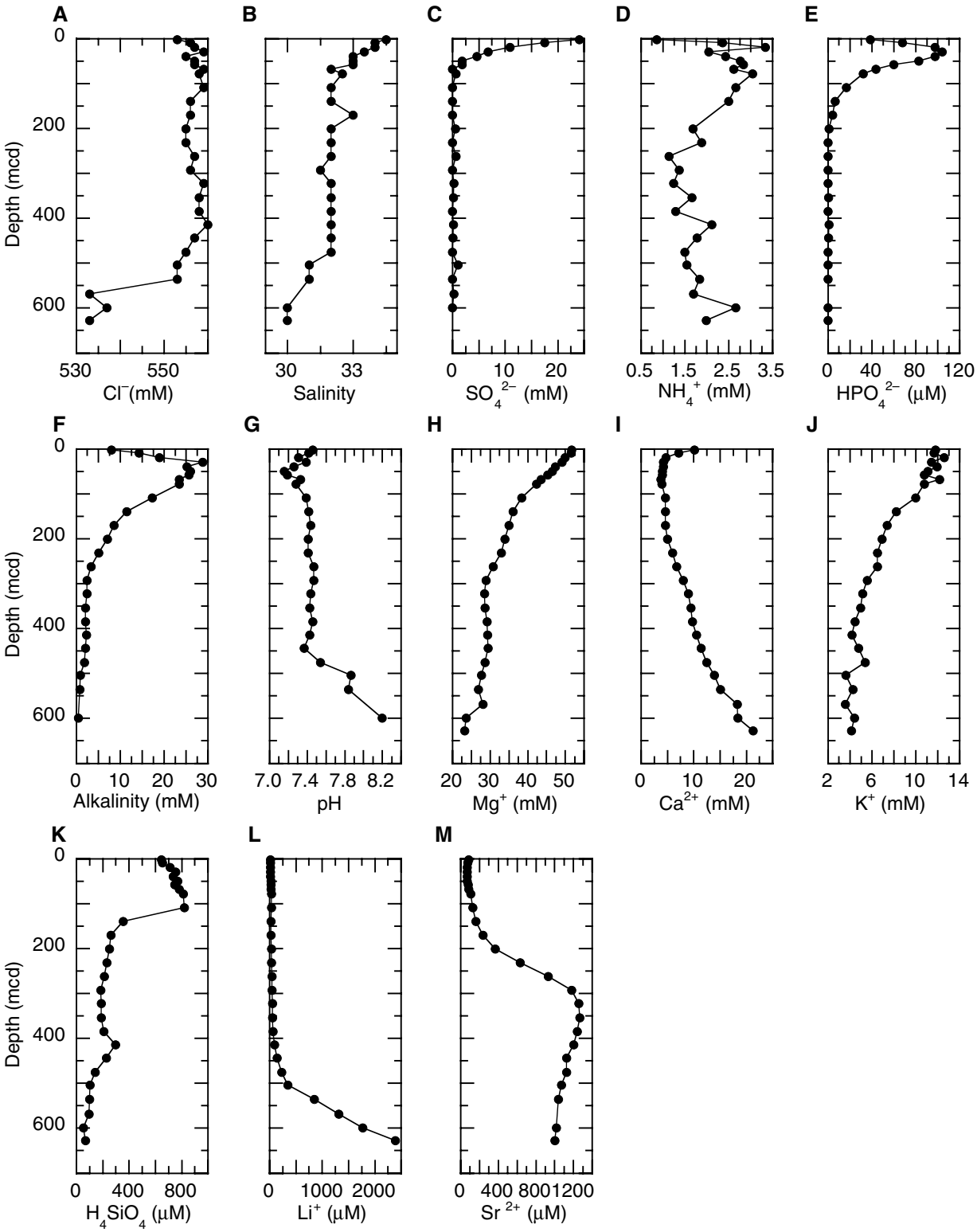

Figure F19. Magnetic susceptibility measurements at Site 1146 plotted for each hole. APC = advanced hydraulic piston corer, XCB = extended core barrel.

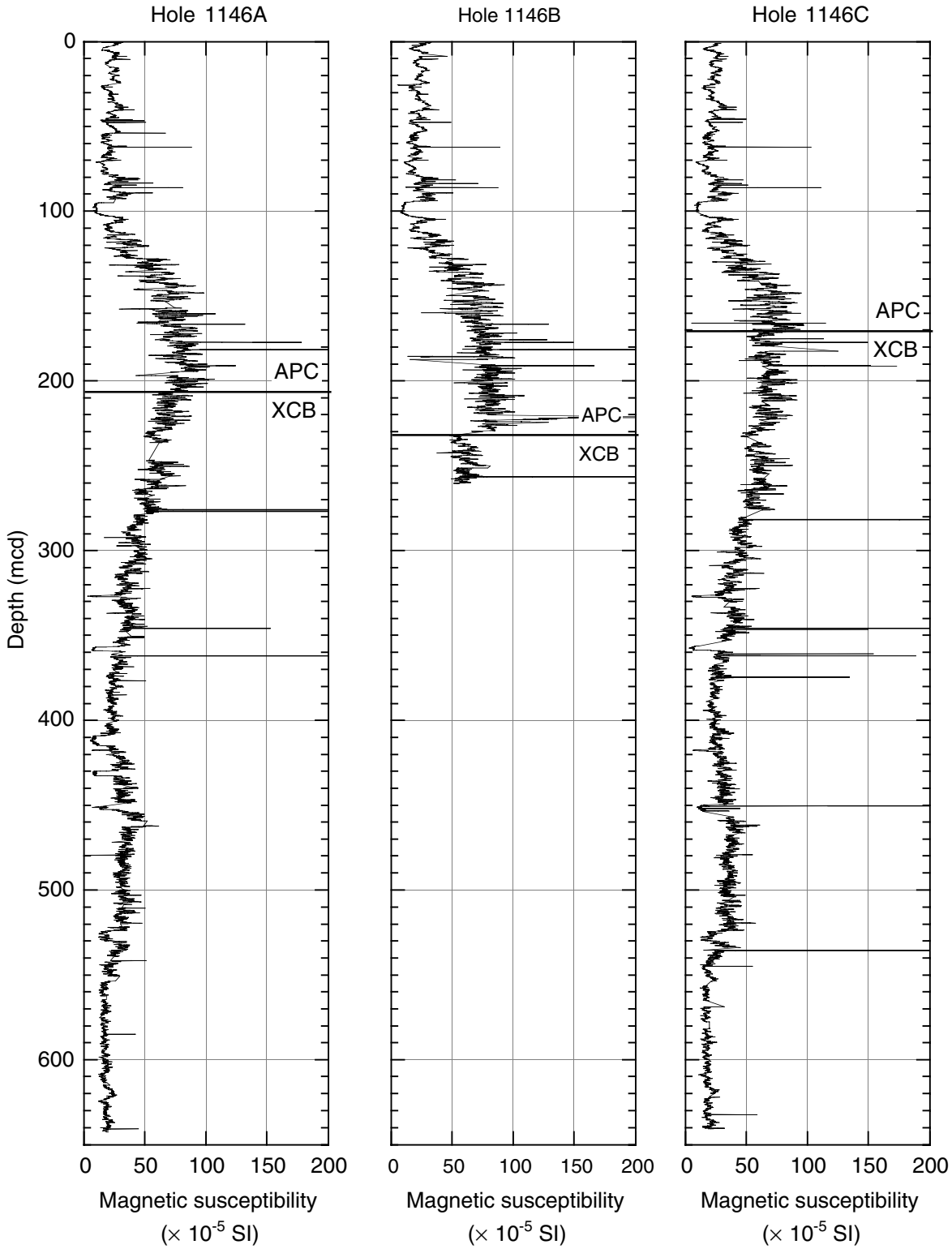

Figure F20. Natural gamma radiation measurements at Site 1146 smoothed with a 20-point moving average, plotted for each hole. APC = advanced hydraulic piston corer, XCB = extended core barrel.

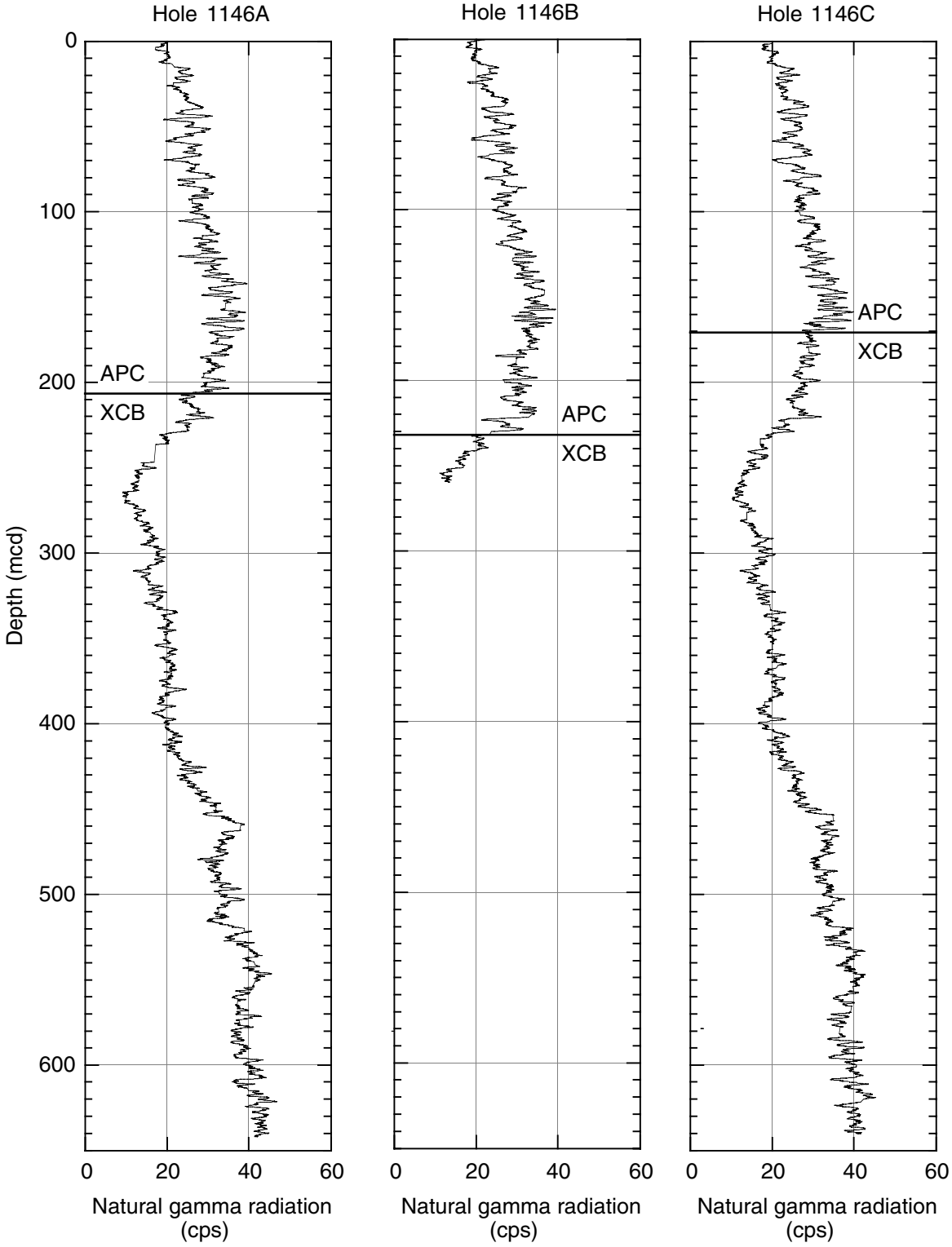

Figure F21. Bulk density measurements from GRA (line) and MAD methods (open circles) at Site 1146 plotted for each hole. APC = advanced hydraulic piston corer, XCB = extended core barrel.

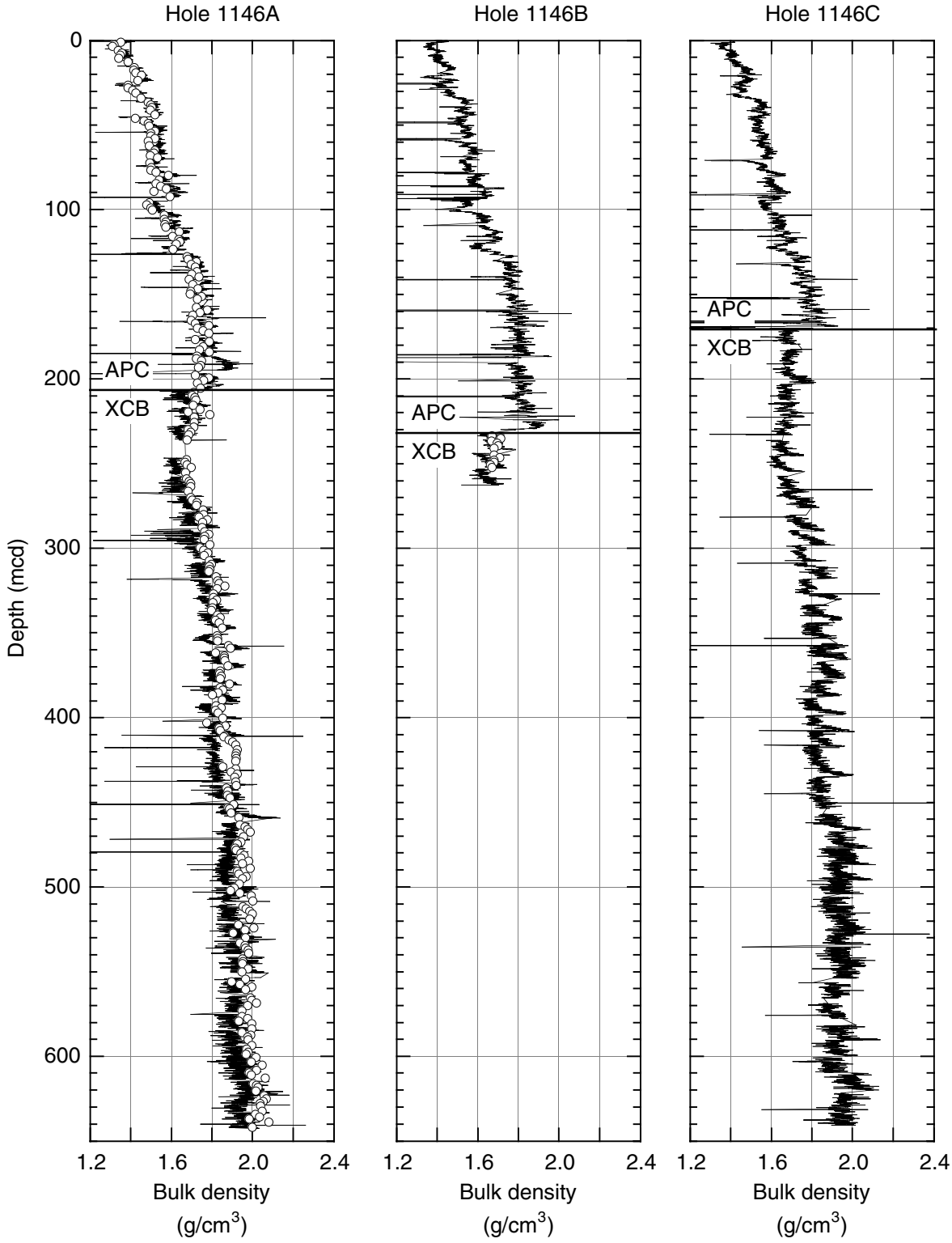

Figure F22. *P*-wave velocity measurements for Hole 1146A. APC = advanced hydraulic piston corer, XCB = extended core barrel.

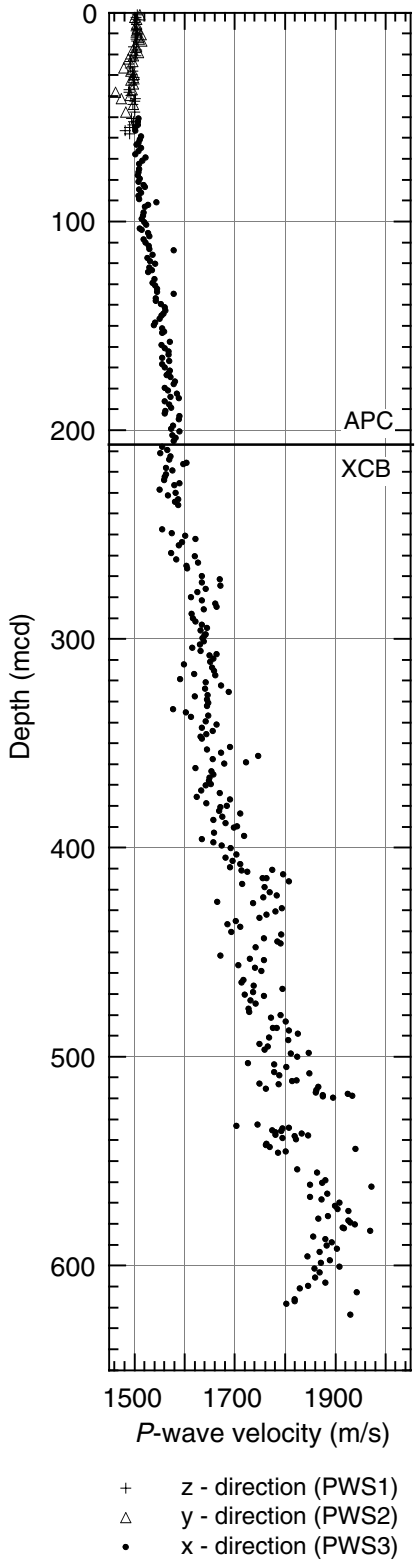

Figure F23. Porosity, grain density, and dry density values obtained from the moisture and density method. Solid circles = Hole 1146A, open circles = Hole 1146B, APC = advanced hydraulic piston corer, XCB = extended core barrel.

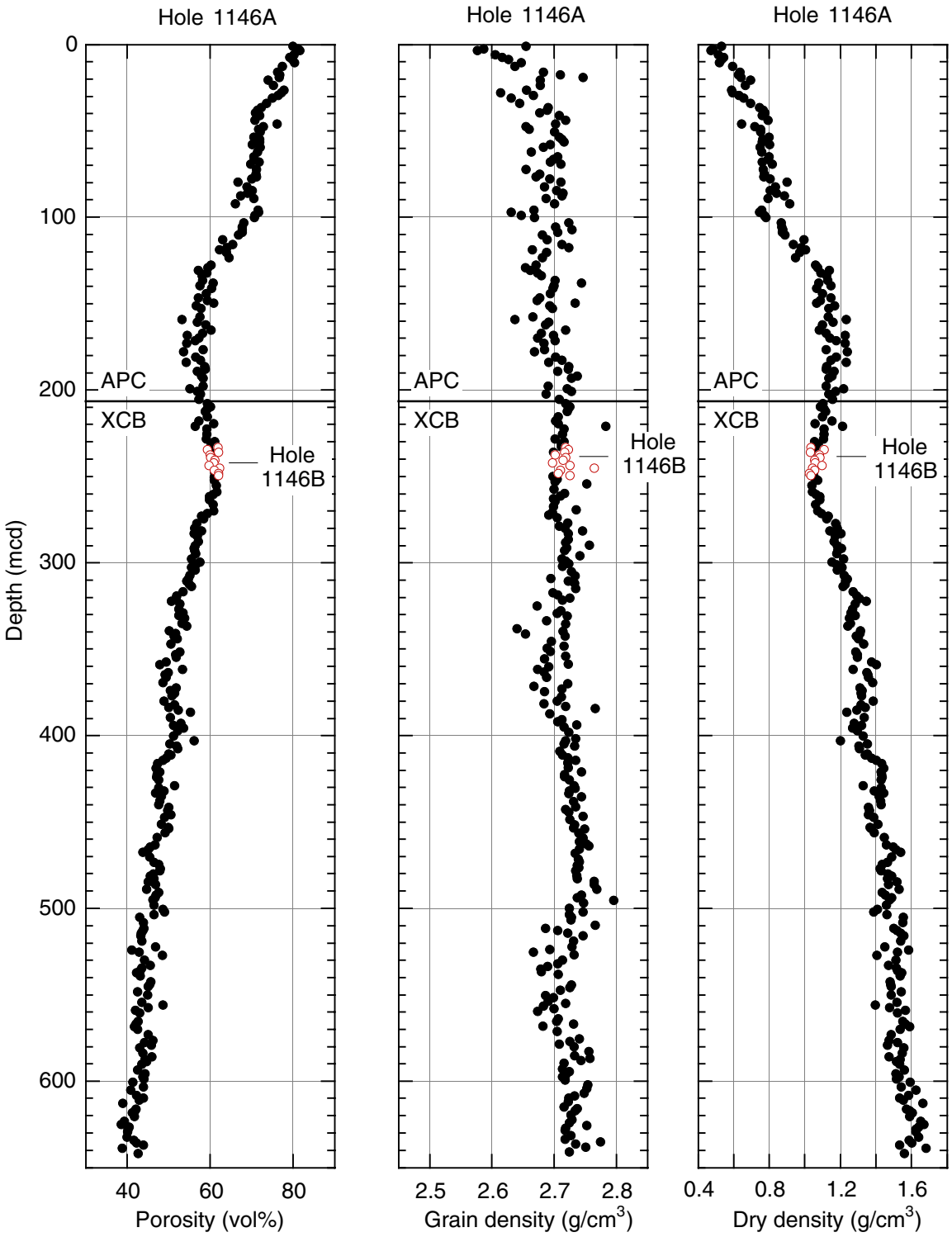

Figure F24. Color reflectance measurements from split-core surfaces at Site 1146 smoothed with a 20-point moving average, plotted for each hole. L*, a*, and b* are standard parameters calculated by the Minolta CM-2002 photospectrometer from the spectral data. L* = black line, a*/ b* = gray line, APC = advanced hydraulic piston corer, XCB = extended core barrel.

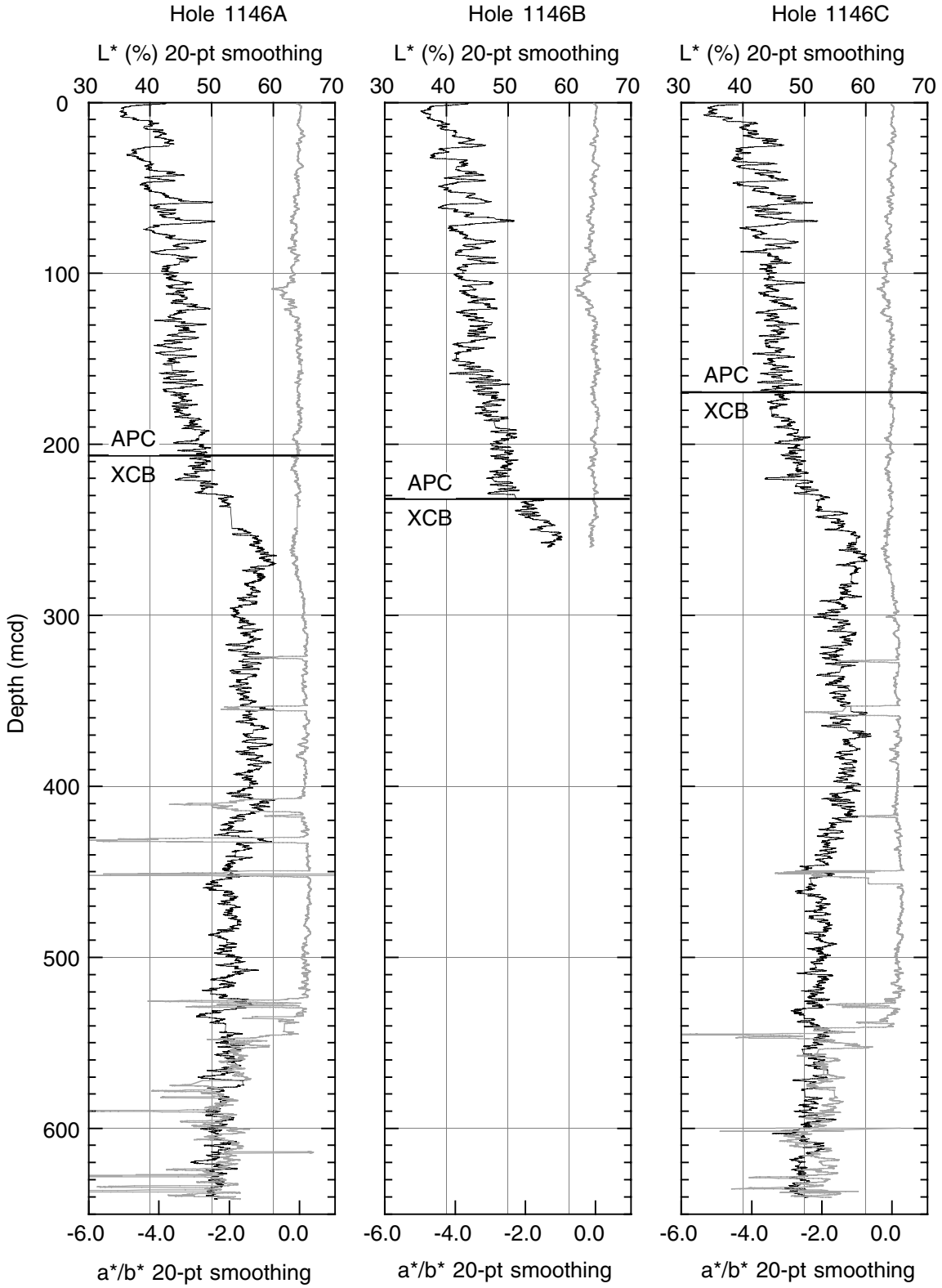

Figure F25. Thermal conductivity measurements for Holes 1146A and 1146B. Open squares = Hole 1146A, solid circles = Hole 1146B, APC = advanced hydraulic piston corer, XCB = extended core barrel.

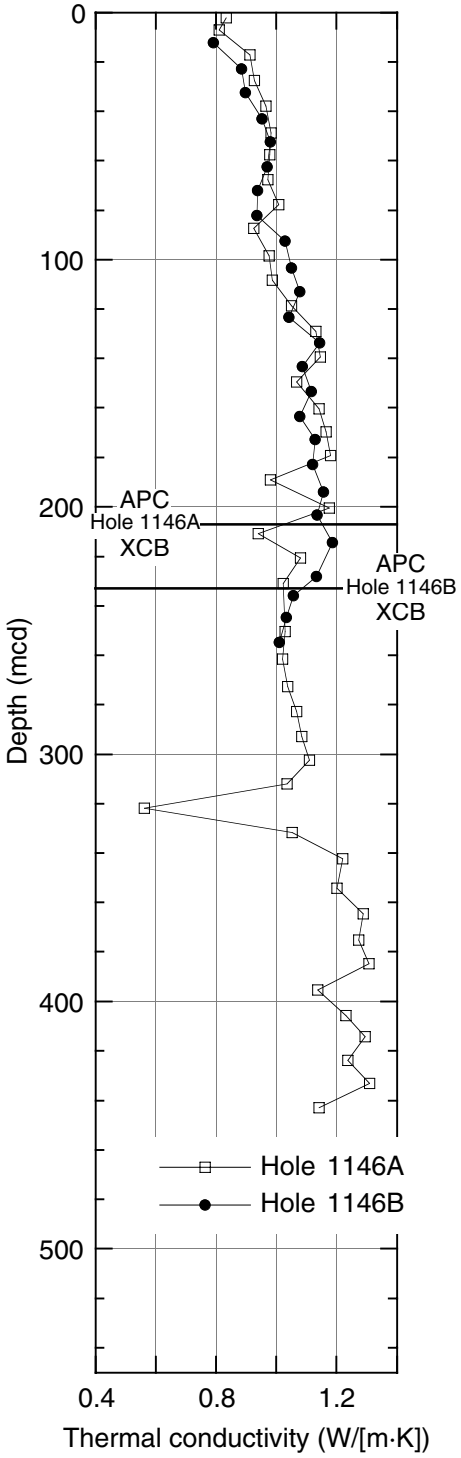

Figure F26. Downhole temperature measurements at Site 1146. **A.** Bottom-water temperature at Hole 1146B taken before Core 184-1146B-1H was shot. This value is taken as approximate bottom-water temperature at Site 1146. **B–E.** Downhole sediment temperature records and calculated equilibrium temperatures at Hole 1146A. Open circles = original temperature measurements, solid circles = selected section of data used in calculating the equilibrium temperature.

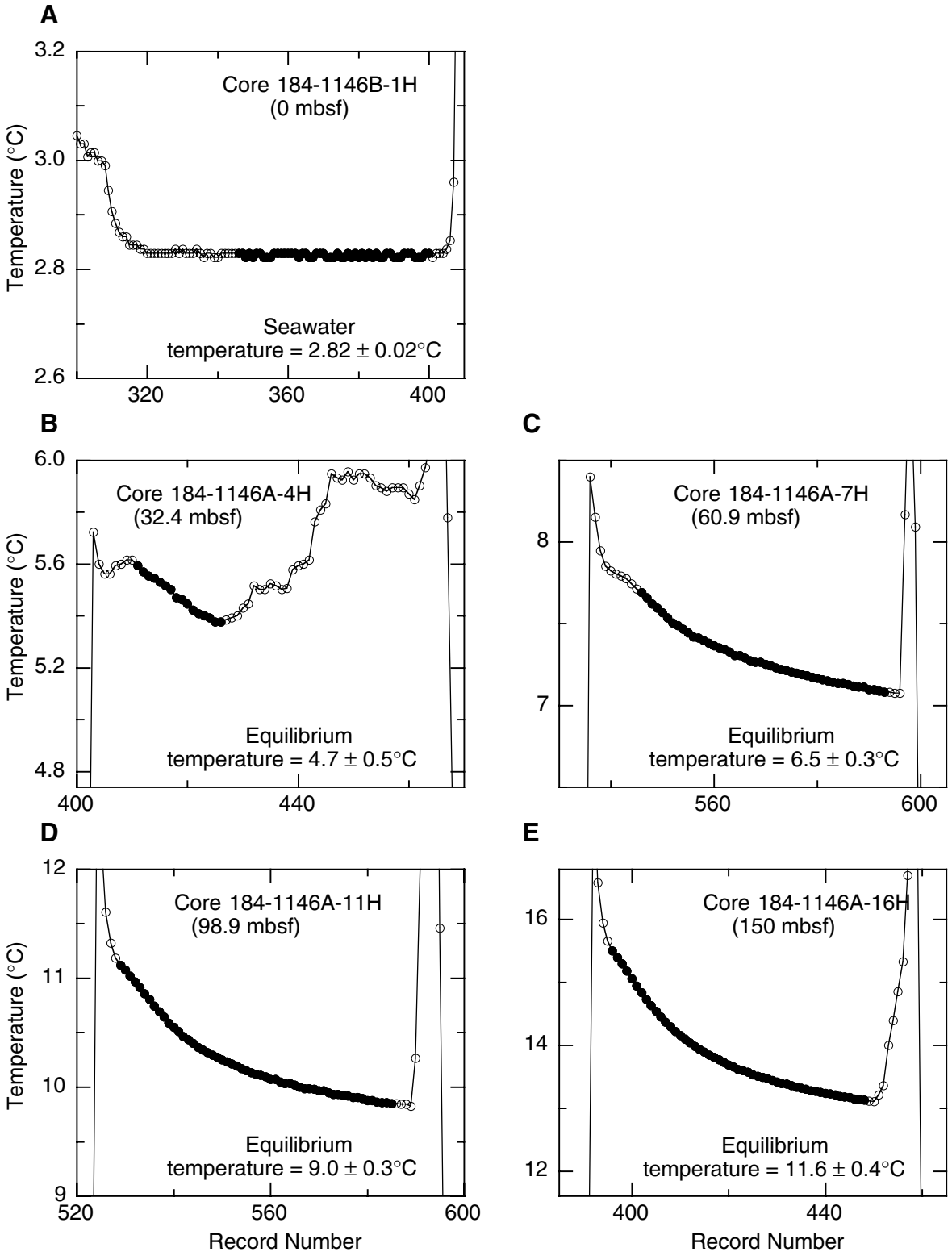

Figure F27. Downhole temperature gradient at Site 1146. T = temperature (°C) at depth (mbsf), R = correlation coefficient.

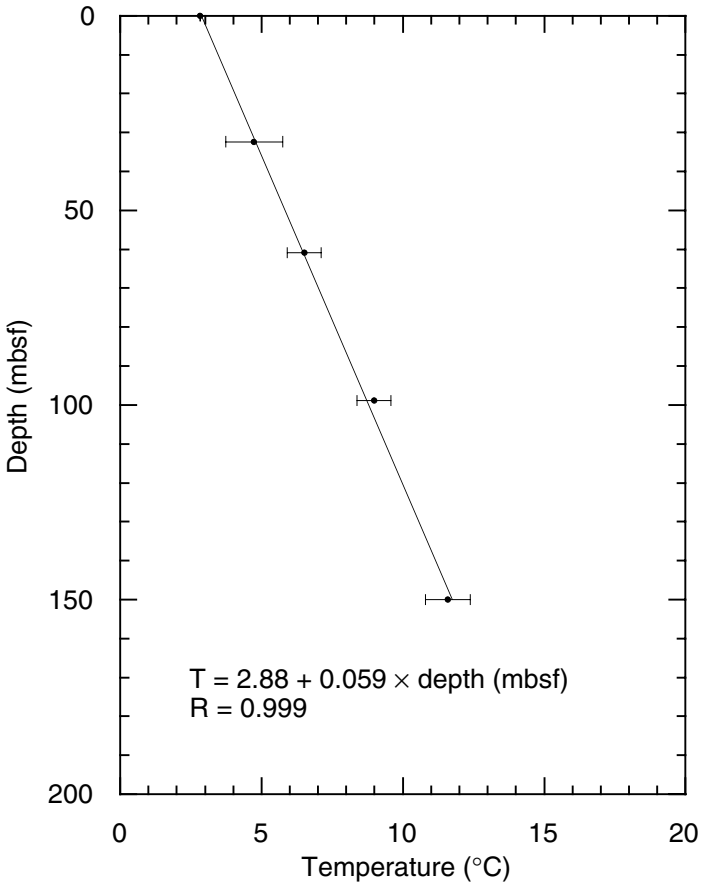

Figure F28. Graphic summary of downhole logging operations for Hole 1146A. The seafloor was identified based on a step in natural gamma activity at the sediment/water boundary. FMS = Formation MicroScanner, LSS = long-spaced sonic, GHMT = geological high-resolution magnetic tool.

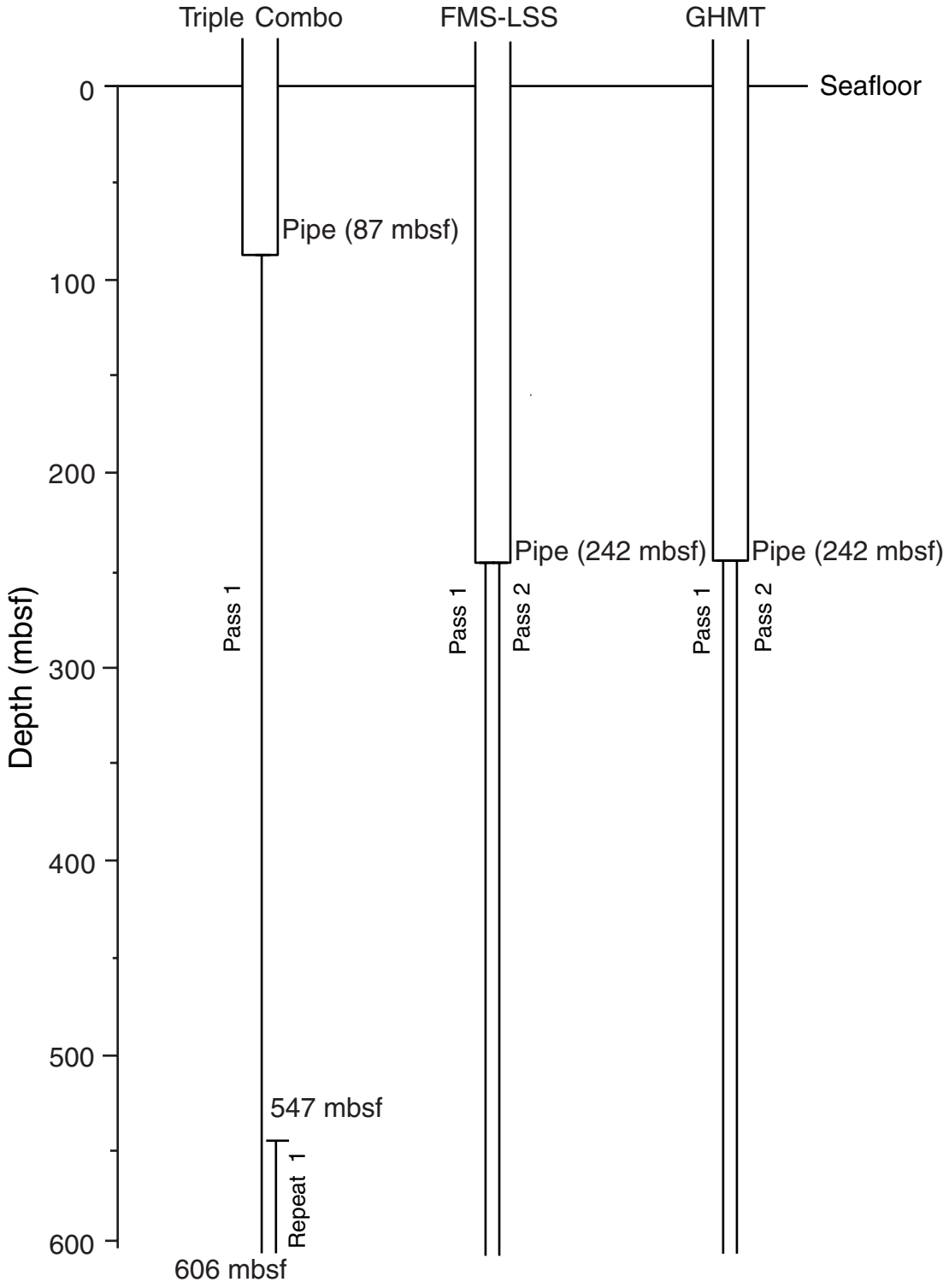

Figure F29. Downhole logs of hole diameter (as measured by caliper opening), neutron porosity (neut.), bulk density, electrical resistivity (SFL = spherically focused log, IMPH = medium induction phasor-processed resistivity, IDPH = deep induction phasor-processed resistivity), magnetic susceptibility (pass 1 and pass 2 of the GHMT tool string), and *P*-wave velocity from Hole 1146A. IU = instrument units.

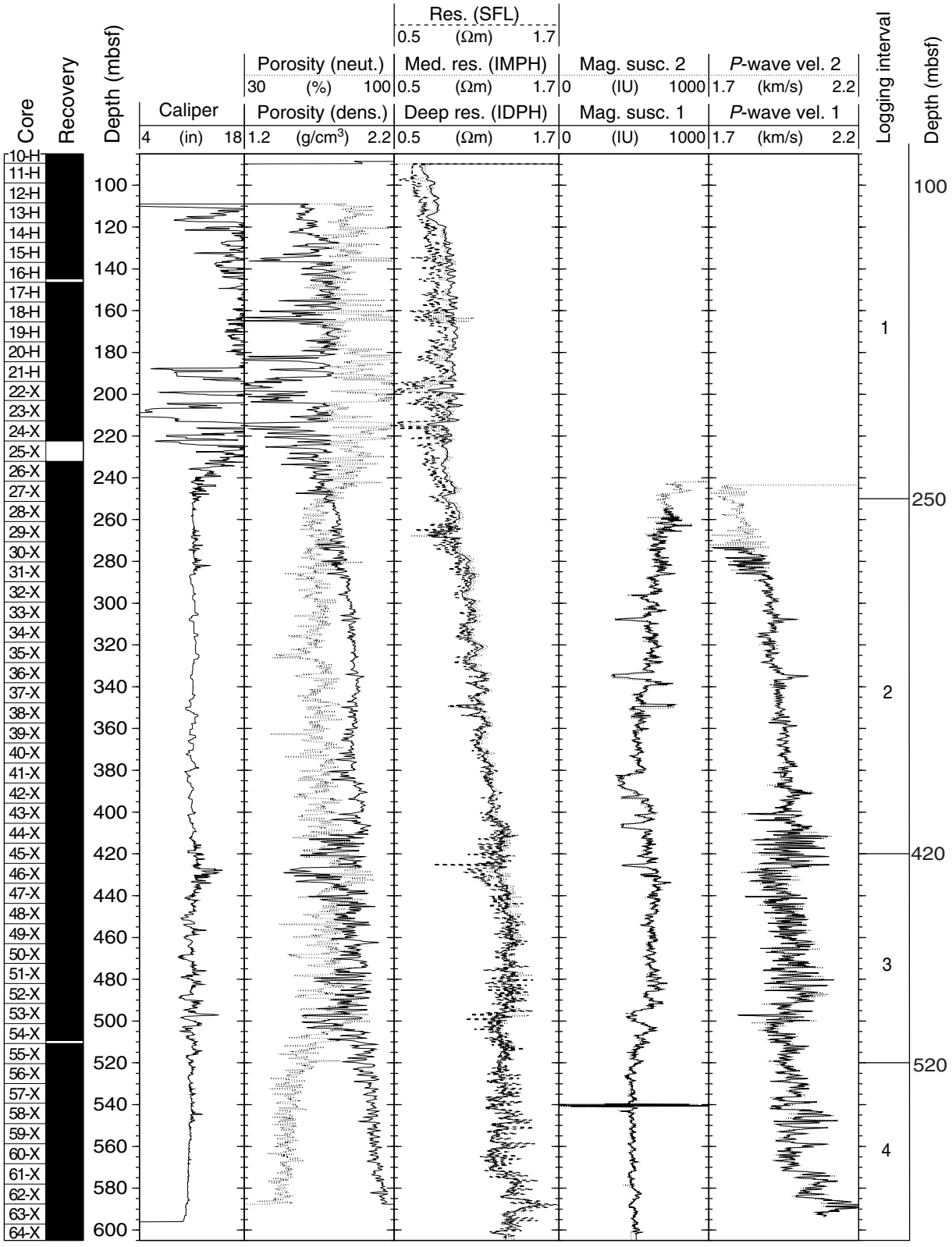

Figure F30. Downhole logs of gamma ray (HSGR = standard gamma ray), computed gamma ray (HCGR = HSGR minus uranium contribution), and potassium, thorium, and uranium from the natural gamma-ray tool (NGT) and hostile environment natural gamma-ray sonde (HNGS). The gamma-ray and computed gamma-ray values are from the HNGS tool.

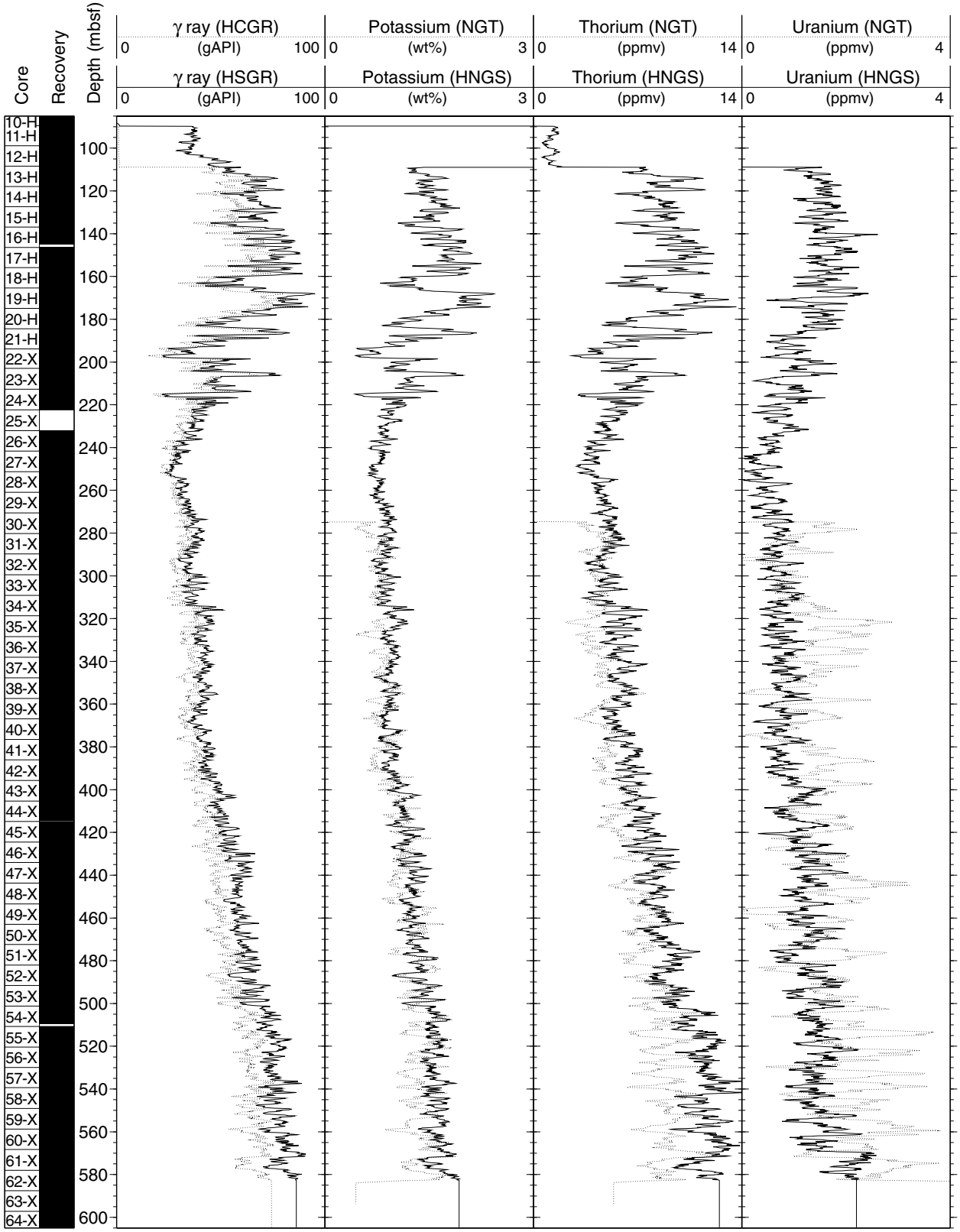

Figure F31. Comparison of magnetic susceptibility from core logging with the multisensor track (MST) measurements of core logs and downhole measurements (pass 1 of the GHMT tool string), of thorium measured by the NGT tool string and photoelectric effect (PEF) from the HLDS, of $CaCO_3$ from core samples and PEF, and of bulk density from downhole and core logging. MAD = moisture and density, GRA = gamma-ray attenuation, IU = instrument units.

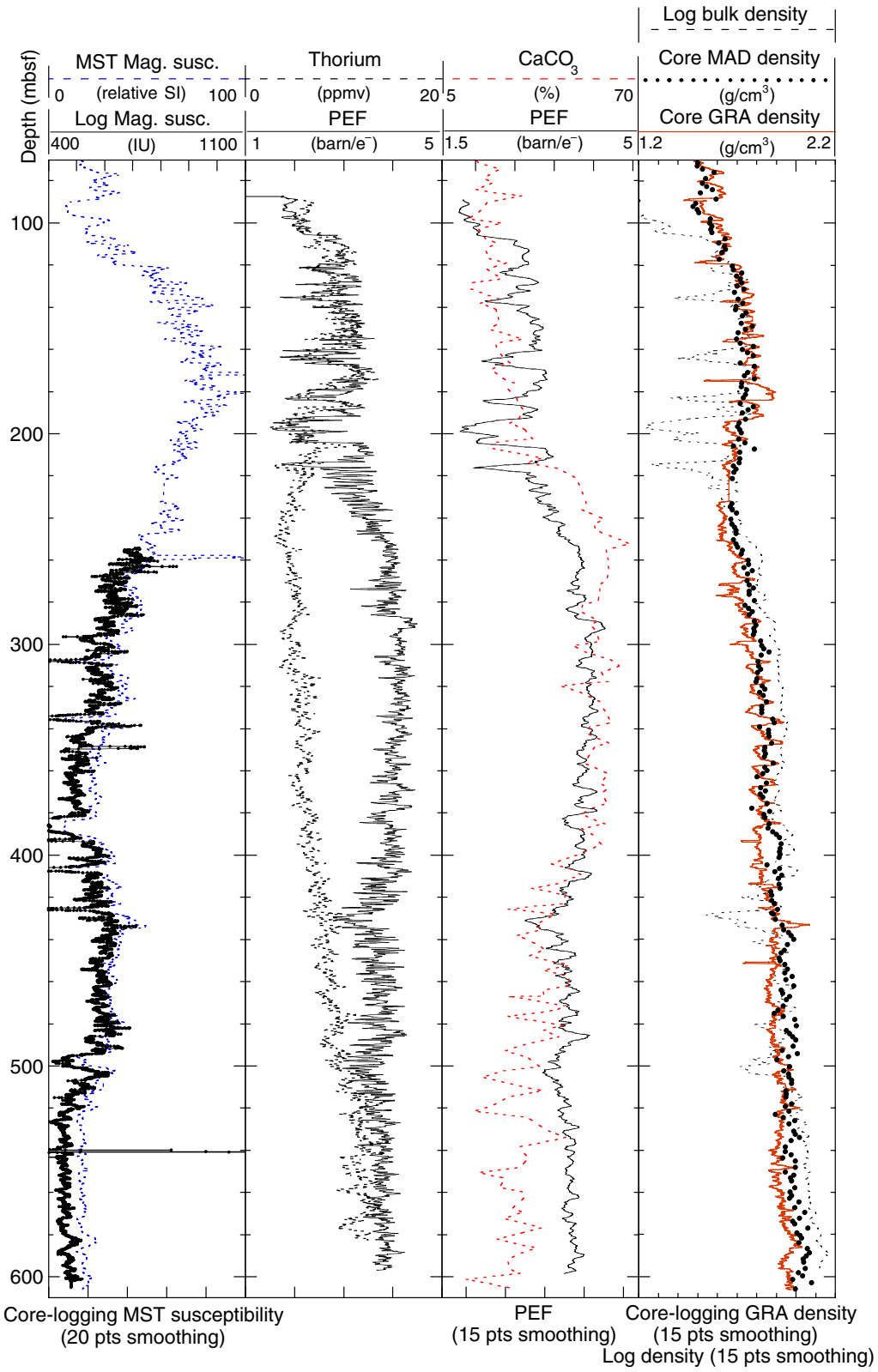

Figure F32. Comparison of core moisture and density (MAD) porosity and downhole log bulk density porosity, and of natural gamma radiation from downhole and core logging. Also shown is total magnetic field from downhole logging. Large-amplitude spikes in the magnetic field were edited out. HSGR = standard gamma ray, HLDS = hostile environment lithodensity sonde, MST = multisensor track, NGR = natural gamma radiation, PWS3 = *P*-wave velocity (sensor).

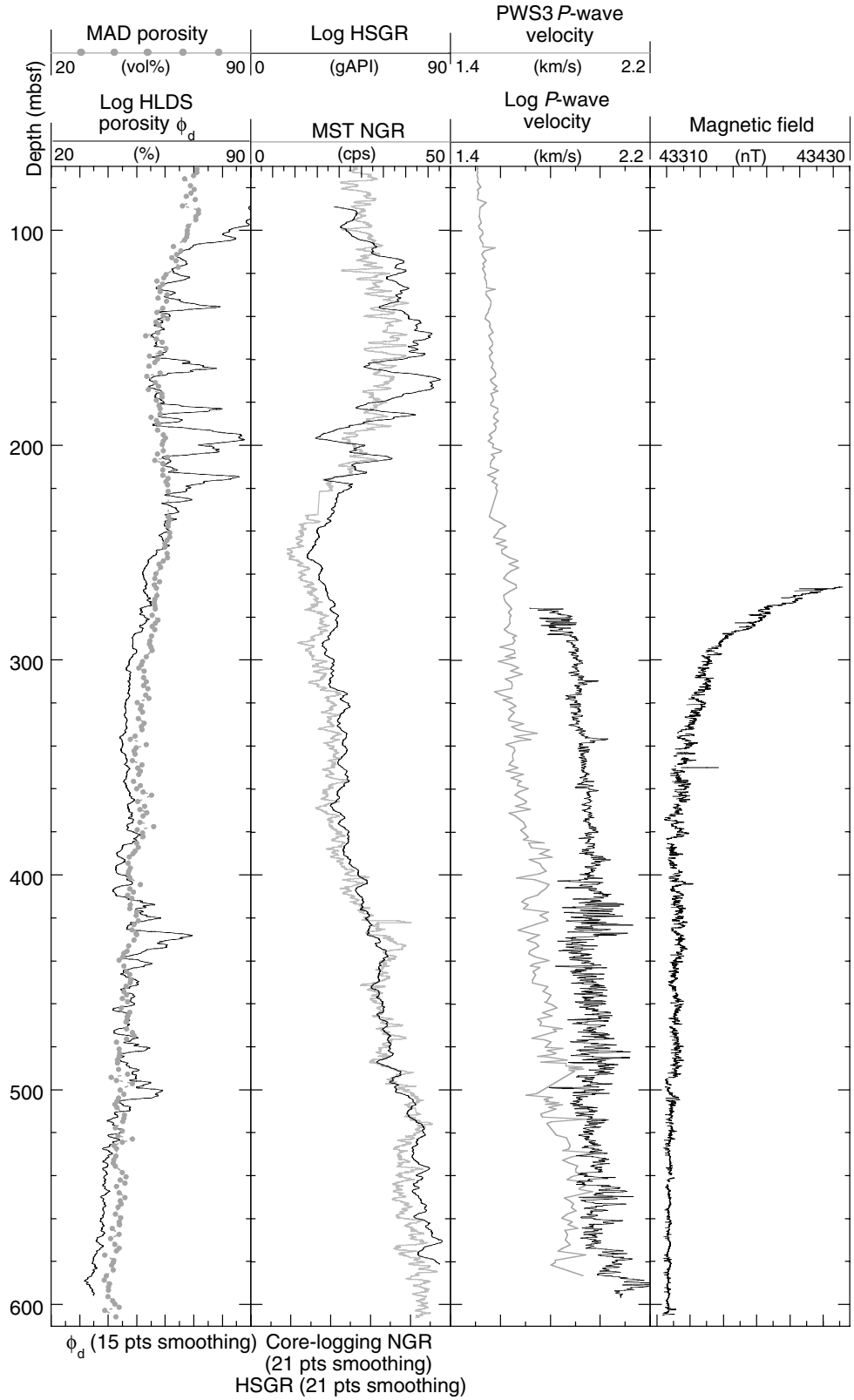

Figure F33. Formation MicroScanner (FMS) image from downhole logging data displaying alternation of relatively conductive (darker) and resistive (lighter) intervals.

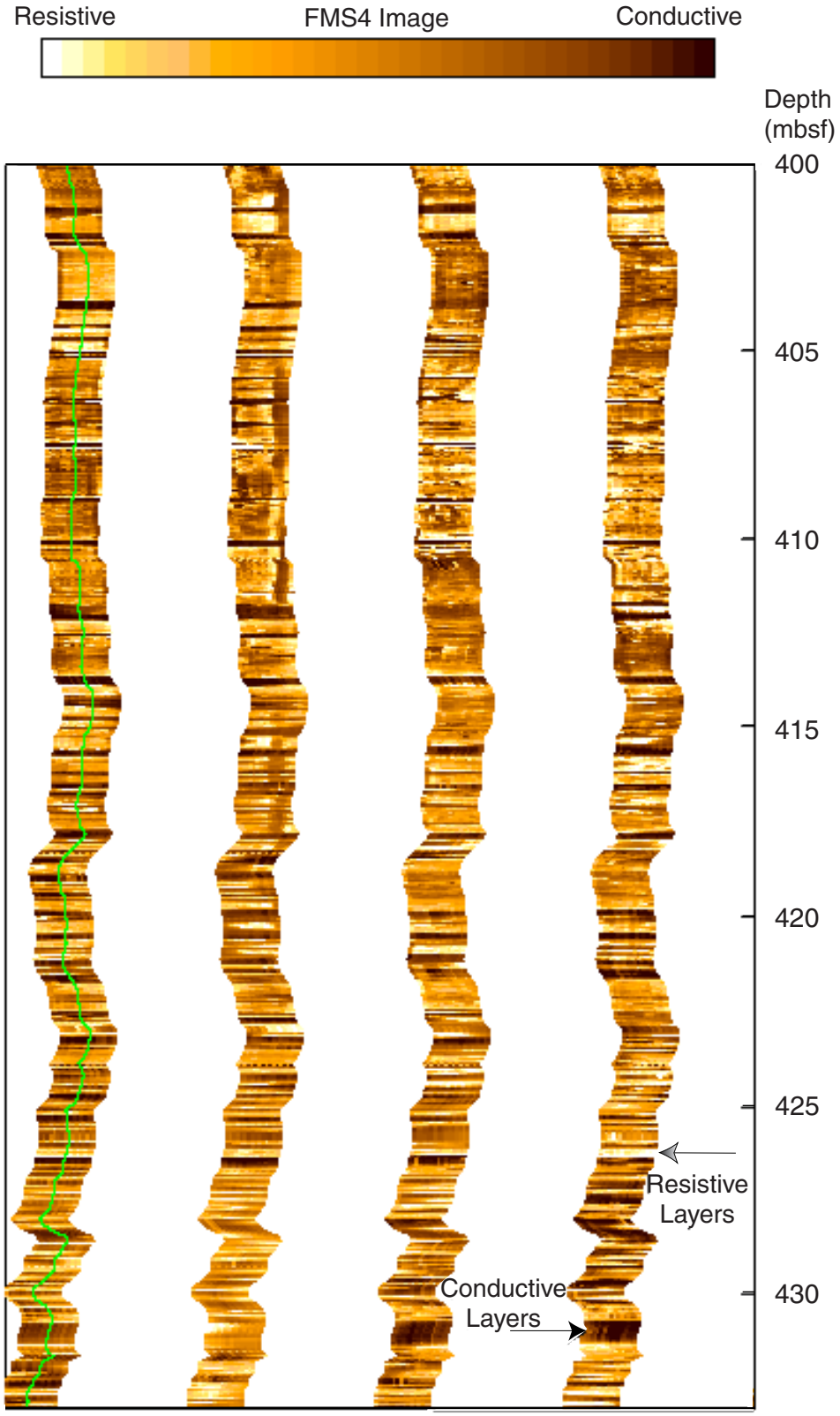

Table T1. Site 1146 coring summary. (See table notes. Continued on next two pages.)

Core	Date (March 1999)	Time (UTC + 8 hr)	Depth Top (mbsf)	Depth Bottom (mbsf)	Depth Top (mcd)	Length (m) Cored	Length (m) Recovered	Recovery (%)
184-1146A-								
1H	22	0515	0.0	3.9	0.00	3.9	3.85	98.7
2H	22	0550	3.9	13.4	4.85	9.5	9.43	99.3
3H	22	0625	13.4	22.9	15.05	9.5	9.77	102.8
4H	22	0730	22.9	32.4	25.50	9.5	9.66	101.7
5H	22	0800	32.4	41.9	35.55	9.5	9.85	103.7
6H	22	0847	41.9	51.4	45.15	9.5	9.04	95.2
7H	22	1000	51.4	60.9	53.90	9.5	9.99	105.2
8H	22	1045	60.9	70.4	63.90	9.5	9.23	97.2
9H	22	1125	70.4	79.9	74.00	9.5	9.89	104.1
10H	22	1210	79.9	89.4	83.70	9.5	9.72	102.3
11H	22	1310	89.4	98.9	94.75	9.5	10.13	106.6
12H	22	1350	98.9	108.4	104.70	9.5	9.73	102.4
13H	22	1430	108.4	117.9	114.90	9.5	9.92	104.4
14H	22	1510	117.9	127.4	125.25	9.5	9.80	103.2
15H	22	1555	127.4	136.9	135.60	9.5	9.95	104.7
16H	22	1655	136.9	146.4	145.75	9.5	7.99	84.1
17H	22	1735	146.4	155.9	156.75	9.5	9.38	98.7
18H	22	1820	155.9	165.4	165.95	9.5	9.56	100.6
19H	22	1905	165.4	174.9	175.55	9.5	9.94	104.6
20H	22	1950	174.9	184.4	185.33	9.5	9.84	103.6
21H	22	2040	184.4	193.9	196.75	9.5	9.42	99.2
22X	22	2135	193.9	203.0	206.95	9.1	9.77	107.4
23X	22	2210	203.0	212.7	216.90	9.7	9.80	101.0
24X	22	2240	212.7	222.4	227.40	9.7	9.69	99.9
25X	22	2310	222.4	232.1	237.10	9.7	0.00	0.0
26X	22	2345	232.1	241.7	246.65	9.6	9.88	102.9
27X	23	0020	241.7	251.3	257.80	9.6	9.70	101.0
28X	23	0110	251.3	260.9	268.94	9.6	9.72	101.3
29X	23	0145	260.9	270.6	279.00	9.7	9.53	98.3
30X	23	0225	270.6	280.2	289.05	9.6	9.69	100.9
31X	23	0305	280.2	289.8	298.65	9.6	9.77	101.8
32X	23	0345	289.8	299.5	308.25	9.7	9.74	100.4
33X	23	0425	299.5	309.1	318.25	9.6	9.60	100.0
34X	23	0505	309.1	318.7	328.05	9.6	9.74	101.5
35X	23	0545	318.7	328.4	338.40	9.7	9.66	99.6
36X	23	0635	328.4	338.1	350.50	9.7	9.87	101.8
37X	23	0715	338.1	347.7	360.85	9.6	9.88	102.9
38X	23	0810	347.7	357.3	371.45	9.6	9.87	102.8
39X	23	0850	357.3	366.9	381.10	9.6	9.75	101.6
40X	23	0935	366.9	376.5	391.70	9.6	9.79	102.0
41X	23	1040	376.5	386.1	402.12	9.6	9.79	102.0
42X	23	1140	386.1	395.7	410.42	9.6	9.43	98.2
43X	23	1250	395.7	405.3	420.17	9.6	9.40	97.9
44X	23	1350	405.3	414.9	429.37	9.6	9.30	96.9
45X	23	1455	414.9	424.5	439.32	9.6	9.84	102.5
46X	23	1605	424.5	434.1	450.42	9.6	9.99	104.1
47X	23	1750	434.1	443.7	462.02	9.6	9.89	103.0
48X	23	1905	443.7	453.4	471.91	9.7	9.89	102.0
49X	23	2015	453.4	463.0	480.54	9.6	9.73	101.4
50X	23	2130	463.0	472.4	489.69	9.4	9.70	103.2
51X	23	2250	472.4	482.0	499.59	9.6	9.76	101.7
52X	24	0005	482.0	491.6	510.44	9.6	9.83	102.4
53X	24	0105	491.6	501.2	521.49	9.6	9.75	101.6
54X	24	0220	501.2	510.8	531.94	9.6	8.20	85.4
55X	24	0320	510.8	520.4	541.44	9.6	9.91	103.2
56X	24	0425	520.4	529.9	553.45	9.5	9.16	96.4
57X	24	0535	529.9	539.4	564.40	9.5	9.93	104.5
58X	24	0645	539.4	549.1	575.27	9.7	9.89	102.0
59X	24	0750	549.1	558.7	584.83	9.6	9.87	102.8
60X	24	0855	558.7	568.3	594.80	9.6	9.86	102.7
61X	24	1010	568.3	578.0	604.29	9.7	9.95	102.6
62X	24	1115	578.0	587.6	614.79	9.6	9.50	99.0
63X	24	1230	587.6	597.2	623.94	9.6	9.82	102.3
64X	24	1410	597.2	607.0	633.19	9.8	9.92	101.2
					Totals:	607.0	603.85	99.5

Table T1 (continued).

Core	Date (March 1999)	Time (UTC + 8 hr)	Depth Top (mbsf)	Depth Bottom (mbsf)	Depth Top (mcd)	Length (m) Cored	Length (m) Recovered	Recovery (%)
184-1146B-								
1H	25	1525	0.0	7.3	0.00	7.3	7.28	99.7
2H	25	1550	7.3	16.8	8.55	9.5	9.36	98.5
3H	25	1640	16.8	26.3	19.10	9.5	9.18	96.6
4H	25	1730	26.3	35.8	28.80	9.5	9.22	97.1
5H	25	1815	35.8	45.3	39.30	9.5	9.29	97.8
6H	25	1905	45.3	54.8	48.70	9.5	9.85	103.7
7H	25	1955	54.8	64.3	58.80	9.5	8.86	93.3
8H	25	2050	64.3	73.8	68.50	9.5	9.95	104.7
9H	25	2135	73.8	83.3	78.60	9.5	9.56	100.6
10H	25	2225	83.3	92.8	88.90	9.5	9.91	104.3
11H	25	2315	92.8	102.3	99.70	9.5	8.39	88.3
12H	26	0005	102.3	111.8	109.30	9.5	9.80	103.2
13H	26	0050	111.8	121.3	119.50	9.5	9.54	100.4
14H	26	0140	121.3	130.8	129.90	9.5	9.78	103.0
15H	26	0220	130.8	140.3	139.60	9.5	7.82	82.3
16H	26	0315	140.3	149.8	149.70	9.5	9.99	105.2
17H	26	0400	149.8	159.3	159.75	9.5	9.35	98.4
18H	26	0450	159.3	168.8	169.05	9.5	9.91	104.3
19H	26	0545	168.8	178.3	179.55	9.5	7.92	83.4
20H	26	0630	178.3	187.8	190.25	9.5	9.89	104.1
21H	26	0720	187.8	197.3	200.85	9.5	9.58	100.8
22H	26	0835	197.3	206.8	210.65	9.5	9.74	102.5
23H	26	0940	206.8	216.3	221.54	9.5	8.54	89.9
24X	26	1115	216.3	225.9	232.05	9.6	9.76	101.7
25X	26	1200	225.9	235.5	241.05	9.6	9.53	99.3
26X	26	1310	235.5	245.1	251.05	9.6	9.71	101.2
					Totals:	245.1	241.71	98.6
184-1146C-								
Drilled			0.0	1.0				
1H	26	1600	1.0	10.5	0.90	9.5	9.68	101.9
2H	26	1640	10.5	20.0	11.10	9.5	9.65	101.6
3H	26	1725	20.0	29.5	20.80	9.5	9.92	104.4
4H	26	1815	29.5	39.0	31.95	9.5	9.55	100.5
5H	26	1900	39.0	48.5	41.20	9.5	9.71	102.2
6H	26	1945	48.5	58.0	51.35	9.5	9.63	101.4
7H	26	2040	58.0	67.5	60.65	9.5	9.85	103.7
8H	26	2120	67.5	77.0	70.95	9.5	9.49	99.9
9H	26	2210	77.0	86.5	81.05	9.5	9.86	103.8
10H	26	2300	86.5	96.0	91.20	9.5	9.65	101.6
11H	26	2350	96.0	105.5	101.95	9.5	9.91	104.3
12H	27	0040	105.5	115.0	111.90	9.5	9.74	102.5
13H	27	0123	115.0	124.5	121.70	9.5	9.88	104.0
14H	27	0210	124.5	134.0	132.10	9.5	9.26	97.5
15H	27	0300	134.0	143.5	142.25	9.5	9.98	105.1
16H	27	0345	143.5	153.0	152.20	9.5	8.99	94.6
17H	27	0445	153.0	162.5	161.95	9.5	8.94	94.1
18X	27	0615	162.5	172.1	170.35	9.6	9.50	99.0
19X	27	0655	172.1	181.7	182.40	9.6	9.80	102.1
20X	27	0735	181.7	191.3	193.10	9.6	9.76	101.7
21X	27	0815	191.3	200.9	202.95	9.6	9.63	100.3
22X	27	0855	200.9	210.5	213.80	9.6	9.60	100.0
23X	27	0930	210.5	220.1	224.25	9.6	9.35	97.4
Drilled			220.1	224.1				
24X	27	1020	224.1	233.7	236.15	9.6	9.72	101.3
25X	27	1105	233.7	243.3	245.25	9.6	9.79	102.0
26X	27	1145	243.3	252.9	257.30	9.6	9.65	100.5
27X	27	1230	252.9	262.5	266.74	9.6	9.65	100.5
28X	27	1315	262.5	272.1	280.35	9.6	9.77	101.8
29X	27	1400	272.1	281.8	289.25	9.7	9.81	101.1
30X	27	1445	281.8	291.5	298.10	9.7	9.80	101.0
31X	27	1530	291.5	301.2	308.50	9.7	9.75	100.5
32X	27	1615	301.2	305.7	318.20	4.5	6.09	135.3
33X	27	1700	305.7	315.3	323.55	9.6	7.32	76.3
34X	27	1745	315.3	324.9	333.15	9.6	9.82	102.3
35X	27	1840	324.9	334.6	343.80	9.7	9.83	101.3
36X	27	1930	334.6	344.2	356.25	9.6	9.98	104.0
37X	27	2020	344.2	353.8	367.30	9.6	9.94	103.5
38X	27	2110	353.8	363.5	377.95	9.7	9.74	100.4
39X	27	2200	363.5	373.1	388.80	9.6	9.82	102.3

Table T1 (continued).

Core	Date (March 1999)	Time (UTC + 8 hr)	Depth Top (mbsf)	Depth Bottom (mbsf)	Depth Top (mcd)	Length (m) Cored	Length (m) Recovered	Recovery (%)
40X	27	2245	373.1	382.8	398.76	9.7	9.94	102.5
41X	27	2330	382.8	392.4	407.62	9.6	9.85	102.6
42X	28	0015	392.4	402.0	415.97	9.6	9.71	101.2
43X	28	0100	402.0	411.6	425.17	9.6	9.76	101.7
44X	28	0145	411.6	421.2	434.92	9.6	9.85	102.6
45X	28	0230	421.2	430.6	444.92	9.4	9.37	99.7
46X	28	0345	430.6	440.2	456.92	9.6	9.82	102.3
47X	28	0450	440.2	449.8	467.57	9.6	9.93	103.4
48X	28	0600	449.8	459.5	477.39	9.7	9.84	101.4
49X	28	0710	459.5	468.7	486.49	9.2	9.89	107.5
50X	28	0810	468.7	478.3	494.59	9.6	9.93	103.4
51X	28	0910	478.3	487.9	506.04	9.6	9.90	103.1
52X	28	1020	487.9	497.5	515.74	9.6	9.92	103.3
53X	28	1125	497.5	507.1	524.59	9.6	9.92	103.3
54X	28	1230	507.1	516.7	535.47	9.6	9.85	102.6
55X	28	1345	516.7	526.4	545.00	9.7	8.95	92.3
56X	28	1500	526.4	536.0	556.45	9.6	9.77	101.8
57X	28	1600	536.0	545.6	568.74	9.6	9.39	97.8
58X	28	1705	545.6	555.3	581.55	9.7	9.90	102.1
59X	28	1815	555.3	564.9	590.91	9.6	9.67	100.7
60X	28	1920	564.9	574.6	600.94	9.7	9.55	98.5
61X	28	2020	574.6	584.2	610.54	9.6	9.89	103.0
62X	28	2200	584.2	593.8	621.84	9.6	9.78	101.9
63X	28	2320	593.8	603.5	631.39	9.7	9.97	102.8
					Cored:	598.5	606.16	101.3
					Drilled:	5.0		
					Total:	603.5		

Notes: UTC = Universal Time Coordinated. This table is also available in **ASCII format.**

Table T2. Site 1146 coring summary by section.

Core	Date (March 1999)	Time (UTC + 8 hr)	Core depth (mbsf) Top	Core depth (mbsf) Bottom	Length (m) Cored	Length (m) Recovered	Recovery (%)	Section	Length (m) Liner	Length (m) Curated	Section depth (mbsf) Top	Section depth (mbsf) Bottom	Top depth (mcd)	Catwalk samples	Comments
184-1146A-															
1H	22	0515	0.0	3.9	3.9	3.85	98.7								
								1	1.50	1.50	0.00	1.50	0.00		
								2	1.50	1.50	1.50	3.00	1.50	IW, IWPL	
								3	0.70	0.70	3.00	3.70	3.00	HS	
								CC(w/3)	0.15	0.15	3.70	3.85	3.70	PAL	
								Totals:	3.85	3.85					
2H	22	0550	3.9	13.4	9.5	9.43	99.3								
								1	1.50	1.50	3.90	5.40	4.85		
								2	1.50	1.50	5.40	6.90	6.35		
								3	1.50	1.50	6.90	8.40	7.85	IW, IWPL	
								4	1.50	1.50	8.40	9.90	9.35	HS	
								5	1.50	1.50	9.90	11.40	10.85		
								6	1.00	1.00	11.40	12.40	12.35		
								7	0.74	0.74	12.40	13.14	13.35		Liner damaged
								CC(w/7)	0.19	0.19	13.14	13.33	14.09	PAL	
								Totals:	9.43	9.43					
3H	22	0625	13.4	22.9	9.5	9.77	102.8								
								1	1.50	1.50	13.40	14.90	15.05		
								2	1.50	1.50	14.90	16.40	16.55		
								3	1.50	1.50	16.40	17.90	18.05	IW, IWPL	
								4	1.50	1.50	17.90	19.40	19.55	HS	
								5	1.50	1.50	19.40	20.90	21.05		
								6	1.50	1.50	20.90	22.40	22.55		
								7	0.57	0.57	22.40	22.97	24.05		
								CC(w/7)	0.20	0.20	22.97	23.17	24.62	PAL	
								Totals:	9.77	9.77					
4H	22	0730	22.9	32.4	9.5	9.66	101.7								Adara
								1	1.50	1.50	22.90	24.40	25.50		
								2	1.50	1.50	24.40	25.90	27.00		
								3	1.50	1.50	25.90	27.40	28.50	IW, IWPL	
								4	1.50	1.50	27.40	28.90	30.00	HS	
								5	1.50	1.50	28.90	30.40	31.50		
								6	1.50	1.50	30.40	31.90	33.00		
								7	0.38	0.38	31.90	32.28	34.50		
								CC(w/7)	0.28	0.28	32.28	32.56	34.88	PAL	
								Totals:	9.66	9.66					
5H	22	0800	32.4	41.9	9.5	9.85	103.7								
								1	1.50	1.50	32.40	33.90	35.55		
								2	1.50	1.50	33.90	35.40	37.05		
								3	1.50	1.50	35.40	36.90	38.55	IW, IWPL	
								4	1.50	1.50	36.90	38.40	40.05	HS	
								5	1.50	1.50	38.40	39.90	41.55		

Notes: UTC = Universal Time Coordinated. The notation "CC(w/x)" refers to the D-tube in which the core catcher is stored, where x is the section number (1–8 or CC). NS = no section, IWPL = interstitial waters plastic Lin, IW = interstitial waters, HS = headspace, PAL = paleontology, IWGM = interstitial waters glass Matsumoto, MAT = Matsumoto, LEV = Leventhal. This table is also available in **ASCII format.**

Table T3. Site 1146 composite depths. (See table note. Continued on next page.)

Core	Depth (mbsf)	Cumulative offset (m)	Depth (mcd)
184-1146A-			
Continuous mcd:			
1H	0.0	0.00	0.00
2H	3.9	0.95	4.85
3H	13.4	1.65	15.05
4H	22.9	2.60	25.50
5H	32.4	3.15	35.55
6H	41.9	3.25	45.15
7H	51.4	2.50	53.90
8H	60.9	3.00	63.90
9H	70.4	3.60	74.00
10H	79.9	3.80	83.70
11H	89.4	5.35	94.75
12H	98.9	5.80	104.70
13H	108.4	6.50	114.90
14H	117.9	7.35	125.25
15H	127.4	8.20	135.60
16H	136.9	8.85	145.75
17H	146.4	10.35	156.75
18H	155.9	10.05	165.95
19H	165.4	10.15	175.55
20H	174.9	10.43	185.33
21H	184.4	12.35	196.75
22X	193.9	13.05	206.95
23X	203.0	13.90	216.90
24X	212.7	14.70	227.40
25X	222.4	14.70	237.10
26X	232.1	14.55	246.65
Floating mcd:			
27X	241.7	16.10	257.80
28X	251.3	17.64	268.94
29X	260.9	18.10	279.00
30X	270.6	18.45	289.05
31X	280.2	18.45	298.65
32X	289.8	18.45	308.25
33X	299.5	18.75	318.25
34X	309.1	18.95	328.05
35X	318.7	19.70	338.40
36X	328.4	22.10	350.50
37X	338.1	22.75	360.85
38X	347.7	23.75	371.45
39X	357.3	23.80	381.10
40X	366.9	24.80	391.70
41X	376.5	25.62	402.12
42X	386.1	24.32	410.42
43X	395.7	24.47	420.17
44X	405.3	24.07	429.37
45X	414.9	24.42	439.32
46X	424.5	25.92	450.42
47X	434.1	27.92	462.02
48X	443.7	28.21	471.91
49X	453.4	27.14	480.54
50X	463.0	26.69	489.69
51X	472.4	27.19	499.59
52X	482.0	28.44	510.44
53X	491.6	29.89	521.49
54X	501.2	30.74	531.94
55X	510.8	30.64	541.44
56X	520.4	33.05	553.45
57X	529.9	34.50	564.40
58X	539.4	35.87	575.27
59X	549.1	35.73	584.83
60X	558.7	36.10	594.80
61X	568.3	35.99	604.29
62X	578.0	36.79	614.79
63X	587.6	36.34	623.94
64X	597.2	35.99	633.19

Core	Depth (mbsf)	Cumulative offset (m)	Depth (mcd)
184-1146B-			
Continuous mcd:			
1H	0.0	0.00	0.00
2H	7.3	1.25	8.55
3H	16.8	2.30	19.10
4H	26.3	2.50	28.80
5H	35.8	3.50	39.30
6H	45.3	3.40	48.70
7H	54.8	4.00	58.80
8H	64.3	4.20	68.50
9H	73.8	4.80	78.60
10H	83.3	5.60	88.90
11H	92.8	6.90	99.70
12H	102.3	7.00	109.30
13H	111.8	7.70	119.50
14H	121.3	8.60	129.90
15H	130.8	8.80	139.60
16H	140.3	9.40	149.70
17H	149.8	9.95	159.75
18H	159.3	9.75	169.05
19H	168.8	10.75	179.55
20H	178.3	11.95	190.25
21H	187.8	13.05	200.85
22H	197.3	13.35	210.65
23H	206.8	14.74	221.54
24X	216.3	15.75	232.05
25X	225.9	15.15	241.05
26X	235.5	15.55	251.05
184-1146C-			
Continuous mcd:			
1H	1.0	–0.10	0.90
2H	10.5	0.60	11.10
3H	20.0	0.80	20.80
4H	29.5	2.45	31.95
5H	39.0	2.20	41.20
6H	48.5	2.85	51.35
7H	58.0	2.65	60.65
8H	67.5	3.45	70.95
9H	77.0	4.05	81.05
10H	86.5	4.70	91.20
11H	96.0	5.95	101.95
12H	105.5	6.40	111.90
13H	115.0	6.70	121.70
14H	124.5	7.60	132.10
15H	134.0	8.25	142.25
16H	143.5	8.70	152.20
17H	153.0	8.95	161.95
18X	162.5	7.85	170.35
19X	172.1	10.30	182.40
20X	181.7	11.40	193.10
21X	191.3	11.65	202.95
22X	200.9	12.90	213.80
23X	210.5	13.75	224.25
24X	224.1	12.05	236.15
25X	233.7	11.55	245.25
26X	243.3	14.00	257.30
Floating mcd:			
27X	252.9	13.84	266.74
28X	262.5	17.85	280.35
29X	272.1	17.15	289.25
30X	281.8	16.30	298.10
31X	291.5	17.00	308.50
32X	301.2	17.00	318.20
33X	305.7	17.85	323.55
34X	315.3	17.85	333.15
35X	324.9	18.90	343.80

Table T3 (continued).

Core	Depth (mbsf)	Cumulative offset (m)	Depth (mcd)
36X	334.6	21.65	356.25
37X	344.2	23.10	367.30
38X	353.8	24.15	377.95
39X	363.5	25.30	388.80
40X	373.1	25.66	398.76
41X	382.8	24.82	407.62
42X	392.4	23.57	415.97
43X	402.0	23.17	425.17
44X	411.6	23.32	434.92
45X	421.2	23.72	444.92
46X	430.6	26.32	456.92
47X	440.2	27.37	467.57
48X	449.8	27.59	477.39
49X	459.5	26.99	486.49
50X	468.7	25.89	494.59
51X	478.3	27.74	506.04
52X	487.9	27.84	515.74
53X	497.5	27.09	524.59
54X	507.1	28.37	535.47
55X	516.7	28.30	545.00
56X	526.4	30.05	556.45
57X	536.0	32.74	568.74
58X	545.6	35.95	581.55
59X	555.3	35.61	590.91
60X	564.9	36.04	600.94
61X	574.6	35.94	610.54
62X	584.2	37.64	621.84
63X	593.8	37.59	631.39

Note: This table is also available in **ASCII format.**

Table T4. Site 1146 splice tie points. (See table note. Continued on next page.)

Hole, core, section, interval (cm)	Depth (mbsf)	Depth (mcd)		Hole, core, section, interval (cm)	Depth (mbsf)	Depth (mcd)
Continuous splice:						
1146B-1H-1, 0	0.00	0.00				
1146B-1H-5, 17	6.17	6.17	Tie to	1146C-1H-4, 77	6.27	6.17
1146C-1H-7, 17	10.17	10.07	Tie to	1146B-2H-1, 152	8.82	10.07
1146B-2H-5, 92	14.22	15.47	Tie to	1146C-2H-3, 137	14.87	15.47
1146C-2H-7, 37	19.87	20.47	Tie to	1146B-3H-1, 137	18.17	20.47
1146B-3H-5, 7	22.87	25.17	Tie to	1146C-3H-3, 137	24.37	25.17
1146C-3H-6, 102	28.52	29.32	Tie to	1146B-4H-1, 52	26.82	29.32
1146B-4H-5, 82	33.12	35.62	Tie to	1146C-4H-3, 67	33.17	35.62
1146C-4H-7, 37	38.87	41.32	Tie to	1146C-5H-1, 12	39.12	41.32
1146C-5H-6, 36	46.86	49.06	Tie to	1146B-6H-1, 36	45.66	49.06
1146B-6H-6, 142	54.22	57.62	Tie to	1146C-6H-5, 27	54.77	57.62
1146C-6H-7, 12	57.62	60.47	Tie to	1146B-7H-2, 17	56.47	60.47
1146B-7H-6, 12	62.42	66.42	Tie to	1146C-7H-4, 127	63.77	66.42
1146C-7H-7, 42	67.42	70.07	Tie to	1146B-8H-2, 7	65.87	70.07
1146B-8H-5, 8	70.38	74.58	Tie to	1146C-8H-3, 62.5	71.13	74.58
1146C-8H-6, 127	76.27	79.72	Tie to	1146B-9H-1, 112	74.92	79.72
1146B-9H-6, 72	82.02	86.82	Tie to	1146C-9H-4, 127	82.77	86.82
1146C-9H-6, 52	85.02	89.07	Tie to	1146B-10H-1, 17	83.47	89.07
1146B-10H-5, 87	90.17	95.77	Tie to	1146C-10H-4, 7	91.07	95.77
1146C-10H-6, 122	95.22	99.92	Tie to	1146B-11H-1, 22	93.02	99.92
1146B-11H-5, 137	100.17	107.07	Tie to	1146C-11H-4, 62	101.12	107.07
1146C-11H-7, 22	105.22	111.17	Tie to	1146B-12H-2, 37	104.17	111.17
1146B-12H-5, 72	109.02	116.02	Tie to	1146C-12H-3, 112	109.62	116.02
1146C-12H-6, 102	114.02	120.42	Tie to	1146B-13H-1, 92	112.72	120.42
1146B-13H-5, 142	119.22	126.92	Tie to	1146C-13H-4, 72	120.22	126.92
1146C-13H-6, 142	123.92	130.62	Tie to	1146B-14H-1, 72	122.02	130.62
1146B-14H-4, 137	127.17	135.77	Tie to	1146C-14H-3, 67	128.17	135.77
1146C-14H-6, 92	132.92	140.52	Tie to	1146B-15H-1, 92	131.72	140.52
1146B-15H-4, 12	135.42	144.22	Tie to	1146C-15H-2, 47	135.97	144.22
1146C-15H-6, 32	141.82	150.07	Tie to	1146B-16H-1, 37	140.67	150.07
1146B-16H-6, 27	148.07	157.47	Tie to	1146C-16H-4, 77	148.77	157.47
1146C-16H-6, 102	152.02	160.72	Tie to	1146B-17H-1, 97	150.77	160.72
1146B-17H-5, 102	156.82	166.77	Tie to	1146A-18H-1, 82	156.72	166.77
1146A-18H-6, 92	164.32	174.37	Tie to	1146B-18H-4, 79.5	164.62	174.37
1146B-18H-7, 22	168.52	178.27	Tie to	1146A-19H-2, 122	168.12	178.27
1146A-19H-7, 47	174.87	185.02	Tie to	1146C-19X-2, 112	174.72	185.02
1146C-19X-6, 77	180.37	190.67	Tie to	1146B-20H-1, 42	178.72	190.67
1146B-20H-6, 142	187.22	199.17	Tie to	1146C-20X-5, 7	187.77	199.17
1146C-20X-7, 28	190.98	202.38	Tie to	1146B-21H-2, 137	189.33	202.38
1146B-21H-6, 42	194.37	207.42	Tie to	1146C-21X-3, 147	195.77	207.42
1146C-21X-7, 32	200.32	211.97	Tie to	1146B-22H-1, 132	198.62	211.97
1146B-22H-6, 62	205.42	218.77	Tie to	1146A-23X-2, 37	204.87	218.77
1146A-23X-6, 112	211.62	225.52	Tie to	1146C-23X-1, 127	211.77	225.52
1146C-23X-5, 82	217.32	231.07	Tie to	1146A-24X-3, 64.5	216.37	231.07
1146A-24X-4, 32	217.52	232.22	Tie to	1146B-24X-1, 17	216.47	232.22
1146B-24X-5, 12	222.42	238.17	Tie to	1146C-24X-2, 52	226.12	238.17
1146C-24X-7, 22	233.32	245.37	Tie to	1146C-25X-1, 12	233.82	245.37
1146C-25X-6, 22	241.42	252.97	Tie to	1146B-26X-2, 42	237.42	252.97
1146B-26X-6, 82	243.82	259.37	Tie to	1146C-26X-2, 52	245.37	259.37
1146C-26X-7, 40	252.70	266.70				
Floating splice:						
1146C-27X-1, 0	252.90	266.74				
1146C-27X-6, 62	261.02	274.86	Tie to	1146A-28X-4, 142	257.22	274.86
1146A-28X-7, 44	260.74	278.38	Append to	1146A-29X-1, 0	260.90	279.00
1146A-29X-2, 52	262.92	281.02	Tie to	1146C-28X-1, 67	263.17	281.02
1146C-28X-7, 27	271.77	289.62	Tie to	1146C-29X-1, 37	272.47	289.62
1146C-29X-7, 16	281.26	298.41	Tie to	1146C-30X-1, 30.5	282.11	298.41
1146C-30X-7, 48	291.28	307.58	Append to	1146A-32X-1, 0	289.80	308.25
1146A-32X-7, 28	299.08	317.53	Append to	1146A-33X-1, 0	299.50	318.25
1146A-33X-7, 36	308.86	327.61	Append to	1146A-34X-1, 0	309.10	328.05
1146A-34X-6, 82	317.42	336.37	Tie to	1146C-34X-3, 19.5	318.52	336.37
1146C-34X-5, 92	322.22	340.07	Tie to	1146A-35X-2, 17	320.37	340.07
1146A-35X-7, 22	327.92	347.62	Tie to	1146C-35X-3, 79.5	328.72	347.62
1146C-35X-6, 137	333.77	352.67	Tie to	1146A-36X-2, 64.5	330.57	352.67
1146A-36X-6, 132	337.22	359.32	Tie to	1146C-36X-3, 7	337.67	359.32
1146C-36X-6, 27	342.37	364.02	Tie to	1146A-37X-3, 17	341.27	364.02

Table T4 (continued).

Hole, core, section, interval (cm)	Depth (mbsf)	Depth (mcd)		Hole, core, section, interval (cm)	Depth (mbsf)	Depth (mcd)
1146A-37X-6, 77	346.37	369.12	Tie to	1146C-37X-2, 29.5	346.02	369.12
1146C-37X-6, 42	352.12	375.22	Tie to	1146A-38X-3, 74.5	351.47	375.22
1146A-38X-5, 82	354.52	378.27	Tie to	1146C-38X-1, 32	354.12	378.27
1146C-38X-4, 122	359.52	383.67	Tie to	1146A-39X-2, 107	359.87	383.67
1146A-39X-6, 27	365.07	388.87	Tie to	1146C-39X-1, 7	363.57	388.87
1146C-39X-5, 142	370.92	396.22	Tie to	1146A-40X-3, 152	371.42	396.22
1146A-40X-5, 132	374.22	399.02	Tie to	1146C-40X-1, 25.5	373.36	399.02
1146C-40X-4, 17	377.77	403.43	Tie to	1146A-41X-1, 130.5	377.81	403.43
1146A-41X-6, 87	384.87	410.49	Tie to	1146A-42X-1, 7	386.17	410.49
1146A-42X-6, 97	394.57	418.89	Tie to	1146C-42X-2, 142	395.32	418.89
1146C-42X-5, 127	399.67	423.24	Tie to	1146A-43X-3, 4.5	398.77	423.24
1146A-43X-6, 148	404.68	429.15	Append to	1146A-44X-1, 0	405.30	429.37
1146A-44X-5, 102	412.32	436.39	Tie to	1146C-44X-1, 147	413.07	436.39
1146C-44X-5, 132	418.92	442.24	Tie to	1146A-45X-2, 142	417.82	442.24
1146A-45X-5, 47	421.37	445.79	Tie to	1146C-45X-1, 87	422.07	445.79
1146C-45X-6, 17	428.87	452.59	Tie to	1146A-46X-2, 67	426.67	452.59
1146A-46X-5, 62	431.12	457.04	Tie to	1146C-46X-1, 12	430.72	457.04
1146C-46X-5, 42	437.02	463.34	Tie to	1146A-47X-1, 132	435.42	463.34
1146A-47X-6, 22	441.82	469.74	Tie to	1146C-47X-2, 64.5	442.37	469.74
1146C-47X-5, 107	447.27	474.64	Tie to	1146A-48X-2, 121	446.43	474.64
1146A-48X-6, 122	452.42	480.63	Tie to	1146C-48X-3, 22.5	453.04	480.63
1146C-48X-6, 17	457.47	485.06	Tie to	1146A-49X-3, 152	457.92	485.06
1146A-49X-6, 102	461.92	489.06	Tie to	1146C-49X-2, 104.5	462.07	489.06
1146C-49X-5, 57	466.07	493.06	Tie to	1146A-50X-3, 34.5	466.37	493.06
1146A-50X-6, 32	470.82	497.51	Tie to	1146C-50X-2, 142	471.62	497.51
1146C-50X-6, 127	477.47	503.36	Tie to	1146A-51X-3, 74.5	476.17	503.36
1146A-51X-6, 77	480.67	507.86	Tie to	1146C-51X-2, 29.5	480.12	507.86
1146C-51X-6, 112	486.92	514.66	Tie to	1146A-52X-3, 122	486.22	514.66
1146A-52X-5, 137	489.37	517.81	Tie to	1146C-52X-2, 57	489.97	517.81
1146C-52X-6, 62	496.02	523.86	Tie to	1146A-53X-2, 87	493.97	523.86
1146A-53X-5, 132	498.92	528.81	Tie to	1146C-53X-3, 122	501.72	528.81
1146C-53X-7, 12	506.62	533.71	Tie to	1146A-54X-2, 27	502.97	533.71
1146A-54X-5, 62	507.82	538.56	Tie to	1146C-54X-3, 7	510.19	538.56
1146C-54X-6, 127	515.89	544.26	Tie to	1146A-55X-2, 129.5	513.62	544.26
1146A-55X-3, 132	515.12	545.76	Tie to	1146C-55X-1, 75.5	517.46	545.76
1146C-55X-6, 117	525.37	553.67	Tie to	1146A-56X-1, 19.5	520.62	553.67
1146A-56X-3, 77	524.17	557.22	Tie to	1146C-56X-1, 74.5	527.17	557.22
1146C-56X-6, 142	535.32	565.37	Tie to	1146A-57X-1, 94.5	530.87	565.37
1146A-57X-4, 87	535.27	569.77	Tie to	1146C-57X-1, 101	537.03	569.77
1146C-57X-6, 72	544.23	576.97	Tie to	1146A-58X-2, 19	541.10	576.97
1146A-58X-6, 82	547.72	583.59	Tie to	1146C-58X-2, 52.5	547.64	583.59
1146C-58X-6, 117	554.27	590.22	Tie to	1146A-59X-4, 87.5	554.49	590.22
1146A-59X-6, 22	556.82	592.55	Tie to	1146C-59X-2, 12.5	556.94	592.55
1146C-59X-5, 112	562.42	598.03	Tie to	1146A-60X-3, 19.5	561.93	598.03
1146A-60X-6, 142	567.66	603.76	Tie to	1146C-60X-2, 129.5	567.72	603.76
1146C-60X-6, 32	572.72	608.76	Tie to	1146A-61X-3, 147	572.77	608.76
1146A-61X-6, 62	576.42	612.41	Tie to	1146C-61X-2, 34.5	576.47	612.41
1146C-61X-7, 42	584.02	619.96	Tie to	1146A-62X-4, 64.5	583.17	619.96
1146A-62X-5, 122	585.22	622.01	Tie to	1146C-62X-1, 17	584.37	622.01
1146C-62X-6, 92	592.62	630.26	Tie to	1146A-63X-5, 29.5	593.92	630.26
1146A-63X-6, 127	596.37	632.71	Tie to	1146C-63X-1, 129.5	595.12	632.71
1146C-63X-7, 52	603.32	640.91				

Note: This table is also available in **ASCII format.**

Table T5. Light-colored, carbonate-rich layers observed in cores recovered at Site 1146.

Inferred isotopic stage	Core, section, interval (cm)	Top		Bottom		Thickness (m)	Remarks/comments
		Depth (mbsf)	Depth (mcd)	Depth (mbsf)	Depth (mcd)		
	184-1146A-						
Holocene	1H-1, 10	0.10	0.10	0.10	0.10	ND	
	7H-3, 120, to 7H-4, 70	55.60	58.10	56.60	59.10	1.00	
	8H-4, 40, to 8H-5, 60	65.80	68.80	67.50	70.50	1.70	With light gray ash layer at interval 1146A-8H-5, 17-19 cm
	9H-5, 30, to 9H-6, 100	76.70	80.30	78.90	82.50	2.20	
	10H-5, 90-130	86.80	90.60	87.20	91.00	0.40	
	184-1146B-						
Holocene	1H-1, 11-120	0.11	0.11	1.20	1.20	1.09	
Stage 5	3H-4, 70, to 3H-5, 20	22.00	24.30	23.00	25.30	1.00	
Stage 7	5H-3, 0-60	38.80	42.30	39.40	42.90	0.60	
Stage 9	5H-5, 10-100	41.90	45.40	42.80	46.30	0.90	
	6H-4, 0-125	49.80	53.20	51.05	54.45	1.25	No green clay layers
	6H-7, 45, to 7H-1, 70	54.75	58.15	55.50	59.50	0.75	Green clay layers only in the lower part
	8H-2, 0-80	65.80	70.00	66.60	70.80	0.80	
	9H-1, 135, to 9H-3, 112	75.15	79.95	77.92	82.72	2.77	
	9H-4, 132, to 9H-5, 90	79.62	84.42	80.70	85.50	1.08	
	10H-2, 9-91	84.89	90.49	85.71	91.31	0.82	
	10H-3, 16-115	86.46	92.06	87.45	93.05	0.99	
	10H-4, 5-78	87.85	93.45	88.58	94.18	0.73	
	11H-4, 10, to 11H-5, 101	97.40	104.30	99.81	106.71	2.41	
	12H-3, 99, to 12H-5, 18	106.29	113.29	108.48	115.48	2.19	
	13H-1, 0, to 13H-2, 44	111.80	119.50	113.74	121.44	1.94	
	14H-1, 0-56	121.30	129.90	121.86	130.46	0.56	
	14H-2, 19-66	122.99	131.59	123.46	132.06	0.47	
	14H-5, 6-86	127.36	135.96	128.16	136.76	0.80	
	15H-1, 31-97	131.11	139.91	131.77	140.57	0.66	
	17H-2, 25-40	151.55	161.50	151.70	161.65	0.15	
	17H-2, 54, to 17H-3, 35	151.84	161.79	153.15	163.10	1.31	
	17H-4, 19-130	154.49	164.44	155.60	165.55	1.11	
	184-1146C-						
Holocene	1H-1, 0-113	1.00	0.90	2.13	2.03	1.13	
Stage 5	3H-3, 76, to 3H-4, 45	23.76	24.56	24.95	25.75	1.19	
Stage 7	5H-1, 20-121	39.20	41.40	40.21	42.41	1.01	No increase in green layers
Stage 9	5H-3, 87, to 5H-4, 45	42.87	45.07	43.95	46.15	1.08	
	6H-5, 50, to 6H-6, 40	55.00	57.85	56.40	59.25	1.40	
	7H-6, 33, to 8H-1, 41	65.83	68.48	67.91	71.36	2.08	No increase in foraminifers
	8H-7, 6, to 9H-2, 20	76.56	80.01	78.70	82.75	2.14	
	9H-3, 80, to 9H-4, 23	80.80	84.85	81.73	85.78	0.93	
	10H-2, 94-137	88.94	93.64	89.37	94.07	0.43	
	11H-2, 84, to 11H-4, 37	98.34	104.29	100.87	106.82	2.53	
	12H-2, 18, to 12H-3, 54	107.18	113.58	109.04	115.44	1.86	
	12H-4, 88, to 12H-5, 69	110.88	117.28	112.19	118.59	1.31	
	12H-5, 110, to 12H-6, 138	112.60	119.00	114.38	120.78	1.78	
	13H-4, 5-50	119.55	126.25	120.00	126.70	0.45	
	13H-6, 30-80	122.80	129.50	123.30	130.00	0.50	
	14H-1, 50-95	125.00	132.60	125.45	133.05	0.45	
	14H-2, 30-110	126.30	133.90	127.10	134.70	0.80	
	14H-4, 55, to 14H-5, 25	129.55	137.15	130.75	138.35	1.20	
	15H-2, 10-135	135.60	143.85	136.85	145.10	1.25	
	15H-5, 30-110	140.30	148.55	141.10	149.35	0.80	
	16H-4, 11-112	148.11	156.81	149.12	157.82	1.01	
	17H-1, 2-110	153.02	161.97	154.10	163.05	1.08	
	17H-2, 90, to 17H-3, 70	155.40	164.35	156.70	165.65	1.30	
	21X-4, 5-60	195.85	207.50	196.40	208.05	0.55	
	22X-1, 0-130	200.90	213.80	202.20	215.10	1.30	
	22X-3, 15-70	204.05	216.95	204.60	217.50	0.55	
	22X-6, 7, to 22X-7, 47	208.47	221.37	210.07	222.97	1.60	
	23X-2, 33-138	212.33	226.08	213.38	227.13	1.05	
	23X-4, 58-150	215.58	229.33	216.50	230.25	0.92	
	23X-5, 13-103	216.63	230.38	217.53	231.28	0.90	

Note: ND = not determined.

Table T6. Volcanic ash layers observed at Site 1146.

Core, section, interval (cm)	Top Depth (mbsf)	Top Depth (mcd)	Bottom Depth (mbsf)	Bottom Depth (mcd)	Thickness (cm)	Remarks/comments
184-1146A-						
2H-2, 102	6.42	7.37	6.42	7.37	<1	Isolated black pumice clast
6H-1, 76-79	42.66	45.91	42.69	45.94	3	Strongly bioturbated ash layer
7H-6, 91-93	59.81	62.31	59.83	62.33	2	Light gray graded ash
8H-5, 17-19	67.07	70.07	67.09	70.09	2	Light gray graded ash
9H-7, 28-29	79.68	83.28	79.69	83.29	1	Graded fine-grained black ash layer
12H-1, 47-48	99.37	105.17	99.38	105.18	1	Black pumic fragment
12H-7, 27-28	108.17	113.97	108.18	113.98	1	White pumice fragment
19H-5, 10-14	171.50	181.65	171.54	181.69	4	Ash layer with basal black pumice fragments
26X-CC, 30-33	241.87	256.42	241.90	256.45	3	Dark gray altered ash layer with zeolites
33X-6, 98-99	307.98	326.73	307.99	326.74	1	Green ash layer at the top of a foraminifer turbidite
36X-5, 143	335.83	357.93	335.83	357.93	<1	Green, volcanic glass layer ending a foraminifer turbidite
184-1146B-						
2H-2, 30	9.10	10.35	9.10	10.35	<1	
7H-3, 49-50	58.29	62.29	58.30	62.30	1	
12H-5, 57-60	108.87	115.87	108.90	115.90	3	Dark ash layer with 1-cm-long glass shards
12H-6, 133	111.13	118.13	111.13	118.13	<1	Ash-filled bioturbations
19H-2, 58-62	170.88	181.63	170.92	181.67	4	Black ash layer with basal pumice fragments
26X-4, 95-98	240.95	256.50	240.98	256.53	3	Graded volcanic ash with pyrite
184-1146C-						
3H-3, 55-57	23.55	24.35	23.57	24.37	2	Pumice lump
5H-4, 9-11	43.59	45.79	43.61	45.81	2	Light gray ash layer
7H-2, 3-7	59.53	62.18	59.57	62.22	4	Light gray ash layer
7H-7, 30-31	67.30	69.95	67.31	69.96	1	Bioturbated ash layer
9H-2, 103-104	79.53	83.58	79.54	83.59	1	Light gray ash layer
9H-4, 65-68	82.15	86.20	82.18	86.23	3	Black patch with volcanic fragment
19X-1, 0-4	172.10	182.40	172.14	182.44	4	Black ash layer with basal pumice fragments
25X-4, 1-11	238.21	249.76	238.31	249.86	10	Dark interval between 1 and 11 cm containing ~35% of altered and fresh volcanic glass mixed with clay (and a lesser amount of nannofossils)
29X-2, 142-145	275.02	292.17	275.05	292.2	3	White ash layer on top of a foraminifer turbidite, with gradational upper boundary

Table T7. Summary of biohorizons at Site 1146. (**See table notes.** Continued on next page.)

Code	Events	Depth range of stratigraphic datums: Top: Core, section, interval (cm)	Top: Depth (mbsf)	Top: Depth (mcd)	Bottom: Core, section, interval (cm)	Bottom: Depth (mbsf)	Bottom: Depth (mcd)	Average depth (mcd)	Age (Ma)	Average sedimentation rate (m/m.y.)
		184-1146A-			184-1146A-					
CN	FO *E. huxleyi* acme	2H-CC, 12-19	13.30	**14.25**	3H-CC, 13-20	23.14	24.79	19.52	0.09	
PF	LO pink *G. ruber*	3H-CC, 13-20	23.14	24.79	4H-CC, 21-28	32.53	**35.13**	29.96	0.12	
CN	FO *E. huxleyi*	7H-CC, 36-43	61.36	**63.86**	8H-CC, 0-7	70.10	73.10	68.48	0.26	192.7
PF	FO pink *G. ruber*	7H-CC, 36-43	61.36	**63.86**	8H-CC, 0-7	70.10	73.10	68.48	0.40	
CN	LO *P. lacunosa**	9H-CC, 26-33	80.26	83.86	10H-CC, 26-31	89.60	**93.40**	88.63	0.46	
BF	LO *Stilostomella*	10H-CC, 26-31	89.60	93.40	11H-CC, 44-50	99.50	**104.85**	99.12	0.75	
CN	LO *R.asanoi*	12H-CC, 26-32	108.60	114.40	13H-CC, 22-28	118.33	**124.83**	119.62	0.83	
CN	FO *R. asanoi*	14H-CC, 20-26	127.67	**135.02**	15H-CC, 25-32	137.32	145.52	140.27	1.16	
CN	LO *C. macintyrei*	17H-CC, 32-38	155.75	166.10	18H-CC, 24-29	165.44	**175.49**	170.79	1.59	
PF	LO *G. fistulosus*	17H-CC, 32-38	155.75	166.10	18H-CC, 24-29	165.44	**175.49**	170.79	1.77	60.4
CN	LO *D. brouweri*	19H-CC, 20-26	175.31	185.46	20H-CC, 25-32	184.71	**195.14**	190.30	1.95	
PF	FO *G. truncatulinoides*	19H-CC, 20-26	175.31	**185.46**	20H-CC, 25-32	184.71	195.14	190.30	2.00	
PF	LO *G. multicamerata*	20H-CC, 25-32	184.71	195.14	21H-CC, 0-5	193.80	**206.15**	200.64	2.40	
CN	LO *D. pentaradiatus*	21H-CC, 0-5	193.80	206.15	22X-CC, 30-35	203.65	**216.70**	211.42	2.52	
CN	LO *D. tamalis**	23X-CC, 22-27	212.78	226.68	24X-CC, 28-33	222.37	**237.07**	231.87	2.83	
					184-1146C-					
PF	LO *G. altispira*	24X-CC, 28-33	222.37	237.07	24X-CC, 24-31	233.79	**245.84**	241.47	3.09	
PF	LO *S. seminulina*	24X-CC, 28-33	222.37	237.07	24X-CC, 24-31	233.79	**245.84**	241.47	3.12	
		184-1146B-			184-1146B-					
CN	LO *Sphenolithus* spp.	24X-CC, 27-34	226.03	241.78	25X-CC, 13-21	235.39	**250.54**	246.20	3.66	
		184-1146C-			184-1146C-					
PF	FO *G. tosaensis*	24X-CC, 24-31	233.79	**245.84**	25X-CC, 20-27	243.46	255.01	250.46	3.35	
		184-1146A-			184-1146A-					
CN	LO *R. pseudoumbilicus*	26X-CC, 35-41	241.95	256.50	27X-CC, 23-30	251.37	**267.47**	262.02	3.82	
PF	LO *G. margaritae*	26X-CC, 35-41	241.95	256.50	27X-CC, 23-30	251.37	**267.47**	262.02	3.58	
PF	*Pullenitina* coiling change	26X-CC, 35-41	241.95	256.50	27X-CC, 23-30	251.37	267.47	262.02	3.95	
PF	LO *G. nepenthes*	27X-CC, 23-30	251.37	267.47	28X-CC, 16-23	260.99	278.63	273.08	4.20	
CN	LO *Amaurolithus* spp.	28X-CC, 16-23	260.99	278.63	29X-CC, 16-23	270.40	**288.50**	283.60	4.8	
CN	LO *C. acutus*	29X-CC, 16-23	270.40	288.50	30X-CC, 37-44	280.26	**298.71**	293.64	4.99	
CN	LO *T. rugosus*	30X-CC, 37-44	280.26	298.71	31X-CC, 23-30	289.94	**308.39**	303.58	5.23	
CN	LO *D. quinqueramus*	31X-CC, 23-30	289.94	308.39	32X-CC, 38-45	299.51	**317.96**	313.21	5.54	
CN	LO *A. amplificus*	33X-CC, 15-22	309.07	327.82	34X-CC, 24-30	318.81	**337.76**	332.82	5.99	
PF	FO *S. dehiscens*	34X-CC, 23-30	318.81	**337.76**	35X-CC, 17-24	328.33	348.03	342.93	5.54	
PF	FO *G. tumida*	35X-CC, 17-24	328.33	**348.03**	36X-CC, 37-44	338.24	360.34	354.22	5.82	
CN	FO *A. amplificus*	35X-CC, 17-24	328.33	**348.03**	36X-CC, 37-44	338.24	360.34	354.22	6.76	28.7
PF	FO *G. conglobatus*	36X-CC, 37-44	338.24	**360.34**	37X-CC, 35-41	347.95	370.70	365.55	6.20	
CN	FO *A. primus*	36X-CC, 37-44	338.24	**360.34**	37X-CC, 35-41	347.95	370.70	365.55	7.39	
CN	FO *D. berggrenii*	39X-CC, 24-31	367.02	**390.82**	40X-CC, 35-42	376.66	401.46	396.17	8.20	
PF	FO *G. plesiotumida*	40X-CC, 35-42	376.66	**401.46**	41X-CC, 24-31	386.26	411.88	406.70	8.58	
PF	FO *G. extremus*	40X-CC, 35-42	376.66	**401.46**	41X-CC, 24-31	386.26	411.88	406.70	8.58	
CN	FO *D. pentaradiatus*	40X-CC, 35-42	376.66	**401.46**	41X-CC, 24-31	386.26	411.88	406.70	8.55	
CN	LO *D. hamatus*	41X-CC, 24-31	386.26	411.88	42X-CC, 28-35	395.50	**419.82**	415.88	9.40	
PF	FO *N. acostaensis*	42X-CC, 28-35	395.50	**419.82**	43X-CC, 33-40	405.07	429.54	424.71	9.82	
CN	FO *D. hamatus*	44X-CC, 44-50	414.57	**438.64**	45X-CC, 33-39	424.71	449.13	443.92	10.38	
PF	LO *G. mayeri*	44X-CC, 44-50	414.57	438.64	45X-CC, 33-39	424.71	**449.13**	443.92	10.49	
CN	FO *C. coalithus*	45X-CC, 33-39	424.71	**449.13**	46X-CC, 55-61	434.46	460.38	454.79	10.79	
CN	LO *D. kugleri*	46X-CC, 55-61	434.46	460.38	47X-CC, 46-52	443.96	**471.88**	466.16	11.52	
PF	FO *G. nepenthes*	46X-CC, 55-61	434.46	**460.38**	47X-CC, 46-52	443.96	471.88	466.16	11.19	
CN	FO *D. kugleri*	48X-CC, 37-42	453.57	**481.78**	49X-CC, 37-44	463.10	490.24	486.04	11.83	
PF	LO *F. fohsi* s.l.*	48X-CC, 37-42	453.57	481.78	49X-CC, 37-44	463.10	**490.24**	486.04	11.68	
CN	FO *T. rugosus*	49X-CC, 37-44	463.10	**490.24**	50X-CC, 31-38	472.67	499.36	494.83	12.62	
CN	LO *C. floriganus*	50X-CC, 31-38	472.67	499.36	51X-CC, 32-39	482.13	**509.32**	504.37	13.19	
PF	FO *F. fohsi* s.l.	50X-CC, 31-38	472.67	**499.36**	51X-CC, 32-39	482.13	509.32	504.37	13.42	
CN	LO *S. heteromorphus*	51X-CC, 32-39	482.13	509.32	52X-CC, 37-43	491.80	**520.24**	514.81	13.57	14.5
PF	FO *F. praefohsi*	51X-CC, 32-39	482.13	**509.32**	52X-CC, 37-43	491.80	520.24	514.81	14.00	
PF	FO *F. peripheroacuta*	52X-CC, 37-43	491.80	**520.24**	53X-CC, 24-32	501.31	531.20	525.76	14.80	
PF	FO *O. universa**	53X-CC, 24-32	501.31	**531.20**	54X-CC, 27-34	509.37	540.11	535.69	15.10	
CN	LO *H. ampliaperta*	54X-CC, 27-34	509.37	540.11	55X-CC, 35-42	520.68	**551.32**	545.75	15.60	
CN	LO *D. deflandrei* acme	57X-CC, 34-41	539.80	574.30	58X-CC, 24-31	549.26	**585.13**	579.75	16.20	38.1
PF	FO *P. sicana*	59X-CC, 34-41	558.94	**594.67**	60X-CC, 27-34	568.53	604.63	599.68	16.40	
PF	LO *C. dissimilis**	61X-CC, 43-50	578.22	614.21	62X-CC, 19-26	587.47	**624.26**	619.62	17.30	
CN	FO *S. heteromorphus*	63X-3, 70	591.30	**627.64**	63X-CC, 33-39	597.39	633.73	630.70	18.20	

Table T7 (continued).

Code	Events	Depth range of stratigraphic datums: Top: Core, section, interval (cm)	Top: Depth (mbsf)	Top: Depth (mcd)	Bottom: Core, section, interval (cm)	Bottom: Depth (mbsf)	Bottom: Depth (mcd)	Average depth (mcd)	Age (Ma)	Average sedimentation rate (m/m.y.)
CN	LO *S. belemnos**	64X-2, 66	599.36	635.35	64X-CC, 35-41	607.09	**643.08**	639.20	18.30	19.6
PF	LO *G. binaiensis*	63X-CC, 33-39	597.39	633.73	64X-CC, 35-41	607.09	**643.08**	638.41	19.10	

Notes: Sources of reference age for all biostratigraphic events are listed in Tables **T2**, p. 42, and **T3**, p. 43, both in the "Explanatory Notes" chapter. CN = calcareous nannofossils, PF = planktonic foraminifers, BF = benthic foraminifers, FO = first occurrence, LO = last occurrence. * = events used in calculating average sedimentation rate. Depth for the top and bottom of biostratigraphic events = the mean of the sample interval. Depth in bold indicates where datum is recorded; depth range between the top and bottom is the interval where the real bioevent may occur. Bars in average sedimentation rate column indicate the range of samples to which the average sedimentation rate applies.

Table T8. Calcareous nannofossil checklist for Site 1146. (**See table notes.** Continued on next page.)

Epoch	Zones	Core, section, interval (cm)	Depth (mcd)	Preservation	Abundance	*Amaurolithus amplificus*	*Amaurolithus delicatus*	*Amaurolithus primus*	*Amaurolithus tricorniculatus*	*Calcidiscus leptoporus*	*Calcidiscus macintyrei*	*Calcidiscus premacintyrei*	*Catinaster calyculus*	*Catinaster coalitus*	*Ceratolithus armatus*	*Ceratolithus cristatus*	*Ceratolithus rugosus*	*Coccolithus miopelagicus*	*Coccolithus pelagicus*	*Coronocyclus nitescens*	*Cyclicargolithus floridanus*	*Discoaster asymmetricus*	*Discoaster bellus*	*Discoaster berggrenii*	*Discoaster bollii*	*Discoaster brouweri*	*Discoaster calcaris*	*Discoaster deflandrei*	*Discoaster druggii*	*Discoaster hamatus*
		184-1146A-																												
		1H-CC, 8-15	3.82	G	A					F									R											
	NN21B	2H-CC, 12-19	14.25	G	A					F																				
		3H-CC, 13-20	24.79	G	A					C						F			R											
		4H-CC, 21-28	35.13	G	A					F						R														
	NN21A	5H-CC, 20-27	45.37	G	A					F						R														
		6H-CC, 35-42	54.16	G	A					R						R														
		7H-CC, 36-43	63.86	G	A					R						R										R				
	NN20	8H-CC, 0-7	73.10	G	A					R	R					R										R				
Pleistocene		9H-CC, 26-33	83.86	G	A					R						R										R				
		10H-CC, 26-31	93.40	G	A					R						R										R				
		11H-CC, 44-50	104.85	G	A					R																R				
		12H-CC, 26-32	114.40	G	A					R						R			R							R				
	NN19b	13H-CC, 22-28	124.83	G	A					R	R					R			R							R				
		14H-CC, 20-26	135.02	G	A					R						R										R				
		15H-CC, 25-32	145.52	G	A					R						R			R							R				
		16H-CC, 25-31	153.71	G	A					R						R										R				
		17H-CC, 32-38	166.10	G	A					R	R					R			R							R				
	NN19a	18H-CC, 24-29	175.49	G	A					R	F					R			R							R				
		19H-CC, 20-26	185.46	G	A					R	F					R										C				
	NN18	20H-CC, 25-32	195.14	G	A					R	R					R										C				
late Pliocene		21H-CC, 0-5	206.14	G	A					R	R					R						R				C				
	NN17	22X-CC, 30-35	216.70	G	A					R	R					R						R				C				
		23X-CC, 22-27	226.68	G	A					R	R					R			R			R				C				
	NN16	24X-CC, 28-33	237.07	M	A					R	C					R			R			R				C				
		26X-CC, 35-41	256.50	M	A					C	C					R	R									F				
	NN15	27X-CC, 23-30	267.47	M	A					C	F					R	R									F				
		28X-CC, 16-23	278.63	M	A				R	F	F					R										F				
early Pliocene	NN 12-14	29X-CC, 16-23	288.50	M	A		R		R	C	F					R			R							C				
		30X-CC, 37-44	298.71	M	A		R		R	C									F							F				
		31X-CC, 23-30	308.39	M	A		R		R	F	R								F							C				
		32X-CC, 38-45	317.96	M	A		R	F	R	C	F				R				R							F				
		33X-CC, 15-22	327.82	M	A		F	R		F	R								C					F		F				
late Miocene	NN11	34X-CC, 23-30	337.76	M	A	R	R	F	R	F	F								C					F		F				
		35X-CC, 17-24	348.03	G	A		R	R		F	R								C					A		C				
		36X-CC, 37-44	360.34	G	A	R				F	F								C					C		F				
		37X-CC, 35-41	370.70	G	A					F	F								C					C		C				
		38X-CC, 36-43	381.29	M	A					F	R								F					F		C				

Core, section, interval (cm)	*Discoaster kugleri*	*Discoaster loeblichii*	*Discoaster moorei*	*Discoaster neohamatus*	*Discoaster neorectus*	*Discoaster pentaradiatus*	*Discoaster petaliformis*	*Discoaster prepentaradiatus*	*Discoaster quinqueramus*	*Discoaster signus*	*Discoaster surculus*	*Discoaster variabilis*	*Discosphaera tubifera*	*Emiliania huxleyi*	*Florisphaera profunda*	*Gephyrocapsa caribbeanica*	*Gephyrocapsa margarelii*	*Gephyrocapsa oceanica*	*Gephyrocapsa* spp. (small)	*Helicosphaera ampliaperta*	*Helicosphaera carteri*	*Helicosphaera hyalina*	*Helicosphaera inversa*	*Helicosphaera wallichii*	*Minylitha convallis*
184-1146A-																									
1H-CC, 8-15														A	A			A	C		C			R	
2H-CC, 12-19														C	A			A	A		F			R	
3H-CC, 13-20														C	A			A	A		F			F	
4H-CC, 21-28														F	A			A	A		C	R	R	R	
5H-CC, 20-27													R		A	R		A	D		F				
6H-CC, 35-42													R		C	C	C	C	A		R				
7H-CC, 36-43						R							R		C	C	C	C	A		R				
8H-CC, 0-7												R	R		C	C	C	C	A		R				
9H-CC, 26-33						R									D	C	C	C	C		R				
10H-CC, 26-31						R						R			D	F	F	C	C		R				
11H-CC, 44-50						R						R			D	R	F	C	C		R				
12H-CC, 26-32						R									D		F	C	C		F				
13H-CC, 22-28						R							R		A	R	F	F	D		F				
14H-CC, 20-26						R							R		A	R	R	R	D		R				
15H-CC, 25-32						R						R			C	F	F	R	D		R				
16H-CC, 25-31						R						R			A	C	F	F	D		C				
17H-CC, 32-38						R						R			A	F	C	F	A		C				
18H-CC, 24-29						R									A						R				
19H-CC, 20-26						F									A						R				
20H-CC, 25-32						F									A						F				
21H-CC, 0-5						F									A						F				
22X-CC, 30-35						C					R	R			A						F				
23X-CC, 22-27						C					R				A						F				
24X-CC, 28-33						A					R				A						F				
26X-CC, 35-41						C					C	F			A						C				
27X-CC, 23-30						C					C	F			C						F				
28X-CC, 16-23						C					F	F			A						C				
29X-CC, 16-23						C					C	C			C						C				
30X-CC, 37-44						C					C	C			A						C				
31X-CC, 23-30						C			F		F	C			A						C				
32X-CC, 38-45						C			C		F	F			C						C				
33X-CC, 15-22						F			A		F	F			A				R		C				
34X-CC, 23-30						F			C		F	F			A				F		F				
35X-CC, 17-24						R			A		F	F			C				R		F				
36X-CC, 37-44						R			C		F	C			C						C				
37X-CC, 35-41						F			C		F	C			C						C				R
38X-CC, 36-43				F		F			C		R	F			C						C				

Core, section, interval (cm)	*Oolithotus antillarum*	*Pontosphaera* spp.	*Pseudoemiliania lacunosa*	*Reticulofenestra asanoi*	*Reticulofenestra pseudoumbilicus*	*Reticulofenestra* (small-medium sized)	*Rhabdosphaera clavigera*	*Scapholithus fossilis*	*Sphenolithus abies/neoabies*	*Sphenolithus belemnos*	*Sphenolithus heteromorphus*	*Syracosphaera pulchra*	*Syracosphaera* spp.	*Thorosphaera flabellata*	*Triquetrorhabdulus rugosus*	*Umbellosphaera irregularis*	*Umbilicosphaera sibogae*
184-1146A-																	
1H-CC, 8-15	R						F	R				C	R	F		F	C
2H-CC, 12-19	R	R					C	F				F				F	C
3H-CC, 13-20	F						F	F				C	R			F	C
4H-CC, 21-28	R						C	F				C				R	C
5H-CC, 20-27	F	F					C	F				C					C
6H-CC, 35-42		R	R				F	R				R	R			R	
7H-CC, 36-43		R	R				F	R				F	R			R	F
8H-CC, 0-7		R	F				R	R				R	R	R		R	F
9H-CC, 26-33		R	C				R					R	R	F		R	F
10H-CC, 26-31		R	C				R	R				R	R	F		R	R
11H-CC, 44-50		R	C				R					R	R	F		R	F
12H-CC, 26-32		R	C	R			R					R		R			R
13H-CC, 22-28		R	C	C			R					R	R	R		R	F
14H-CC, 20-26		R	A	R		R	R					R		R			F
15H-CC, 25-32		R	A	R		R	R					R		R		R	F
16H-CC, 25-31		R	A			R	R	R				R		R			R
17H-CC, 32-38		R	A			R	R					R		R			R
18H-CC, 24-29		R	A			F	R	R				R		R			R
19H-CC, 20-26		R	C			A	F	R				R		R			R
20H-CC, 25-32		R	C			A	F					R		R			R
21H-CC, 0-5		R	C			A	F					R		R			R
22X-CC, 30-35		R	C		R	A	F					R		R			R
23X-CC, 22-27		R	C			A	F					R	F	R			F
24X-CC, 28-33		R	C		R	A	R	R	F			R		R			R
26X-CC, 35-41					C	A	R		A			F					C
27X-CC, 23-30					C	A	F		A			F					C
28X-CC, 16-23					C	D	R		A			R					C
29X-CC, 16-23					C	A	F		A			F					C
30X-CC, 37-44					C	A	F		A			F			R		C
31X-CC, 23-30					F	A	F	R	A			F			F		C
32X-CC, 38-45					C	A			A						R		C
33X-CC, 15-22					C	A			A						R		C
34X-CC, 23-30					C	A	R	R	A			R			R		C
35X-CC, 17-24					C	A			A			R			F		C
36X-CC, 37-44					F	A			A						F		F
37X-CC, 35-41						C			A						F		C
38X-CC, 36-43	C				R	A			A						F		C

Table T8 (continued).

Epoch	Zones	Core, section, interval (cm)	Depth (mcd)	Preservation	Abundance	*Amaurolithus amplificus*	*Amaurolithus delicatus*	*Amaurolithus primus*	*Amaurolithus tricorniculatus*	*Calcidiscus leptoporus*	*Calcidiscus macintyrei*	*Calcidiscus premacintyrei*	*Catinaster calyculus*	*Catinaster coalitus*	*Ceratolithus armatus*	*Ceratolithus cristatus*	*Ceratolithus rugosus*	*Coccolithus miopelagicus*	*Coccolithus pelagicus*	*Coronocyclus nitescens*	*Cyclicargolithus floridanus*	*Discoaster asymmetricus*	*Discoaster bellus*	*Discoaster berggrenii*	*Discoaster bollii*
late Miocene	NN11	39X-CC, 24-31	390.82	M	A					F	F								C				F		
	NN10	40X-CC, 35-42	401.46	G	A					C	F								C				F		
		41X-CC, 24-31	411.88	G	A					F	F								F				F		
	NN 9	42X-CC, 28-35	419.82	G	A					F	F		F	F					F				C		C
		43X-CC, 33-40	429.54	G	A					F	F		C	C					F				C		
		44X-CC, 44-50	438.64	G	A					R	F		C	C					R				C		
	NN 8	45X-CC, 33-39	449.13	M	A					R	F								R				F		F
middle Miocene	NN 7	46X-CC, 55-61	460.38							F	F								F				R		F
		47X-CC, 46-52	471.88	M	A					C	C								F				R		F
		48X-CC, 37-42	481.78	M	A					C	C								C						F
	NN 6	49X-CC, 37-44	490.24	P	A					F	F	R							C						F
		50X-CC, 31-38	499.36	P	A					F	F	F						R	C	R	C				C
		51X-CC, 32-39	509.32	P	F						R	R							C	R	C				C
	NN 5	52X-CC, 37-43	520.24	P	A					F	R	F						R	C	R	C				C
		53X-CC, 24-32	531.20	P	A						R							F	F	R	C				F
		54X-CC, 27-34	540.11	P	A					F	R	R						F	F	R	C				C
	NN 4	55X-CC, 35-42	551.32	P	A					F	R	F						F	C	R	C				C
		56X-CC, 0-8	562.57	P	A					R	R							R	F	R	A				C
		57X-CC, 34-41	574.30	M	A						R								C	F	A				C
		58X-CC, 24-31	585.13	M	A						R							F	F	F	A				C
early Miocene		59X-CC, 34-41	594.67	P	A						R							R	C	F	A				F
		60X-CC, 27-34	604.63	M	A					F	R							F	C	F	A				C
		61X-CC, 43-50	614.21	M	A						R	R						F	F	R	C				F
		62X-CC, 19-26	624.26	M	A						R							F	C	F	A				F
		63X-CC, 33-39	633.73	M	A						R							F	F	R	C				F
	NN 3	64X-CC, 35-41	643.08	M	A						R							F	F	R	C				F

Core, section, interval (cm)	*Discoaster brouweri*	*Discoaster calcaris*	*Discoaster deflandrei*	*Discoaster druggii*	*Discoaster hamatus*	*Discoaster kugleri*	*Discoaster loeblichii*	*Discoaster moorei*	*Discoaster neohamatus*	*Discoaster neorectus*	*Discoaster pentaradiatus*	*Discoaster petaliformis*	*Discoaster prepentaradiatus*	*Discoaster quinqueramus*	*Discoaster signus*	*Discoaster surculus*	*Discoaster variabilis*	*Discosphaera tubifera*	*Emiliania huxleyi*	*Florisphaera profunda*	*Gephyrocapsa caribbeanica*	*Gephyrocapsa margarelii*	*Gephyrocapsa oceanica*	*Gephyrocapsa* spp. (small)	*Helicosphaera ampliaperta*
39X-CC, 24-31	C								C		R		F	F			F			C					
40X-CC, 35-42	C								C				C	F			F			C					
41X-CC, 24-31	C								F					F			C			C					
42X-CC, 28-35	C			C	F		F		F	F				F			C			C					
43X-CC, 33-40	C			C	F		F		F	F				F			C			C					
44X-CC, 44-50	C						F			F			F				C			C					
45X-CC, 33-39	C	C								F			F				C			C					
46X-CC, 55-61	F	C				F		F									C			C					
47X-CC, 46-52	F	F	F			F		F					F				C			C					
48X-CC, 37-42	R	C						F									C			C					
49X-CC, 37-44	R	F						F							R		C			C					
50X-CC, 31-38	R	F	F					F							R		C			C					
51X-CC, 32-39			F					F									C			C					
52X-CC, 37-43			F								R	F					F			C					
53X-CC, 24-32								R				F					F			A					
54X-CC, 27-34		R	C									C					R			A					
55X-CC, 35-42			C									C								C					
56X-CC, 0-8		F	C									R					F			C					
57X-CC, 34-41			C	F													F								
58X-CC, 24-31			C														F								
59X-CC, 34-41			C																	C					R
60X-CC, 27-34			C	F																C					F
61X-CC, 43-50			C	F													F			F					F
62X-CC, 19-26			C	F													F								F
63X-CC, 33-39			C	F													F								F
64X-CC, 35-41			C	F													F								F

Core, section, interval (cm)	*Helicosphaera carteri*	*Helicosphaera hyalina*	*Helicosphaera inversa*	*Helicosphaera wallichii*	*Minylitha convallis*	*Oolithotus antillarum*	*Pontosphaera* spp.	*Pseudoemiliania lacunosa*	*Reticulofenestra asanoi*	*Reticulofenestra pseudoumbilicus*	*Reticulofenestra* (small-medium sized)	*Rhabdosphaera clavigera*	*Scapholithus fossilis*	*Sphenolithus abies/neoabies*	*Sphenolithus belemnos*	*Sphenolithus heteromorphus*	*Syracosphaera pulchra*	*Syracosphaera* spp.	*Thorosphaera flabellata*	*Triquetrorhabdulus rugosus*	*Umbellosphaera irregularis*	*Umbilicosphaera sibogae*
39X-CC, 24-31	C					F				R	A			A						R		C
40X-CC, 35-42	C					C				C	C			A						R		C
41X-CC, 24-31	C									C	C			C						R		F
42X-CC, 28-35	F						R			C	C			C						R		
43X-CC, 33-40	F						R			C	C			C						R		R
44X-CC, 44-50	R						R			C	A		R	A					R	R		R
45X-CC, 33-39	F						R			C	A			A						R		R
46X-CC, 55-61	F									C	C			C						R		
47X-CC, 46-52	F						F			C	C			C						R		
48X-CC, 37-42	F						R			C	C			C						R		
49X-CC, 37-44	F						R			C	C			C								
50X-CC, 31-38	F									C	C	F		C								C
51X-CC, 32-39	F									F	C	R		F		C						C
52X-CC, 37-43	C									R	C	R		F		C						C
53X-CC, 24-32	F										A	R		F		C						C
54X-CC, 27-34	F										C			F		C						C
55X-CC, 35-42	C										C			F		C						C
56X-CC, 0-8	F										C			F		C						F
57X-CC, 34-41	F										C					A						F
58X-CC, 24-31	F									R	C					A						F
59X-CC, 34-41	F									R	C					C						F
60X-CC, 27-34	F									F	C					A						C
61X-CC, 43-50	C									F	C			F		C						F
62X-CC, 19-26	C									C	C			F								F
63X-CC, 33-39	C									F	C			F	C							F
64X-CC, 35-41	C									F	C			F	C							

Notes: D = dominant, A = abundant, C = common, F = few/frequent, R = rare, G = good, M = moderate, P = poor. See **"Biostratigraphy,"** p. 9, in the "Explanatory Notes" chapter.

Table T9. Planktonic foraminifer checklist for Site 1146. (**See table notes.** Continued on next page.)

Epoch	Zone	Core, section interval (cm)	Depth (mcd)	Abundance	Preservation	*Catapsydrax dissimilis*	*Fohsella fohsi* s.l.	*Fohsella praefohsi*	*Globoturborotalita nepenthes*	*Globigerinatella insueta*	*Globigerinoides conglobatus*	*Globigerinoides extremus*	*Globigerinoides fistulosus*	*Globigerinoides obliquus*	*Globigerinoides ruber*	*Globigerinoides ruber* (pink)	*Globoquadrina altispira*	*Globoquadrina binaiensis*	*Globoquadrina dehiscens*	*Globorotalia birnageae*	*Globorotalia crassaformis*	*Globorotalia inflata*	*Globorotalia lenguaensis*	*Globorotalia margaritae*	*Globorotalia mayeri*	*Globorotalia menardii*	*Globorotalia merotumida*	*Globorotalia multicamerata*	*Globorotalia peripheroacuta*	*Globorotalia peripheronda*	*Globorotalia plesiotumida*	*Globorotalia praescitula*	*Globorotalia siakensis*	*Globorotalia tosaensis*	*Globorotalia truncatulinoides*	*Globorotalia tumida*	*Neogloboquadrina acostaensis*	*Neogloboquadrina dutertrei*	*Orbulina universa*	*Praeorbulina glomerosa*	*Praeorbulina sicana*	*Pulleniatina* (dextral)	*Pulleniatina* (sinistral)	*Pulleniatina obliquiloculata*	*Sphaeroidinella dehiscens*	*Sphaeroidinellopsis kochi*	*Sphaeroidinellopsis seminulina*
		184-1146A-																																										
Pleistocene	N22	1H-CC, 8-15	3.82	A	V						R				A							R				F										A					F			
		2H-CC, 12-19	14.25	A	V						R				A						F	R				F										F					F			
		3H-CC, 13-20	24.79	A	V						R				A							R				R									P		F					A	P		
		4H-CC, 21-28	35.13	A	V						R				A							R				A									R	R	F					F	P		
		5H-CC, 20-27	45.37	A	V						R				F	P						R				A									F		F					F	P		
		6H-CC, 35-42	54.16	A	V										F	R						F				F											A					A			
		7H-CC, 36-43	63.86	A	V										A	P						A													R		A					F			
		8H-CC, 0-7	73.10	A	V										A						P																A					F			
		9H-CC, 26-33	83.86	A	V										A							F				F											A					P			
	N22	10H-CC, 26-31	93.40	A	V																					F									R		A					A	F		
		11H-CC, 44-50	104.85	A	V										A							A													P		A					R			
		12H-CC, 26-32	114.40	A	V										A							F				F									P							A			
		13H-CC, 22-28	124.83	A	V										A						R	A													P		A								
		14H-CC, 20-26	135.02	A	V										A											F									P							A	F		
		15H-CC, 25-32	145.52	A	V						F				A											F									P							A	F		
		16H-CC, 25-31	153.71	A	V						R											F													P		A					R	R		
		17H-CC, 32-38	166.10	A	V										A							F													P		A						R		
late Pliocene		18H-CC, 24-29	175.49	A	V								P		A																			P							A	F		
		19H-CC, 20-26	185.46	A	G								P		A											R									P		A						R		
	N21	20H-CC, 25-32	195.14	A	V						R	P	P													F												F					A	F		
		21H-CC, 0-5	206.15	A	V						R				F													F											F					A	F		
		22X-CC, 30-35	216.70	A	V										F													R						P		R						F	F		
		23X-CC, 22-27	226.68	A	V							P														F		R								R						R	R		
		24X-CC, 28-33	237.07	A	V							P			A													R															R		
	N20	26X-CC, 35-41	256.50	A	V												R											F													F			R		R
early Pliocene	N19	27X-CC, 23-30	267.47	A	V							A					F							P				R														A			
		28X-CC, 16-23	278.63	A	V				P								R							P				P														R		P	
		29X-CC, 16-23	288.50	A	V				P															P				R														R		P	R	
		30X-CC, 37-44	298.71	A	V				P								R							P				R																P	P	
		31X-CC, 23-30	308.39	A	V						P						R							P				P																P	R	
		32X-CC, 38-45	317.96	A	V				P		P	F					R											P																P	R	
		33X-CC, 15-22	327.82	A	V						P						R											P																P	R	
		34X-CC, 23-30	337.76	A	V												R											P																P	R	
	N18	35X-CC, 17-24	348.03	A	V				P		P						R											P																P	P	R
late Miocene	N17	36X-CC, 37-44	360.34	A	V						P						F		P																									P		
		37X-CC, 35-41	370.70	A	V							P					F														P														R	R	
		38X-CC, 36-43	381.29	A	V							F					R														R														R	R	
		39X-CC, 24-31	390.82	A	V				P			F																		P							P							R		
		40X-CC, 35-42	401.46	A	V							R					R														P														P	P	
	N16	41X-CC, 24-31	411.88	A	V									R												R											P								P	P	

Table T9 (continued).

Epoch	Zone	Core, section interval (cm)	Depth (mcd)	Abundance	Preservation	*Catapsydrax dissimilis*	*Fohsella fohsi* s.l.	*Fohsella praefohsi*	*Globoturborotalita nepenthes*	*Globigerinatella insueta*	*Globigerinoides conglobatus*	*Globigerinoides extremus*	*Globigerinoides fistulosus*	*Globigerinoides obliquus*	*Globigerinoides ruber*	*Globigerinoides ruber* (pink)	*Globoquadrina altispira*	*Globoquadrina binaiensis*	*Globoquadrina dehiscens*	*Globorotalia birnageae*	*Globorotalia crassaformis*	*Globorotalia inflata*	*Globorotalia lenguaensis*	*Globorotalia margaritae*	*Globorotalia mayeri*	*Globorotalia menardii*	*Globorotalia merotumida*	*Globorotalia multicamerata*	*Globorotalia peripheroacuta*	*Globorotalia peripheroronda*	*Globorotalia plesiotumida*	*Globorotalia praescitula*	*Globorotalia siakensis*	*Globorotalia tosaensis*	*Globorotalia truncatulinoides*	*Globorotalia tumida*	*Neogloboquadrina acostaensis*	*Neogloboquadrina dutertrei*	*Orbulina universa*	*Praeorbulina glomerosa*	*Praeorbulina sicana*	*Pulleniatina* (dextral)	*Pulleniatina* (sinistral)	*Pulleniatina obliquiloculata*	*Sphaeroidinella dehiscens*	*Sphaeroidinellopsis kochi*	*Sphaeroidinellopsis seminulina*
middle Miocene	N16	42X-CC, 28-35	419.82	A	V				R					P					R			P				R										P							P	
	N15	43X-CC, 33-40	429.54	A	V				R					P			R																												
		44X-CC, 44-50	438.64	A	V									A			R		R																										
	N14	45X-CC, 33-39	449.13	A	V				P					F			R		R						R							R												
		46X-CC, 55-61	460.38	A	V				P					P	A		R								P							P											R	
	N13	47X-CC, 46-52	471.88	A	V									A											A							A												
		48X-CC, 37-42	481.78	A	V										A		R								A							A											R	
	N12	49X-CC, 37-44	490.24	A	V		P								F				F						A							F												
		50X-CC, 31-38	499.36	A	V		P	P							F				F																			F						
	N11	51X-CC, 32-39	509.32	A	V			P							F				F										P														
	N10	52X-CC, 37-43	520.24	A	V																				F				R	P			F					F						
	N9	53X-CC, 24-32	531.20	A	V																				R					R			F					P						
	N8	54X-CC, 27-34	540.11	A	V					P															P					R			R					P						
		55X-CC, 35-42	551.32	A	V					P																				R								P	P					
		56X-CC, 0-8	562.57	A	G					P																				R								P	P					
		57X-CC, 34-41	574.30	A	G					P																				P		P						P						
		58X-CC, 24-31	585.13	A	G					P																				P								P						
		59X-CC, 34-41	594.67	A	V					P																					P								P						
early Miocene	N7	60X-CC, 27-34	604.63	A	V																P									P	R													
		61X-CC, 43-50	614.21	A	V																P										R													
	N6	62X-CC, 19-26	624.26	A	V	P																								P														
		63X-CC, 33-39	633.73	A	V	R																								P														
	N5	64X-CC, 35-41	643.08	A	V	P												P													R													

Notes: D = dominant, A = abundant, C = common, F = frequent/few, R = rare, V = very good, G = good, M = moderate, P = poor. See **"Biostratigraphy,"** p. 9, in the "Explanatory Notes" chapter.

Table T10. Age-depth relationship derived from the magnetic polarity time scale, Site 1146.

Polarity event	Age (Ma)	Depth (mcd) Hole 1146A	Hole 1146B	Hole 1146C	Average depth (mcd)
Brunhes/Matuyama	0.78	116.7	114.9	114.8	115.5
upper Jaramillo	0.99		132.5	132.5	132.5
lower Jaramillo	1.07		137.7	138.1	137.9
upper Olduvai	1.77		160.5	162.3	161.4

Table T11. Sedimentation and accumulation rates for selected intervals, based on age-depth model and rates presented in Figure F15, p. 53.

	Bottom of interval					
	Age (Ma)	Depth (mcd)	LSR total (m/m.y.)	LSR carbonate (m/m.y.)	MAR total ($g/cm^2/k.y.$)	MAR carbonate ($g/cm^2/k.y.$)
NN21/NN20	0.26	60.5	289	53.0	19.1	3.60
Brunhes/Matuyama	0.78	115.5	105	23.0	8.6	1.90
Pleistocene/Pliocene	1.77	177.6	65	14.2	7.1	1.55
Pliocene/Miocene	5.32	308.0	38	16.1	4.3	1.81
upper/middle Miocene	11.20	463.3	27	14.1	3.6	1.88
middle/lower Miocene	16.40	587.3	27	8.9	4.0	1.35
Bottom of hole	19.50	643.1	30	8.6	4.6	1.34

Note: LSR = linear sedimentation rate for total sediment and inorganic carbonate, MAR = mass accumulation rate for total sediment and inorganic carbonate.

Table T12. Methane, ethane, and propane concentrations as obtained by headspace analysis, Holes 1146A and 1146C. (**See table notes.** Continued on next page.)

Core, section, interval (cm)	Depth (mbsf)	Depth (mcd)	C_1/C_2	C_1 (ppmv)	C_2 (ppmv)	C_3 (ppmv)
184-1146A-						
1H-3, 0-5	3.0	3.00	—	3	0	0.0
2H-4, 0-5	8.4	9.35	—	6	0	0.0
3H-4, 0-5	17.9	19.55	—	8	0	0.0
4H-4, 0-5	27.4	30.00	—	10	0	0.0
5H-4, 0-5	36.9	40.05	—	9	0	0.0
6H-4, 0-5	46.4	49.65	—	10	0	0.0
7H-4, 0-5	55.9	58.40	—	8	0	0.0
8H-4, 0-5	65.4	68.40	—	8	0	0.0
9H-4, 0-5	74.9	78.50	—	8	0	0.0
10H-4, 0-5	84.4	88.20	—	10	0	0.0
11H-4, 0-5	93.9	99.25	—	11	0	0.0
12H-4, 0-5	103.4	109.20	—	11	0	0.0
13H-4, 0-5	112.9	119.42	—	14	0	0.0
14H-4, 0-5	122.4	129.75	—	12	0	0.0
15H-4, 0-5	131.9	140.10	—	12	0	0.0
16H-4, 0-5	141.4	150.25	—	12	0	0.0
17H-4, 0-5	150.9	161.25	—	13	0	0.0
18H-4, 0-5	160.4	170.45	—	16	0	0.0
19H-4, 0-5	169.9	180.05	—	13	0	0.0
20H-4, 0-5	179.4	189.83	—	16	0	0.0
21H-4, 0-5	188.9	201.25	—	17	0	0.0
22X-4, 0-5	198.4	211.45	—	26	0	0.0
23X-4, 0-5	207.5	221.40	—	23	0	0.0
24X-4, 0-5	217.2	231.90	—	29	0	0.0
26X-4, 0-5	236.6	251.15	—	82	0	0.0
27X-4, 0-5	246.2	262.30	—	131	0	0.0
28X-4, 0-5	255.8	273.44	—	104	0	0.0
29X-4, 0-5	265.4	283.50	—	276	0	0.0
30X-4, 0-5	275.1	293.55	—	396	0	0.0
31X-4, 0-5	284.7	303.15	—	1,089	0	0.0
32X-4, 0-5	294.3	312.75	—	1,499	0	0.0
33X-4, 0-5	304.0	322.75	—	1,677	0	0.0
34X-4, 0-5	313.6	332.55	—	2,244	0	0.0
35X-4, 0-5	323.2	342.90	—	4,211	0	0.0
36X-4, 0-5	332.9	355.00	—	2,344	0	0.0
37X-4, 0-5	342.6	365.35	—	4,465	0	0.0
38X-4, 0-5	352.2	375.95	—	4,885	0	0.0
39X-4, 0-5	361.8	385.60	—	9,968	0	0.0
40X-4, 0-5	371.4	396.20	—	9,917	0	0.0
41X-4, 0-5	381.0	406.62	—	7,783	0	0.0
42X-4, 0-5	390.6	414.92	—	11,496	0	0.0
43X-4, 0-5	400.2	424.67	—	13,871	0	0.0
44X-4, 0-5	409.8	433.87	—	8,734	0	0.0
45X-4, 0-5	419.4	443.82	—	13,665	0	0.0
46X-4, 0-5	429.0	454.92	—	19,239	0	0.0
47X-4, 0-5	438.6	466.52	—	7,917	0	0.0
48X-4, 0-5	448.2	476.41	—	16,051	0	0.0
49X-4, 0-5	457.9	485.04	—	17,788	0	0.0
50X-4, 0-5	467.5	494.19	—	27,016	0	0.0
51X-4, 0-5	476.9	504.09	—	13,275	0	0.0
52X-4, 0-5	486.5	514.94	—	18,316	0	0.0
53X-4, 0-5	496.1	525.99	—	5,400	0	0.0
54X-4, 0-5	505.7	536.44	2,461	24,120	10	0.0
55X-4, 0-5	515.3	545.94	1,475	23,595	16	0.0
56X-4, 0-5	524.9	557.95	934	56,883	61	0.0
57X-4, 0-5	534.4	568.90	740	53,093	72	1.1
58X-4, 0-5	543.9	579.77	659	45,609	69	0.0
59X-4, 0-5	553.6	589.33	587	74,735	127	2.2
60X-4, 0-5	563.2	599.34	660	85,205	129	2.6
61X-4, 0-5	572.8	608.79	478	73,802	155	7.3
62X-4, 0-5	582.5	619.29	375	40,252	107	7.3
63X-4, 0-5	592.1	628.44	422	31,493	75	5.5
64X-4, 0-5	601.7	637.69	345	5,627	16	1.8

Table T12 (continued).

Core, section, interval (cm)	Depth (mbsf)	Depth (mcd)	C_1/C_2	C_1 (ppmv)	C_2 (ppmv)	C_3 (ppmv)
184-1146C-						
53X-4, 0-5	502.0	529.09	3,140	24,802	8	0.0
54X-4, 0-5	511.6	539.99	1,643	28,422	17	0.0
55X-4, 0-5	521.2	549.50	1,126	37,030	33	0.0
56X-4, 0-5	530.9	560.95	780	37,668	48	0.0
57X-4, 0-5	540.5	573.25	685	43,408	63	1.2
58X-4, 0-5	550.1	586.05	618	40,199	65	0.0
59X-4, 0-5	559.8	595.41	508	34,114	67	2.6
60X-4, 0-5	569.4	605.44	450	28,680	64	2.9
61X-4, 0-5	579.1	615.04	456	47,839	105	5.6
62X-4, 0-5	588.7	626.34	438	56,987	130	9.0
63X-4, 0-5	598.3	635.89	399	32,544	82	6.7

Notes: C_1 = methane, C_2 = ethane, C_3= propane. — = no C_2.

Table T13. Inorganic carbon, carbonate, total carbon, total organic carbon, total nitrogen, and total sulfur contents at Site 1146. (**See table notes.** Continued on next two pages.)

Core, section, interval (cm)	Depth (mbsf)	Depth (mcd)	IC (wt%)	$CaCO_3$ (wt%)	TC (wt%)	TOC (wt%)	TN (wt%)	TS (wt%)	C/N
184-1146A-									
1H-1, 107-108	1.07	1.07	2.56	21.4	3.16	0.60	0.09	0.10	6.6
2H-1, 107-108	4.97	5.92	1.67	14.0					
2H-3, 107-108	7.97	8.92	1.84	15.4	2.83	0.99	0.11	0.30	9.0
2H-5, 107-108	10.97	11.92	2.42	20.2					
3H-1, 107-108	14.47	16.12	0.94	7.9					
3H-3, 107-108	17.47	19.12	2.23	18.6	2.92	0.68	0.09	0.15	7.6
3H-5, 107-108	20.47	22.12	3.19	26.6					
4H-1, 107-108	23.97	26.57	2.50	20.9					
4H-3, 107-108	26.97	29.57	1.59	13.3	2.50	0.91	0.10	0.52	9.1
4H-5, 107-108	29.97	32.57	1.20	10.0					
5H-1, 107-108	33.47	36.62	1.90	15.9					
5H-3, 107-108	36.47	39.62	1.48	12.4	2.12	0.64	0.08	0.23	8.0
5H-5, 107-108	39.47	42.62	3.22	26.8					
6H-1, 107-108	42.97	46.22	2.38	19.9					
6H-3, 107-108	45.97	49.22	2.77	23.1	3.63	0.85	0.10	0.40	8.5
6H-6, 107-108	50.47	53.72	2.29	19.1					
7H-1, 107-108	52.47	54.97	2.47	20.6					
7H-3, 107-108	55.47	57.97	3.82	31.9	4.17	0.34	0.07	0.37	4.9
7H-6, 107-108	59.97	62.47	3.11	26.0					
8H-1, 107-108	61.97	64.97	3.33	27.8					
8H-3, 107-108	64.97	67.97	2.65	22.1	3.13	0.48	0.08	0.13	6.0
8H-5, 107-108	67.97	70.97	3.35	27.9					
8H-6, 108-109	69.48	72.48	1.92	16.1					
9H-1, 107-108	71.47	75.07	2.03	16.9					
9H-3, 107-108	74.47	78.07	2.91	24.3	3.60	0.68	0.09	0.20	7.6
9H-6, 107-108	78.97	82.57	2.23	18.6					
10H-1, 107-108	80.97	84.77	2.65	22.1					
10H-3, 107-108	83.97	87.77	1.94	16.2	2.47	0.53	0.09	0.42	5.8
10H-5, 107-108	86.97	90.77	3.75	31.3					
11H-1, 107-108	90.47	95.82	2.38	19.8					
11H-3, 107-108	93.47	98.82	2.22	18.5	2.86	0.64	0.08	0.20	8.0
11H-6, 107-108	97.97	103.32	1.63	13.6					
12H-1, 107-108	99.97	105.77	2.99	24.9					
12H-3, 107-108	102.97	108.77	2.05	17.1	2.40	0.35	0.07	0.12	5.0
12H-6, 107-108	107.47	113.27	2.32	19.3					
13H-1, 107-108	109.47	115.97	2.78	23.2					
13H-3, 107-108	112.47	118.97	2.33	19.4	2.74	0.41	0.07	0.07	5.8
13H-6, 107-108	117.01	123.51	2.46	20.6					
14H-1, 107-108	118.97	126.32	3.17	26.4					
14H-3, 107-108	121.97	129.32	2.38	19.8	2.71	0.33	0.06	0.05	5.5
14H-6, 107-108	126.47	133.82	2.98	24.8					
15H-1, 107-108	128.47	136.67	1.80	15.0					
15H-3, 107-108	131.47	139.67	1.74	14.5	2.13	0.39	0.06	0.20	6.5
15H-6, 107-108	135.99	144.19	2.85	23.8					
16H-1, 107-108	137.97	146.82	2.11	17.6					
16H-3, 107-108	140.97	149.82	2.74	22.8	3.19	0.45	0.07	0.00	6.4
17H-1, 107-108	147.47	157.82	2.87	23.9					
17H-3, 107-108	150.47	160.82	2.46	20.5	2.82	0.35	0.06	0.05	5.9
17H-6, 107-108	154.97	165.32	3.80	31.7					
18H-1, 107-108	156.97	167.02	2.71	22.6					
18H-3, 107-108	159.97	170.02	2.78	23.2	3.11	0.32	0.06	0.10	5.4
18H-6, 75-76	164.15	174.20	3.05	25.5					
19H-1, 107-108	166.47	176.62	3.31	27.6					
19H-3, 107-108	169.47	179.62	2.52	21.1	2.87	0.34	0.05	0.05	6.8
19H-6, 107-108	173.97	184.12	3.02	25.2					
20H-1, 107-108	175.97	186.40	3.47	28.9					
20H-3, 107-108	178.97	189.40	3.21	26.8	3.52	0.31	0.05	0.00	6.1
20H-6, 107-108	182.99	193.42	3.56	29.7					
21H-1, 107-108	185.47	197.82	3.63	30.3					
21H-3, 107-108	188.47	200.82	3.81	31.7	4.11	0.30	0.05	0.06	6.0
21H-6, 107-108	192.97	205.32	3.66	30.5					
22X-1, 107-108	194.97	208.02	3.28	27.4					
22X-3, 107-108	197.97	211.02	3.87	32.3	4.13	0.26	0.04	0.00	6.5
22X-6, 107-108	202.47	215.52	4.19	35.0					

Table T13 (continued).

Core, section, interval (cm)	Depth (mbsf)	Depth (mcd)	IC (wt%)	$CaCO_3$ (wt%)	TC (wt%)	TOC (wt%)	TN (wt%)	TS (wt%)	C/N
23X-1, 107-108	204.07	217.97	2.74	22.9					
23X-3, 107-108	207.07	220.97	2.60	21.7	2.87	0.27	0.05	0.00	5.4
23X-6, 107-108	211.57	225.47	4.59	38.3					
24X-1, 107-108	213.77	228.47	3.95	33.0					
24X-3, 107-108	216.77	231.47	5.26	43.8	5.39	0.13	0.04	0.00	3.2
24X-6, 107-108	221.27	235.97	5.94	49.5					
26X-1, 107-108	233.17	247.72	6.31	52.6					
26X-3, 107-108	236.17	250.72	6.14	51.2	6.29	0.15	0.02	0.00	7.4
26X-6, 107-108	240.67	255.22	7.01	58.5					
27X-1, 107-108	242.77	258.87	6.64	55.3					
27X-3, 107-108	245.77	261.87	6.67	55.6	6.79	0.11	0.02	0.00	5.7
27X-6, 107-108	250.27	266.37	7.68	64.1					
28X-1, 107-108	252.37	270.01	8.05	67.1					
28X-3, 107-108	255.37	273.01	7.10	59.2	7.18	0.07	0.02	0.00	3.7
28X-6, 107-108	259.87	277.51	7.20	60.0					
29X-1, 107-108	261.97	280.07	7.17	59.7					
29X-3, 107-108	264.97	283.07	7.22	60.2	7.28	0.05	0.03	0.00	1.8
29X-6, 107-108	269.47	287.57	7.14	59.5					
30X-1, 107-108	271.67	290.12	6.83	57.0					
30X-3, 107-108	274.67	293.12	6.87	57.2	6.95	0.08	0.02	0.00	4.0
30X-6, 107-108	279.17	297.62	6.80	56.7					
31X-1, 107-108	281.27	299.72	6.18	51.5					
31X-3, 107-108	284.27	302.72	6.10	50.8	6.17	0.07	0.03	0.00	2.3
31X-6, 107-108	288.77	307.22	6.79	56.6					
32X-1, 107-108	290.87	309.32	6.49	54.1					
32X-3, 107-108	293.87	312.32	6.72	56.0	6.91	0.18	0.03	0.00	6.1
32X-6, 107-108	298.37	316.82	6.84	57.0					
33X-1, 107-108	300.57	319.32	5.79	48.2					
33X-3, 107-108	303.57	322.32	6.25	52.1	6.30	0.05	0.03	0.00	1.6
33X-6, 113-114	308.13	326.88	7.45	62.1					
34X-1, 107-108	310.17	329.12	7.61	63.5					
34X-3, 107-108*	313.17	332.12	6.91	57.6	7.07	0.16	0.02	0.00	6.4
34X-6, 107-108	317.67	336.62	7.18	59.9					
35X-1, 107-108	319.77	339.47	5.28	44.0					
35X-3, 107-108*	322.77	342.47	6.06	50.5	6.38	0.32	0.04	0.00	7.3
35X-6, 107-108	327.27	346.97	6.84	57.1					
36X-1, 107-108	329.47	351.57	6.95	57.9					
36X-3, 107-108	332.47	354.57	7.10	59.2	7.26	0.15	0.07	0.03	2.2
36X-6, 107-108	336.97	359.07	7.32	61.0					
37X-1, 107-108	339.17	361.92	6.47	53.9					
37X-3, 107-108	342.17	364.92	6.34	52.9	6.51	0.16	0.06	0.00	2.7
37X-6, 107-108	346.67	369.42	7.23	60.2					
38X-1, 107-108	348.77	372.52	6.64	55.4					
38X-3, 107-108	351.77	375.52	6.49	54.1	6.66	0.17	0.04	0.00	4.1
38X-6, 107-108	356.27	380.02	6.23	51.9					
39X-1, 107-108	358.37	382.17	6.67	55.6					
39X-3, 107-108	361.37	385.17	7.21	60.1	7.42	0.20	0.04	0.00	5.1
39X-6, 107-108	365.87	389.67	6.86	57.2					
40X-1, 107-108	367.97	392.77	7.20	60.0					
40X-3, 107-108	370.97	395.77	6.93	57.8	7.09	0.16	0.04	0.01	3.9
40X-6, 107-108	375.47	400.27	7.16	59.6					
41X-1, 107-108	377.57	403.19	6.56	54.7					
41X-3, 107-108	380.57	406.19	6.12	51.0	6.30	0.18	0.03	0.01	5.9
41X-6, 107-108	385.07	410.69	7.05	58.8					
42X-1, 107-108	387.17	411.49	6.13	51.1					
42X-3, 107-108*	390.17	414.49	6.59	54.9	6.74	0.15	0.04	0.00	4.3
42X-6, 107-108*	394.67	418.99	6.92	57.7	7.26	0.34	0.03	0.00	17.2
43X-1, 107-108	396.77	421.24	6.53	54.4					
43X-3, 107-108	399.77	424.24	6.02	50.2	6.23	0.20	0.04	0.00	5.1
43X-6, 107-108	404.27	428.74	4.94	41.2					
44X-1, 107-108	406.37	430.44	5.66	47.2					
44X-3, 107-108	409.37	433.44	6.10	50.9	6.11	0.00	0.04	0.00	0.1
44X-6, 107-108	413.87	437.94	5.11	42.6					
45X-1, 87-88	415.77	440.19	4.15	34.6					
45X-3, 98-99	418.88	443.30	5.52	46.0	5.65	0.12	0.09	0.00	1.4
45X-6, 72-73	423.12	447.54	5.38	44.8					
46X-1, 107-108	425.57	451.49	3.21	26.8					
46X-3, 43-44	427.93	453.85	5.08	42.4	5.23	0.14	0.08	0.00	1.8
46X-6, 104-105	433.04	458.96	4.29	35.8					
47X-1, 130-131	435.40	463.32	4.54	37.9					

Table T13 (continued).

Core, section, interval (cm)	Depth (mbsf)	Depth (mcd)	IC (wt%)	$CaCO_3$ (wt%)	TC (wt%)	TOC (wt%)	TN (wt%)	TS (wt%)	C/N
47X-3, 101-102	438.11	466.03	3.59	29.9	3.68	0.09	0.09	0.00	1.0
47X-6, 80-81	442.40	470.32	4.35	36.3					
48X-1, 107-108	444.77	472.98	4.67	38.9					
48X-3, 107-108	447.77	475.98	4.07	34.0	4.16	0.08	0.08	0.02	1.0
48X-6, 107-108	452.27	480.48	5.66	47.2					
49X-1, 107-108	454.47	481.61	4.62	38.5					
49X-3, 107-108	457.47	484.61	5.62	46.8	5.68	0.06	0.09	0.00	0.7
49X-6, 107-108	461.97	489.11	5.66	47.2					
50X-1, 107-108	464.07	490.76	4.59	38.3					
50X-3, 107-108*	467.07	493.76	4.66	38.8	4.89	0.23	0.09	0.00	3.0
50X-3, 125-127*	467.25	493.94	3.22	26.9	3.60	0.38	0.05	0.03	8.0
50X-3, 126-127	467.26	493.95	3.43	28.6	3.58	0.15	0.09	0.07	1.6
50X-6, 107-108	471.57	498.26	5.51	45.9					
51X-1, 107-108	473.47	500.66	5.10	42.5					
51X-3, 107-108	476.47	503.66	3.23	26.9	3.31	0.08	0.13	0.02	0.6
51X-6, 107-108	480.97	508.16	5.38	44.9					
52X-1, 107-108	483.07	511.51	4.63	38.6					
52X-3, 107-108	486.07	514.51	5.24	43.7	5.11	0.00	0.04	0.00	0.0
52X-6, 107-108	490.57	519.01	3.62	30.2					
53X-1, 107-108	492.67	522.56	3.10	25.9					
53X-3, 107-108	495.67	525.56	3.97	33.1	4.17	0.20	0.10	0.00	2.0
53X-6, 107-108	500.17	530.06	4.45	37.1					
54X-1, 107-108	502.27	533.01	3.02	25.2					
54X-3, 107-108	505.27	536.01	2.20	18.4	2.34	0.13	0.09	0.01	1.5
55X-1, 107-108	511.87	542.51	4.58	38.2					
55X-3, 107-108*	514.87	545.51	3.28	27.4	3.48	0.20	0.12	0.03	1.5
55X-6, 107-108	519.37	550.01	2.46	20.5					
56X-1, 107-108	521.47	554.52	1.85	15.5					
56X-3, 107-108*	524.47	557.52	3.98	33.2	4.33	0.35	0.11	0.03	3.1
57X-1, 107-108	530.97	565.47	4.81	40.1					
57X-3, 107-108	533.97	568.47	5.51	46.0	5.59	0.07	0.04	0.00	1.8
57X-6, 107-108	538.47	572.97	3.69	30.8					
58X-1, 107-108	540.47	576.34	3.79	31.6					
58X-3, 107-108	543.47	579.34	4.01	33.4	3.91	0.00	0.05	0.05	0.0
58X-6, 107-108	547.97	583.84	3.73	31.1					
59X-1, 125-126	550.35	586.08	2.05	17.1					
59X-3, 101-102	553.11	588.84	3.10	25.9	3.22	0.11	0.09	0.06	1.3
59X-6, 118-119	557.78	593.51	2.85	23.8					
60X-1, 107-108	559.77	595.87	3.78	31.5					
60X-3, 107-108	562.78	598.88	3.85	32.1	4.00	0.14	0.09	0.02	1.6
60X-6, 107-108	567.31	603.41	3.39	28.3					
61X-1, 107-108	569.37	605.36	3.83	31.9					
61X-3, 107-108	572.37	608.36	3.04	25.4	3.18	0.13	0.06	0.00	2.2
61X-6, 107-108	576.87	612.86	4.54	37.8					
62X-1, 107-108	579.07	615.86	3.80	31.7					
62X-3, 107-108*	582.07	618.86	2.78	23.2	2.93	0.15	0.11	0.07	1.4
62X-6, 97-98*	586.47	623.26	4.32	36.0	4.53	0.21	0.04	0.00	8.0
63X-1, 110-111	588.70	625.04	3.74	31.2					
63X-3, 110-111	591.70	628.04	3.19	26.6	3.35	0.16	0.10	0.00	1.6
63X-6, 109-110	596.19	632.53	3.28	27.3					
64X-1, 107-108	598.27	634.26	3.70	30.9					
64X-3, 107-108	601.27	637.26	1.56	13.0	1.69	0.13	0.10	0.00	1.3
64X-6, 107-108	605.77	641.76	3.44	28.7					

Notes: IC = inorganic carbon, $CaCO_3$ = carbonate, TC = total carbon, TOC = total organic carbon, TN = total nitrogen, TS = total sulfur, C/N = carbon/nitrogen ratio. * = TOC (TC) average of duplicate analyses.

Table T14. Rock-Eval pyrolysis results for Site 1146.

Core, section, interval (cm)	Depth (mbsf)	Depth (mcd)	Mass weight (mg)	T_{max}	S_1	S_2	S_3	PI	HI	OI	TOC (R-E)	TOC (TC – IC)
184-1146A-												
3H-3, 107-108	17.5	19.1	72.7	377	0.09	0.38	3.16	0.20	95	790	0.40	0.68
6H-3, 107-108	46.0	49.2	78.2	402	0.11	0.60	2.71	0.16	98	444	0.61	0.85
9H-3, 107-108	29.0	82.6	96.0	392	0.09	0.39	2.72	0.19	76	530	0.51	0.68
16H-3, 107-108	141.0	149.8	120.0	378	0.04	0.15	2.07	0.22	48	667	0.31	0.45
19H-3, 107-108	169.5	179.6	58.5	409	0.01	0.05	1.43	0.17	23	680	0.21	0.34
29H-3, 107-108	265.0	283.1	123.0	*	0.01	0.01	1.23	0.50	33	4100	0.03	0.05
35H-3, 107-108	322.8	342.5	123.0	*	0.01	0.02	1.30	0.50	40	2600	0.05	0.32
35RH-3, 107-108	322.8	342.5	72.2	*	0.01	0.00	0.51	*	0	1275	0.04	0.32
37H-3, 107-108	342.2	64.9	70.0	334	0.01	0.02	0.58	0.50	50	1450	0.04	0.16
40H-3, 107-108	371.0	95.8	84.2	*	0.03	0.04	1.25	0.50	100	3125	0.04	0.16
50H-3, 107-108	467.0	93.8	106.0	365	0.02	0.05	0.96	0.33	83	1600	0.06	0.23
53H-3, 107-108	495.7	525.6	102.0	335	0.02	0.06	1.03	0.25	75	1287	0.08	0.20
58H-3, 107-108	543.5	579.3	77.6	337	0.03	0.07	1.01	0.30	100	1442	0.07	0.00
60H-3, 107-108	562.8	603.4	104.0	370	0.03	0.12	1.24	0.21	133	1377	0.09	0.14
184-1146C-												
7H-2, 96-97 wood	60.5	63.1	6	329	8	13.66	22.5	0.37	155	255	8.81	10

Notes: T_{max} = temperature (°C) of maximum release of pyrolysis HC, S_1= mg/g volatile HC, S_2 = pyrolysis HC mg/g, S_3 = pyrolysis CO_2 mg/g, PI = production index, HI = hydrogen index, OI = oxygen index, TOC = total organic carbon, R-E = Rock-Eval, R = replicate, TC = total carbon, IC = inorganic carbon. * = values not identified.

Table T15. Composition of interstitial waters, Hole 1146A.

Core, section, interval (cm)	Depth (mbsf)	Depth (mcd)	pH	Alkalinity (mM)	Salinity	Cl^- (mM)	Cl^- (mM)*	Na^+ (mM)	K^+ (mM)	Mg^{2+} (mM)	Ca^{2+} (mM)	SO_4^{2-} (mM)	HPO_4^{2-} (µM)	NH_4^+ (mM)	H_4SiO_4 (µM)	Li^+ (µM)	Sr^{2+} (µM)
184-1146A-																	
1H-2, 145-150	2.98	2.98	7.46	8.02	34.5	553	540	459.6396	11.8	51.7	10.2	24.1	38.8	0.9	645	24	87
2H-3, 145-150	8.38	9.33	7.42	14.27	34.0	556	553	470.6592	11.7	51.6	7.2	17.5	68.1	2.4	654	21	78
3H-3, 145-150	17.88	19.53	7.31	18.90	34.0	557	558	473.3028	12.6	50.0	4.7	10.9	97.4	3.3	712	22	70
4H-3, 145-150	27.38	29.98	7.39	28.82	33.5	559	558	480.1268	11.4	49.2	4.2	6.8	103.9	2.1	755	23	69
5H-3, 145-150	36.88	40.03	7.26	25.17	33.0	555	557	473.8808	11.9	47.4	4.2	4.7	97.4	2.4	736	24	70
6H-3, 145-150	46.38	49.63	7.16	25.98	33.0	557	560	474.3564	11.1	46.6	4.1	1.8	82.7	2.8	772	27	71
7H-3, 145-150	55.88	58.38	7.19	25.61	33.0	557	562	478.7908	10.8	45.3	4.1	1.8	59.9	2.8	746	31	79
8H-3, 145-150	65.38	68.38	7.33	23.48	32.0	559	558	471.7672	12.2	43.6	3.8	0.0	43.6	2.6	781	34	88
9H-3, 145-150	74.88	78.48	7.28	23.48	32.5	558	559	477.2434	10.8	42.3	4.0	0.7	32.2	3.1	815	37	107
12H-3, 145-150	103.38	109.18	7.39	17.28	32.0	559	557	475.3062	10.0	38.4	4.6	0.0	16.6	2.7	820	39	129
15H-3, 145-150	131.85	140.08	7.42	11.54	32.0	556	555	473.9610	8.2	36.1	4.7	0.0	6.5	2.5	355	32	165
18H-3, 145-150	160.35	170.43	7.44	8.56	33.0	556	557	478.3414	7.4	35.0	4.7	0.0	4.2		264	31	238
21H-3, 145-150	188.85	201.23	7.41	7.12	32.0	555	555	475.8628	7.0	34.0	5.0	0.6	0.9	1.7	254	35	367
24X-3, 145-150	217.15	231.88	7.41	5.06	32.0	555	557	474.3912	6.5	33.0	6.0	0.0	0.1	1.9	232	43	633
27X-3, 140-150	246.15	262.25	7.47	3.34	32.0	557	556	476.0202	6.5	30.8	6.8	0.7	0.1	1.1	213	48	931
30X-3, 140-150	275.05	293.50	7.47	2.48	31.5	556	555	474.0752	5.6	29.0	8.1	0.1	0.1	1.4	185	51	1182
33X-3, 140-150	303.95	322.70	7.44	2.42	32.0	559	557	475.7852	5.1	28.6	9.0	0.3	0.1	1.2	189	55	1260
36X-3, 140-150	332.85	354.95	7.43	2.08	32.0	558	558	474.9236	5.0	28.7	9.5	0.2	0.3	1.7	189	61	1268
39X-3, 140-150	361.75	385.55	7.46	2.15	32.0	558	558	473.9012	4.5	29.2	9.8	0.0	0.1	1.3	208	71	1244
42X-3, 140-150	390.55	414.87	7.43	2.28	32.0	560	559	472.9028	4.2	29.4	10.6	0.2	0.9	2.1	299	97	1201
45X-3, 140-150	419.35	443.77	7.37	2.06	32.0	557	559	470.4056	4.8	29.5	11.4	0.1	0.3	1.8	230	143	1126
48X-3, 135-150	448.13	476.36	7.54	1.83	32.0	555	559	469.0482	5.4	28.7	12.5	0.0	0.1	1.5	142	232	1130
51X-3, 135-150	476.83	504.02	7.87	0.88	31.0	553	557	469.2032	3.6	27.7	13.9	1.1	0.1	1.6	103	353	1072
54X-3, 135-150	505.63	536.37	7.84	0.83	31.0	553	550	457.7902	4.3	26.9	15.1	0.0	0.1	1.8	101	855	1038
57X-3, 135-150	534.33	568.83				533	532		3.6	28.1	18.3	0.3		1.7	97	1320	
60X-3, 135-153	563.15	599.25	8.20	0.51	30.0	537	539	444.6232	4.4	23.6	18.4	0.0	0.1	2.7	56	1770	1017
63X-3, 135-153	591.95	628.37			30.0	533	526		4.1	23.2	21.3		0.1	2.0	71	2390	1004

Note: * = chromatography results.

Table T16. Thermal conductivity measurements at Site 1146. (See table note. Continued on next three pages.)

Leg	Site	Hole	Core	Type	Section	Top interval (cm)	Depth (mbsf)	Depth (mcd)	Thermal conductivity (W/[m·K])	Thermal conductivity (3-pt mean)
184	1146	A	1	H	2	75	2.25	2.25	0.829	
184	1146	A	1	H	2	75	2.25	2.25	0.833	
184	1146	A	1	H	2	75	2.25	2.25	0.839	0.83
184	1146	A	2	H	2	75	6.15	7.10	0.812	
184	1146	A	2	H	2	75	6.15	7.10	0.812	
184	1146	A	2	H	2	75	6.15	7.10	0.805	0.81
184	1146	A	3	H	2	75	15.65	17.30	0.914	
184	1146	A	3	H	2	75	15.65	17.30	0.911	
184	1146	A	3	H	2	75	15.65	17.30	0.910	0.91
184	1146	A	4	H	2	75	25.15	27.75	0.928	
184	1146	A	4	H	2	75	25.15	27.75	0.933	
184	1146	A	4	H	2	75	25.15	27.75	0.925	0.93
184	1146	A	5	H	2	75	34.65	37.80	0.978	
184	1146	A	5	H	2	75	34.65	37.80	0.966	
184	1146	A	5	H	2	75	34.65	37.80	0.952	0.97
184	1146	A	6	H	3	75	45.65	48.90	0.956	
184	1146	A	6	H	3	75	45.65	48.90	0.998	
184	1146	A	6	H	3	75	45.65	48.90	0.996	0.98
184	1146	A	7	H	3	75	55.15	57.65	0.977	
184	1146	A	7	H	3	75	55.15	57.65	0.965	
184	1146	A	7	H	3	75	55.15	57.65	0.993	0.98
184	1146	A	8	H	3	75	64.65	67.65	0.933	
184	1146	A	8	H	3	75	64.65	67.65	0.997	
184	1146	A	8	H	3	75	64.65	67.65	0.985	0.97
184	1146	A	9	H	3	75	74.15	77.75	1.041	
184	1146	A	9	H	3	75	74.15	77.75	0.997	
184	1146	A	9	H	3	75	74.15	77.75	0.988	1.01
184	1146	A	10	H	3	75	83.65	87.45	0.912	
184	1146	A	10	H	3	75	83.65	87.45	0.925	
184	1146	A	10	H	3	75	83.65	87.45	0.939	0.93
184	1146	A	11	H	3	75	93.15	98.50	0.959	
184	1146	A	11	H	3	75	93.15	98.50	0.969	
184	1146	A	11	H	3	75	93.15	98.50	0.999	0.98
184	1146	A	12	H	3	75	102.65	108.45	0.994	
184	1146	A	12	H	3	75	102.65	108.45	0.967	
184	1146	A	12	H	3	75	102.65	108.45	1.002	0.99
184	1146	A	13	H	3	75	112.15	118.65	1.090	
184	1146	A	13	H	3	75	112.15	118.65	1.033	
184	1146	A	13	H	3	75	112.15	118.65	1.031	1.05
184	1146	A	14	H	3	75	121.65	129.00	1.130	
184	1146	A	14	H	3	75	121.65	129.00	1.130	
184	1146	A	14	H	3	75	121.65	129.00	1.133	1.13
184	1146	A	15	H	3	75	131.15	139.35	1.162	
184	1146	A	15	H	3	75	131.15	139.35	1.150	
184	1146	A	15	H	3	75	131.15	139.35	1.128	1.15
184	1146	A	16	H	3	75	140.65	149.50	1.057	
184	1146	A	16	H	3	75	140.65	149.50	1.072	
184	1146	A	16	H	3	75	140.65	149.50	1.073	1.07
184	1146	A	17	H	3	75	150.15	160.50	1.116	
184	1146	A	17	H	3	75	150.15	160.50	1.170	
184	1146	A	17	H	3	75	150.15	160.50	1.141	1.14
184	1146	A	18	H	3	75	159.65	169.70	1.174	
184	1146	A	18	H	3	75	159.65	169.70	1.158	
184	1146	A	18	H	3	75	159.65	169.70	1.167	1.17
184	1146	A	19	H	3	75	169.15	179.30	1.158	
184	1146	A	19	H	3	75	169.15	179.30	1.191	
184	1146	A	19	H	3	75	169.15	179.30	1.189	1.18
184	1146	A	20	H	3	75	178.65	189.08	0.994	
184	1146	A	20	H	3	75	178.65	189.08	0.977	
184	1146	A	20	H	3	75	178.65	189.08	0.970	0.98
184	1146	A	21	H	3	75	188.15	200.50	1.201	
184	1146	A	21	H	3	75	188.15	200.50	1.205	

Table T16 (continued).

Leg	Site	Hole	Core	Type	Section	Top interval (cm)	Depth (mbsf)	Depth (mcd)	Thermal conductivity (W/[m·K])	Thermal conductivity (3-pt mean)
184	1146	A	21	H	3	75	188.15	200.50	1.121	1.18
184	1146	A	22	X	3	75	197.65	210.70	0.984	
184	1146	A	22	X	3	75	197.65	210.70	0.924	
184	1146	A	22	X	3	75	197.65	210.70	0.913	0.94
184	1146	A	23	X	3	75	206.75	220.65	1.086	
184	1146	A	23	X	3	75	206.75	220.65	1.085	
184	1146	A	23	X	3	75	206.75	220.65	1.069	1.08
184	1146	A	24	X	3	75	216.45	231.15	1.014	
184	1146	A	24	X	3	75	216.45	231.15	1.028	
184	1146	A	24	X	3	75	216.45	231.15	1.027	1.02
184	1146	A	26	X	3	75	235.85	250.40	1.036	1.03
184	1146	A	27	X	3	75	245.45	261.55	1.042	
184	1146	A	27	X	3	75	245.45	261.55	0.994	
184	1146	A	27	X	3	75	245.45	261.55	1.026	1.02
184	1146	A	28	X	3	75	255.05	272.69	1.066	
184	1146	A	28	X	3	75	255.05	272.69	1.023	
184	1146	A	28	X	3	75	255.05	272.69	1.028	1.04
184	1146	A	29	X	3	75	264.65	282.75	1.079	
184	1146	A	29	X	3	75	264.65	282.75	1.064	
184	1146	A	29	X	3	75	264.65	282.75	1.062	1.07
184	1146	A	30	X	3	75	274.35	292.80	1.084	
184	1146	A	30	X	3	75	274.35	292.80	1.093	
184	1146	A	30	X	3	75	274.35	292.80	1.076	1.08
184	1146	A	31	X	3	75	283.95	302.40	1.130	
184	1146	A	31	X	3	75	283.95	302.40	1.103	
184	1146	A	31	X	3	75	283.95	302.40	1.100	1.11
184	1146	A	32	X	3	75	293.55	312.00	1.034	
184	1146	A	32	X	3	75	293.55	312.00	1.029	
184	1146	A	32	X	3	75	293.55	312.00	1.044	1.04
184	1146	A	33	X	3	75	303.25	322.00	0.576	
184	1146	A	33	X	3	75	303.25	322.00	0.551	
184	1146	A	33	X	3	75	303.25	322.00	0.558	0.56
184	1146	A	34	X	3	75	312.85	331.80	1.053	
184	1146	A	34	X	3	75	312.85	331.80	1.049	
184	1146	A	34	X	3	75	312.85	331.80	1.059	1.05
184	1146	A	35	X	3	75	322.45	342.15	1.264	
184	1146	A	35	X	3	75	322.45	342.15	1.226	
184	1146	A	35	X	3	75	322.45	342.15	1.173	1.22
184	1146	A	36	X	3	75	332.15	354.25	1.165	
184	1146	A	36	X	3	75	332.15	354.25	1.198	
184	1146	A	36	X	3	75	332.15	354.25	1.241	1.20
184	1146	A	37	X	3	75	341.85	364.60	1.303	
184	1146	A	37	X	3	75	341.85	364.60	1.277	
184	1146	A	37	X	3	75	341.85	364.60	1.282	1.29
184	1146	A	38	X	3	75	351.45	375.20	1.250	
184	1146	A	38	X	3	75	351.45	375.20	1.299	
184	1146	A	38	X	3	75	351.45	375.20	1.275	1.27
184	1146	A	39	X	3	75	361.05	384.85	1.295	
184	1146	A	39	X	3	75	361.05	384.85	1.316	
184	1146	A	39	X	3	75	361.05	384.85	1.316	1.31
184	1146	A	40	X	3	75	370.65	395.45	1.148	
184	1146	A	40	X	3	75	370.65	395.45	1.138	
184	1146	A	40	X	3	75	370.65	395.45	1.128	1.14
184	1146	A	41	X	3	75	380.25	405.87	1.253	
184	1146	A	41	X	3	75	380.25	405.87	1.205	
184	1146	A	41	X	3	75	380.25	405.87	1.236	1.23
184	1146	A	42	X	3	75	389.85	414.17	1.286	
184	1146	A	42	X	3	75	389.85	414.17	1.306	
184	1146	A	42	X	3	75	389.85	414.17	1.292	1.29
184	1146	A	43	X	3	75	399.45	423.92	1.213	
184	1146	A	43	X	3	75	399.45	423.92	1.265	
184	1146	A	43	X	3	75	399.45	423.92	1.232	1.24
184	1146	A	44	X	3	75	409.05	433.12	1.303	
184	1146	A	44	X	3	75	409.05	433.12	1.311	
184	1146	A	44	X	3	75	409.05	433.12	1.317	1.31
184	1146	A	45	X	3	75	418.65	443.07	1.141	
184	1146	A	45	X	3	75	418.65	443.07	1.145	
184	1146	A	45	X	3	75	418.65	443.07	1.143	1.14
184	1146	B	2	H	3	75	11.05	12.30	0.784	
184	1146	B	2	H	3	75	11.05	12.30	0.793	

Table T16 (continued).

Leg	Site	Hole	Core	Type	Section	Top interval (cm)	Depth (mbsf)	Depth (mcd)	Thermal conductivity (W/[m·K])	Thermal conductivity (3-pt mean)
184	1146	B	2	H	3	75	11.05	12.30	0.800	0.79
184	1146	B	3	H	3	75	20.55	22.85	0.899	
184	1146	B	3	H	3	75	20.55	22.85	0.874	
184	1146	B	3	H	3	75	20.55	22.85	0.879	0.88
184	1146	B	4	H	3	75	30.05	32.55	0.888	
184	1146	B	4	H	3	75	30.05	32.55	0.893	
184	1146	B	4	H	3	75	30.05	32.55	0.910	0.90
184	1146	B	5	H	3	75	39.55	43.05	0.950	
184	1146	B	5	H	3	75	39.55	43.05	0.937	
184	1146	B	5	H	3	75	39.55	43.05	0.975	0.95
184	1146	B	6	H	3	75	49.05	52.45	0.966	
184	1146	B	6	H	3	75	49.05	52.45	0.997	
184	1146	B	6	H	3	75	49.05	52.45	0.979	0.98
184	1146	B	7	H	3	75	58.55	62.55	0.967	
184	1146	B	7	H	3	75	58.55	62.55	0.974	
184	1146	B	7	H	3	75	58.55	62.55	0.971	0.97
184	1146	B	8	H	3	75	68.05	72.25	0.921	
184	1146	B	8	H	3	75	68.05	72.25	0.961	
184	1146	B	8	H	3	75	68.05	72.25	0.933	0.94
184	1146	B	9	H	3	75	77.55	82.35	0.934	
184	1146	B	9	H	3	75	77.55	82.35	0.935	
184	1146	B	9	H	3	75	77.55	82.35	0.940	0.94
184	1146	B	10	H	3	75	87.05	92.65	1.020	
184	1146	B	10	H	3	75	87.05	92.65	1.012	
184	1146	B	10	H	3	75	87.05	92.65	1.055	1.03
184	1146	B	11	H	3	75	96.55	103.45	1.072	
184	1146	B	11	H	3	75	96.55	103.45	1.037	
184	1146	B	11	H	3	75	96.55	103.45	1.042	1.05
184	1146	B	12	H	3	75	106.05	113.05	1.098	
184	1146	B	12	H	3	75	106.05	113.05	1.073	
184	1146	B	12	H	3	75	106.05	113.05	1.061	1.08
184	1146	B	13	H	3	75	115.55	123.25	1.054	
184	1146	B	13	H	3	75	115.55	123.25	1.049	
184	1146	B	13	H	3	75	115.55	123.25	1.023	1.04
184	1146	B	14	H	3	75	125.05	133.65	1.193	
184	1146	B	14	H	3	75	125.05	133.65	1.126	
184	1146	B	14	H	3	75	125.05	133.65	1.116	1.15
184	1146	B	15	H	3	75	134.55	143.35	1.081	
184	1146	B	15	H	3	75	134.55	143.35	1.064	
184	1146	B	15	H	3	75	134.55	143.35	1.116	1.09
184	1146	B	16	H	3	75	144.05	153.45	1.116	
184	1146	B	16	H	3	75	144.05	153.45	1.107	
184	1146	B	16	H	3	75	144.05	153.45	1.125	1.12
184	1146	B	17	H	3	75	153.55	163.50	1.093	
184	1146	B	17	H	3	75	153.55	163.50	1.073	
184	1146	B	17	H	3	75	153.55	163.50	1.066	1.08
184	1146	B	18	H	3	75	163.05	172.80	1.152	
184	1146	B	18	H	3	75	163.05	172.80	1.125	
184	1146	B	18	H	3	75	163.05	172.80	1.112	1.13
184	1146	B	19	H	3	40	172.20	182.95	1.144	
184	1146	B	19	H	3	40	172.20	182.95	1.110	
184	1146	B	19	H	3	40	172.20	182.95	1.112	1.12
184	1146	B	20	H	3	75	182.05	194.00	1.157	
184	1146	B	20	H	3	75	182.05	194.00	1.165	
184	1146	B	20	H	3	75	182.05	194.00	1.151	1.16
184	1146	B	21	H	3	75	190.20	203.25	1.167	
184	1146	B	21	H	3	75	190.20	203.25	1.108	
184	1146	B	21	H	3	75	190.20	203.25	1.135	1.14
184	1146	B	22	H	3	75	201.05	214.40	1.168	
184	1146	B	22	H	3	75	201.05	214.40	1.185	
184	1146	B	22	H	3	75	201.05	214.40	1.206	1.19
184	1146	B	23	H	5	75	213.46	228.20	1.131	
184	1146	B	23	H	5	75	213.46	228.20	1.134	
184	1146	B	23	H	5	75	213.46	228.20	1.135	1.13
184	1146	B	24	X	3	75	220.05	235.80	1.027	
184	1146	B	24	X	3	75	220.05	235.80	1.067	
184	1146	B	24	X	3	75	220.05	235.80	1.075	1.06
184	1146	B	25	X	3	75	229.65	244.80	1.002	
184	1146	B	25	X	3	75	229.65	244.80	1.042	
184	1146	B	25	X	3	75	229.65	244.80	1.059	1.03

Table T16 (continued).

Leg	Site	Hole	Core	Type	Section	Top interval (cm)	Depth (mbsf)	Depth (mcd)	Thermal conductivity (W/[m·K])	Thermal conductivity (3-pt mean)
184	1146	B	26	X	3	75	239.25	254.80	1.028	
184	1146	B	26	X	3	75	239.25	254.80	1.003	
184	1146	B	26	X	3	75	239.25	254.80	0.998	1.01

Note: This table is also available in **ASCII format.**

Table T17. Summary of logging operations at Site 1146.

Date (March 1999)	Time (local)	
24	1600	Hole preparation complete. Rig up wireline.
24	1732	Rig into hole with HNGS-APS-HLDS-DIT.
24	1941	Uplog at 275 m/hr from 606 to 547 mbsf. Rig into hole to total depth.
24	2005	Uplog at 275 m/hr from 606 mbsf to EOP. Pull out of hole.
		Pipe trip to new EOP at 242 mbsf.
25	0105	Rig into hole with NGT-FMS-LSS.
25	0246	Uplog at 275 m/hr from 606 mbsf to EOP. Rig into hole to total depth.
25	0410	Uplog at 275 m/hr from 606 mbsf to EOP. Pull out of hole.
25	0707	Rig into hole with NGT-GHMT-GPIT.
25	0851	Uplog at 550 m/hr from 606 mbsf to EOP. Rig into hole to total depth.
		Total magnetic field tool failed and then fixed.
25	0945	Uplog at 550 m/hr from 606 mbsf to EOP. Rig into hole to total depth.
25	1025	Uplog at 550 m/hr from 606 mbsf to EOP. Pull out of hole.
25	1235	End of logging operations.

Note: HNGS = hostile environment natural gamma-ray sonde, APS = accelerator porosity sonde, HLDS = hostile environment lithodensity sonde, DIT = dual-induction tool, EOP = end of pipe, NGT = natural gamma-ray tool, FMS = Formation MicroScanner, LSS = long-spaced sonic logging tool, GHMT = geological high-resolution magnetic tool, GPIT = general-purpose inclinometer tool.